

AD-A050 658

ILLINOIS UNIV AT URBANA-CHAMPAIGN DEPT OF MECHANICAL --ETC F/6 20/4
BASE PRESSURE PROBLEMS ASSOCIATED WITH AN AXISYMMETRIC TRANSONIC--ETC(U)

NOV 77 J S LIU, W L CHOW

DAA629-76-G-0199

UNCLASSIFIED

ME-TR-395-5

ARO-13510.3-E

NL

1 OF 2
AD
A050 658



AD A 050658

ME-TR-395-5

'ARO 13510.3-E

UILU ENG 77-4013

(12)

BASE PRESSURE PROBLEMS ASSOCIATED WITH
AN AXISYMMETRIC TRANSONIC FLOW PAST
A BACKWARD FACING STEP

J. S. K. Liu

W. L. Chow

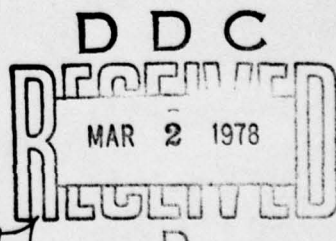
November 1977

U.S. Army Research Office

Grant DAAG29-76-G-0199

Engineering Experiment Station
Department of Mechanical and Industrial Engineering
University of Illinois at Urbana-Champaign
Urbana, IL 61801

Approved for Public Release;
Distribution Unlimited.



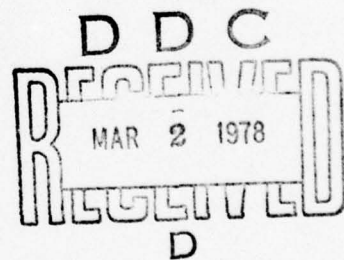
REPORT DOCUMENTATION PAGE		READ INSTRUCTIONS BEFORE COMPLETING FORM
1. REPORT NUMBER 14) ME-TR-395-5, UILU ENG 77-4013	2. GOVT ACCESSION NO.	3. RECIPIENT'S CATALOG NUMBER
4. TITLE (and Subtitle) Base Pressure Problems associated with an Axi-symmetric Transonic Flow past a Backward Facing Step.	5. TYPE OF REPORT & PERIOD COVERED 9) Technical Report,	
7. AUTHOR(s) J. S. K. Liu W. L. Chow	6. PERFORMING ORG. REPORT NUMBER UILU ENG 77-4013✓	
8. CONTRACT OR GRANT NUMBER(s) 15) DAAG29-76-G-0199new	10. PROGRAM ELEMENT, PROJECT, TASK AREA & WORK UNIT NUMBERS	
9. PERFORMING ORGANIZATION NAME AND ADDRESS Department of Mechanical and Industrial Engr. University of Ill. at Urbana-Champaign Urbana, IL 61801	11. REPORT DATE 11 NOV 77	
11. CONTROLLING OFFICE NAME AND ADDRESS U. S. Army Research Office Post Office Box 12211 Research Triangle Park, NC 27709	13. NUMBER OF PAGES One hundred (100) 12/109 p.	
14. MONITORING AGENCY NAME & ADDRESS (if different from Controlling Office) 18) ARO 19) 13510.3-E	15. SECURITY CLASS. (of this report) Unclassified	
16. DISTRIBUTION STATEMENT (of this Report) Approved for public release; distribution unlimited.		
17. DISTRIBUTION STATEMENT (of the abstract entered in Block 20, if different from Report) NA		
18. SUPPLEMENTARY NOTES The findings in this report are not to be construed as an official Department of the Army position, unless so designated by other authorized documents.		
19. KEY WORDS (Continue on reverse side if necessary and identify by block number) Transonic separated flows, recompression and reattachment, saddle point singularity, and transonic base pressure		
20. ABSTRACT (Continue on reverse side if necessary and identify by block number) The base pressure problem of a transonic flow past a backward facing step in the axisymmetric configuration has been examined. The inviscid flow field is generated from an equivalent body with a characteristic parameter and the value of this parameter is determined through the viscous flow analysis. The full axisymmetric potential equation is solved by numerical relaxation while the viscous flow is analyzed through integral formulations. The point of reattachment behaves as a saddle point singularity. The base pressure results are in reasonable agreement with available experimental data.		

400833
jeh

FOREWORD

This research investigation was carried out under the partial financial support from the U.S. Army Research Office through Research Grant DAAG29-76-0199 entitled "Separated Flow Problems within the Transonic and Supersonic Flow Regimes." Dr. Robert E. Singleton from the Army Research Office acted as technical monitor for this project while Dr. Donald J. Spring at the U.S. Army Missile Research and Development Command, Redstone Arsenal, Alabama, served as the principle liaison officer.

Classification for	
DTIS	White Section <input checked="" type="checkbox"/>
DDC	Buff Section <input type="checkbox"/>
UNARMORIZED	
IDENTIFICATION	
BY	
DISTINCTION/AVAILABILITY CODES	
Dist.	AVAIL. AND/OR SPECIAL
A	



ABSTRACT

A flow model has been devised to study the viscid-inviscid interaction within the transonic flow regime. Specifically, the base pressure problem of a transonic flow past a backward facing step in axisymmetric configuration has been examined. It is recognized that the flow field is established as a result of interaction between the viscid and inviscid streams and the problem can be solved by simultaneously considering the influences from both streams. The basic idea employed in this analysis is to interpret the inviscid flow field as if it were generated from an equivalent body whose geometrical description relies upon some characteristic parameters and the values of these parameters are to be determined through the viscous flow analysis. Inviscid flow field is established from solving the full axisymmetric potential equation by numerical method of relaxation while the viscous flow is analyzed through integral formulations. It is found that the point of reattachment behaves as a saddle point singularity for the system of equations governing recompression of the viscous flow and this unique behavior serves to determine the aforementioned parameters. Extensive calculations have been carried out to investigate the influences of the initial momentum thickness of the boundary layer prior to separation, the size of the sting, the shape of the equivalent inviscid body geometry, and the spread rate parameter within the turbulent jet mixing region. The base pressure results are in reasonable agreement with available experimental data. Furthermore, they showed clearly the rise of base drag as the sonic free stream Mach number is approached. Further improvements of the analysis have been also suggested and discussed.

TABLE OF CONTENTS

	Page
1. INTRODUCTION-----	1
2. INVISCID FLOW ANALYSIS-----	13
3. VISCOUS FLOW ANALYSIS-----	20
3.1 QUASI-CONSTANT PRESSURE JET MIXING PROCESS-----	21
3.2 RECOMPRESSION AND REATTACHMENT-----	27
3.3 REDEVELOPMENT OF FLOW-----	36
4. METHOD OF CALCULATIONS-----	38
5. RESULTS AND DISCUSSION-----	41
6. CONCLUSIONS-----	50
BIBLIOGRAPHY-----	93
APPENDIX-----	98

NOMENCLATURE

AB1,AB2,AB3	Coefficient functions defined in Eq. (2.16)
AP1,AP2,AP3	Coefficient functions defined in Eq. (2.17)
B	Stretch parameter
BB1,BB2,BB3	Coefficient functions defined in Eq. (2.16)
BP1,BP2,BP3	Coefficient functions defined in Eq. (2.17)
C	Crocco number, $C^2 = M^2/[2/(\gamma-1) + M^2]$, also dimensionless speed of sound
c	Local speed of sound
C_p	Pressure coefficient
C_{pb}	Base pressure coefficient
F1 ~ F28	Integrals associated with the viscous layer (see APPENDIX)
g	Constant of proportionality defined in Eq. (3.32)
H	Step height
h_b	Thickness of backflow viscous layer
JR	Number of times in the calculation of corresponding inviscid flow due to successive refinement of grid spacings
ℓ_m	Length of mixing region
M	Mach number
m	Power of z in equivalent body coordinate defined in Eq. (2.1)
P	Pressure
R	Radius of curvature
R^*	Dimensionless body radius ($R^* = R_o/H$)

R_b	Dimensionless equivalent body coordinate
R_d	Radius of dividing streamline
R_o	Body radius
R_s	Sting radius
r	Radial distance normal to the axis of centerline
s	Slope of velocity profile at the dividing streamline
Sh	Shape factor of equivalent body
U	Dimensionless velocity component in axial direction
u	Velocity component in axial direction
V	Dimensionless velocity component in radial direction
v	Velocity component in radial direction
x_r	Length along the recompression region
z_R	Location of rear stagnation point of corresponding inviscid flow
β	Streamline angle
γ	Ratio of specific heats
δ	Thickness of shear layer
δ^{**}	Momentum thickness of boundary layer
ϵ	Eddy diffusivity
ζ	Transformed radial coordinate, also dimensionless coordinates within the viscous flow region
η	Dimensionless coordinate of the mixing process
θ_b	Angle of equivalent body coordinate
θ_c	Angle between x-axis and axis of centerline in the recompression region
ξ	Transformed axial coordinate

ρ	Density
σ	Spread rate parameter
τ	Turbulent shear stress
ϕ	Velocity potential function
ϕ	Disturbed potential function, or dimensionless viscous flow velocity

Subscripts

a	Viscous layer above dividing streamline
b	Viscous layer below dividing streamline or backflow
d	Dividing streamline
e	Free stream condition at edge of viscous layer
j	Index for grid points
l	Viscous layer below dividing streamline
m	Edge flow condition of viscous layer within mixing region or the end of mixing section
w	Wall (sting) or axis of centerline
o	Stagnation state
1	Initial section of jet mixing region
∞	Approaching free stream

Superscripts

k	Index for grid points
---	-----------------------

1. INTRODUCTION*

When a flow passes a body with a blunt trailing edge, it is unable to follow the abrupt change in the wall geometry and the flow separates at the base, forming a wake behind the body. A typical picture of such a separated flow is shown in Fig. 1. The pressure within the wake, usually termed base pressure, is generally lower than that of the free stream and it contributes to a large portion of drag suffered by the body. This phenomenon exists irrespective of whether the problem is in the low-speed or high-speed flow regime. The base pressure problem has been the subject of intensive study within the last two decades because of its academic interest as well as its practical importance.

After flow separates at the base, usually a turbulent jet mixing process occurs along the wake boundary. Mixing process is responsible to energize the low energy fluid and entrains mass immediately behind the base. A recompression process subsequently occurs as the main inviscid flow turns toward the original flow direction. As a result of this recompression, part of the fluid entrained within the viscous layer is turned back to form the recirculatory wake flow while the rest of the flow will proceed downstream.

Subsequent to flow reattachment, additional recompression coupled with adjustments as a result of viscous flow redevelopment occurs which generally leads to a pressure plateau higher than that of the free stream (static pressure overshoot).** Afterward, the static pressure decays asymptotically toward the free stream value. Throughout the region of flow, both viscous and

*The major part of the material discussed in this report is based on a Ph.D. thesis by the first author [1]. (Numbers in brackets denote REFERENCES.)

**Overshoot phenomenon does not occur for two-dimensional supersonic flow past a backward facing step. Under this situation, flow redevelopment coupled with a continuous rise of pressure occurs until the original free stream level is reached.

and inviscid streams coexist. It is understood that while the viscous flow is guided more or less by the inviscid flow in the sense of the boundary layer concept, the inviscid flow configuration, as well as the pressure level prevailing within the wake (base pressure) relies equally on the viscous flow mechanisms of mixing, recompression, and redevelopment. Thus the overall flow pattern is established as a result of interaction between the viscous and inviscid streams. This type of mutual influence between the streams is now properly classified as strong interaction, indicating that the viscous and inviscid flows play the same important roles and no solution can be reached without simultaneously considering the influence from each stream.

Korst, Page, and Childs [2] reviewed the earlier work dealing with base pressure problems. Since then, a large amount of effort has been directed to the study of these problems. An excellent review of theories and literature concerning separated flow problems has been published by Wuerer and Clayton [3], Carpenter and Tabakoff [4], Chang [5], Berger [6], and recently Page [7].

The first approach to base pressure problem within the supersonic flow regime was based on the mixing theory developed earlier by Crocco and Lees [8]. They pointed out that in the interaction between a viscous or dissipative flow and an "outer" nearly isentropic stream, the "external flow" cannot be regarded as known datum for the calculation of the "internal" dissipative flow. By introducing an empirical mixing coefficient, the mixing rate is taken to be proportional to the mass flux density of the isentropic stream and the equations of motion are reduced to a single nonlinear ordinary differential equation that can be integrated numerically. It has been found that a critical point exists for the supersonic wake flow. This critical point acts much like the throat of a nozzle in determining the

flow inclination angle and the base pressure after the flow expansion around the corner for the given approaching flow conditions at the base. Following this concept of Crocco and Lees, Lees and Reeves [9,10] formed an integral approach by employing the first moment of momentum equation in addition to the usual momentum integral equation which is capable of treating the attached and separated flows under one single framework. Stewartson's reverse-flow velocity profiles for flow over a solid surface [11] has been used to represent the wake flow. The critical point similar to that of Crocco and Lees exists downstream of the wake. The flow solution for a particular problem is reached when the flow passes smoothly through this critical point. This approach produced very good results for laminar base flow problems.

Alber [12] and Alber and Lees [13] extended the same approach to fully turbulent base flows. By assuming that the shear stress follows the Boussinesq's formulation, turbulent eddy viscosity was obtained from compressible transformation from that of an incompressible flow. The obtained base pressure results were too high when compared with experimental data, especially for cases with thin initial boundary layers. However, this analysis provided a means to predict the base pressure as well as the structure of the flow.

Todisco and Reeves [14] investigated turbulent separated and reattaching flows over compression corners using a strong interaction, wake-like model of the flow and produced results which compare favorably with experiments. Hunter and Reeves [15] applied the aforementioned turbulent interaction model for separated and reattaching flows to several important problems associated with control surfaces on high-speed aircraft and

maneuvering re-entry vehicles. Shamroth and McDonald [16] included a normal momentum integral equation in their analysis and a solution method was devised to eliminate this saddle-point singularity downstream of the reattachment.

Recently, Strahle and Mehta [17] and Strahle, et al. [18], extended the Crocco-Lees theory to axisymmetric turbulent wake flows. In their analysis, the external flow is assumed to be isentropic and is treated with an approximate method of characteristics. Only flows without base bleed have been considered.

Some of the earlier analytical studies were performed by Chapman [19,20]. Analysis was made of base pressure in an inviscid fluid, both for two-dimensional and axially-symmetric flows. It was found that there were an infinite number of possible solutions satisfying all necessary boundary conditions at any given free-stream Mach number. An approximate semi-empirical theory for base pressure in a viscous fluid is developed to account for the effects of Mach number, Reynolds number, profile shape, and type of boundary layer flow. Korst [21] formulated a theoretical treatment of the base pressure problem which utilized Chapman's model but included additional viscous flow considerations. Four flow components are integrated in this model, namely, the flow approaching the trailing edge, the expansion around the corner, the mixing within the free jet boundary, and the recompression at the end of the wake. An "escape concept" for determining the base pressure was suggested in conjunction with the isentropic recompression process along the dividing streamline prior to the rear stagnation point. It specifies that the dividing streamline should attain a level of mechanical energy at the end of the jet mixing region which would allow an isentropic recompression by the

complete conversion of the kinetic energy to the ambient pressure. The base pressure is thus determined by the condition that the stagnation pressure of the dividing streamline shall be equal to the static pressure impressed behind the oblique shock downstream of the wake. However, experimental data showed that the pressure at the rear stagnation point is much lower than what is impressed behind the shock. The asymptotic jet-mixing solution [22,23] was applied to this base pressure problem as "restricted theory" which corresponds to a vanishingly small approaching boundary layer thickness. Results obtained with this restriction represent the lowest possible base-pressure value for a given configuration and approaching flow Mach number. This analysis yields very good predictions of base pressure for planar and quasi-planar flows; however, it provides no information about the detailed flow structure in the recompression region. Korst, Chow, and Zumwalt [24] had extended this analysis to develop a general theory for pressures and temperatures in separated transonic and supersonic flows. Chapman, Kuehn, and Larson [25,26] made a similar consideration of Korst's recompression model for fully developed laminar flow. They instead imposed a reversible adiabatic recompression for the adjacent free stream.

Numerous attempts have been made to improve the component analysis in the Korst theory. Nash [27] introduced an empirical factor to account for the fact that the discriminating streamline does not stagnate at the peak of the pressure distribution. Since the "restricted theory" does not consider the effect of finite Reynolds number, other authors tried to include the influence of the initial boundary layer. Carriere and Sirieix [28], Golik [29], and Nash [27] showed that the effect of an initial boundary layer would be represented as an "equivalent mass bleed"

into the base region. Hill and Page [30] applied the apparent mixing origin shift concept to calculate the flow properties for developing flows within the constant pressure jet mixing region.

Several attempts have been made to extend the Korst theory to the axisymmetric base pressure problem. Zumwalt [31] assumed that the flow recompresses, in a locally planar process, on an imaginary sting which extends from the base. Mueller [32] stipulated that recompression occurs either on a sting with a radius of one-half of the base radius, or on a sting equivalent to the experimentally observed radius of the wake after recompression.

McDonald [33] formulated an approach to predict the two-dimensional turbulent base pressure for flows which reattach to a solid wall. In this analysis, base pressure is assumed and a momentum integral approach gives the velocity profile thickness parameters at reattachment by ignoring the viscosity effect during the abrupt pressure rise. The effect of remaining pressure rise on the now attached boundary layer is estimated using the Squire and Young formula to modify the moment of momentum equation of the ordinary boundary layer theory. Thus, thickness parameters at the end of the pressure rise are obtained. Equating the drag of the backstep to the final momentum thickness would serve to estimate the base pressure by an iterative process. The shape parameter of the attached boundary layer has been assumed to be of the flat-plate type. McDonald [34] also extended his analysis to the axisymmetric turbulent supersonic base flow by means of Mangler's transformation. A unique solution is obtained by specifying the shape of the rehabilitated boundary layer velocity profile. This analysis produced reasonably good prediction of the base pressure; however, it was impossible to obtain a solution to the problem of a vanishingly small sting and the initial boundary layer thickness was restricted to be thin when compared with the body radius.

Among other authors, Nielson, Lynes, and Goodwin [35] studied the laminar wake flow based upon the method of integral relations. Roache and Mueller [36] obtained numerical solutions to the Navier-Stokes equations. Lamb and Hood [37], Reda and Page [38], and Gerhart [39] developed control volume analysis for the recompression region, respectively.

Chow [40] recently developed an integral method of analysis for the turbulent recompression and reattachment process associated with a two-dimensional supersonic free shear layer. The flow field was divided into two subregions along the dividing streamline. The external supersonic free stream guides and interacts with the upper viscous layer and the pressure difference across this layer was estimated from the normal momentum relationship. The lower viscous layer consists of a forward flow characterized by the dividing streamline velocity and a backflow characterized by a maximum backflow velocity. The difference in pressure across this layer was also accounted for. In conjunction with the flow conditions prevailing at the end of the constant pressure jet mixing region, the system of equations may be integrated and solved numerically. It was shown that by linking the dividing streamline velocity with its slope, calculations of these flows can be performed up to the point of reattachment. For a given flow problem, the correct value of base pressure and the location along the wake boundary where recompression starts were established through iterations until the conditions at the rear stagnation point were satisfied. This analysis yielded reasonable results.

Later, Chow and Spring [41,42] also studied the flow redevelopment after reattachment with supersonic turbulent separated flows. The flow redevelopment was interpreted as a process of relaxation of the pressure

difference across the viscous layer. Upon coupling the pressure difference with a slope parameter of the velocity profile, the system of equations governing the redevelopment of flow would produce a saddle-point singularity corresponding to the fully rehabilitated asymptotic flow condition which provided the closure condition for the Chapman-Korst model of base flows. Reasonably good agreement with experimental data has also been observed.

Weng [43] extended Chow's analysis to axisymmetric external flow configurations within the supersonic flow regime. The Prandtl mixing length theory has been used to compute the turbulent shear stresses in the constant pressure jet mixing region and a spatial variation of eddy viscosity had been used in the recompression region for the same purpose. The obtained base pressure and wall pressure distribution agreed well with experimental data. Peters and Phares [44] developed a scheme to include the effect of base bleed which applies equally well to two-dimensional as well as the axisymmetric supersonic turbulent near-wake flows. Reasonably good prediction for base pressure and flow field structure has been observed.

Chow and Spring [45,46] studied low-speed separated flow problems with the same viscous flow analysis combined with the conformal mapping technique for the establishment of the outer inviscid flow. It was suggested that the corresponding inviscid flow of these problems can be described by the free streamline theory with few unspecified parameters and their values were determined by the viscous flow considerations. It was found that the point of reattachment behaves as a saddle-point type singularity in the system of differential equations describing the viscous recompression flow process. This feature was employed to determine the aforementioned free parameters and thus establish the overall corresponding inviscid flow field. The

resulting base pressure coefficient for the specific case agrees reasonably well with the available experimental data. Warpinska and Chow [47,48] extended this study to investigate the incompressible separated flows associated with wedges. The effect of wind tunnel wall interference has also been studied.

For transonic flows, due to the nonlinear and mixed character of the inviscid potential equation, the lack of an adequate and efficient method to calculate accurately the inviscid flow field hampered the analysis of separated within this flow regime. Only recently, because of its practical importance as well as its relation to fully three-dimensional flow via the area rule, there has been a considerable amount of activity in this area. Murman and Cole [49] calculated the flow past thin airfoils including cases with imbedded shock waves on the basis of the transonic small disturbance equation. An analytical expression was developed for the far field of an airfoil which is used as a boundary condition for the numerical computation. In the near field, the governing transonic potential equation was solved numerically using a mixed finite difference system. Separate difference formulas are used in the elliptic and hyperbolic regions to account properly for the local domain of dependence of the differential equation. The difference equations were solved numerically by an iterative line relaxation procedure. For the circular arc airfoil, the results were good when compared with experiments.

Krupp and Murman [50] computed the transonic flow past lifting airfoils and slender bodies. An asymptotic solution had been used for the far-field potential at the boundary of a finite cylinder surrounding the

body. The solution is restricted to subsonic free stream Mach numbers. Bailey [51] also extended the small disturbance treatment to calculate transonic flow past slender bodies of revolution. In this analysis, stretched grid systems had been used in the radial direction.

Steger and Lomax [52] had treated the two-dimensional inviscid full potential equation governing compressible flow by successive over-relaxation procedure. South and Jameson [53] also had similar consideration to the axisymmetric configurations. Successive mesh refinement has been suggested during the course of iteration. A considerable saving in computer time can be achieved by first obtaining a converged solution on a coarse grid, then halving the mesh size in both directions and restarting the solution after interpolating the coarser solution on the new mesh.

Chow, Bober, and Anderson [54,55] investigated the effect of boattail junction shape on the drag of certain afterbodies under transonic flow conditions. In this investigation, they employed finite difference calculations to solve the full transonic-potential equation and the integral boundary-layer technique to account for the viscous displacement effect. It was found that under this transonic flow condition, the growth of the viscous layer indeed contributes significantly to the resulting pressure distribution on the afterbody and the small disturbance simplification is not adequate to describe the flow. The final results of calculations agree well with the experimental flow.

Deiwert [56] studied the two-dimensional compressible Navier-Stokes equations by using MacCormack's second-order accurate finite difference method for the separated transonic turbulent flow field over an airfoil. Four different algebraic eddy viscosity models were employed to estimate

the Reynolds stress. A considerable amount of computing time was used for calculations and only limited success was achieved. It clearly indicates that the essential problem of modeling the turbulent mechanism in the separated region remains.

As an effective method of calculating the transonic inviscid flow field becomes available, the preliminary study of the viscous-inviscid interaction associated with the two-dimensional flow past a backward facing step within the transonic regime has also been carried out by Chow and Shih [57,58]. The basic idea employed in this analysis was to interpret the flow field as if it were produced by an equivalent inviscid body geometry whose description usually relies upon some characteristic parameters. The viscous-inviscid interaction can be properly illustrated by the fact that the viscous flow analysis would determine the correct values of these parameters.

In the present study, the same idea is employed to study the transonic flow past an axisymmetric backward facing step. It is assumed that the isoenergetic flow field prevails throughout the flow so that the consideration of the energy equation is conveniently eliminated. The basic purpose of the present study lies in the hope of determining the base pressure associated with axisymmetric blunt based bodies within the transonic flow regime. This information is urgently needed for all practical flow configurations within this flight regime. The importance of axially symmetric geometry throughout the whole flow field can readily be seen in analytical treatment of this problem.

Extensive calculations have been carried out for different approaching flow Mach numbers, initial momentum thicknesses, and sting radius ratios to explore their effects on the results. It should be noted that the present treatment can be considered only as a first approximation to the problem. Additional improvements to the solution of the problem based on present approach will be discussed in detail in Chapter 5.

2. INVISCID FLOW ANALYSIS

From the introductory discussion, it is understood that for the problem of high subsonic or transonic Mach number flow approaching a backward facing step in axisymmetric configuration, the corresponding inviscid flow field should be first established. For an initially uniform flow approaching the base, it may be expected that the flow will separate at the corner of the base and a turbulent jet mixing process usually occurs along the wake boundary. Since the mixing region is thin in the sense of the boundary layer concept, it may be anticipated that the boundary of the corresponding inviscid flow should assume a geometry which is more or less similar to the path of the dividing streamline. It is thus suggested for the present problem that the corresponding inviscid flow can be established from a flow past an equivalent body shape which is given (see Fig. 2) by

$$\begin{aligned}
 R_b &= (Sh) R^* && \text{for } z < 0 \\
 R_b &= (Sh)(R^* - z^m) && \text{for } 0 \leq z \leq 1 \\
 R_b &= (Sh)(R^* - 1) && \text{for } z > 1
 \end{aligned} \tag{2.1}$$

where Sh ($Sh = H/z_R$) is the shape factor of the equivalent body and $R^* = R_o/H$, R_b is the body profile already normalized by z_R . The point $z = 1$, $R_b = R_s$ corresponds to the inviscid rear stagnation point (which is not the point of reattachment of the real flow) whose location for a given step height H is yet unknown.

The model described above is essentially deducted from the boundary layer concept. It should be noted that the physical region in the vicinity of the bounding streamline of this corresponding inviscid geometry will actually be occupied by viscous flows and adoption of such

a configuration would yield a reasonable description of the inviscid flow which will provide proper guidance and influence to the attached viscous flow in the sense of the boundary layer concept.

For the present series of calculations, $m = 3$ is selected in Eq. (2.1) in order to avoid the introduction of a curvature discontinuity at the corner of the base. However, this is not mandatory for the real flow case. Some results obtained from $m = 2$ will also be presented for comparison purposes.

With the body geometry given by Eq. (2.1), the corresponding inviscid flow field under transonic or high subsonic Mach number conditions may be established through numerical calculations [55]. The axisymmetric inviscid flow field may be described by the potential equation given by

$$\left(1 - \frac{\phi_z^2}{c^2}\right)\phi_{zz} + \left(1 - \frac{\phi_r^2}{c^2}\right)\phi_{rr} - 2\frac{\phi_r \phi_z}{c^2}\phi_{rz} + \frac{\phi_r}{r} = 0 \quad (2.2)$$

where the subscripts indicate partial differentiation and c is the local speed of sound obtained from

$$c^2 = c_0^2 - \frac{\gamma - 1}{2} (\phi_z^2 + \phi_r^2). \quad (2.3)$$

Upon defining

$$\Phi = V_\infty(z + \phi), \quad U = u/V_\infty, \quad V = v/V_\infty, \quad C = c/V_\infty. \quad (2.4)$$

The disturbed potential function ϕ satisfies

$$\left(1 - \frac{U^2}{C^2}\right)\phi_{zz} + \left(1 - \frac{V^2}{C^2}\right)\phi_{rr} - 2\frac{UV}{C}\phi_{rz} + \frac{\phi_r}{r} = 0 \quad (2.5)$$

where

$$U = 1 + \phi_z; \quad V = \phi_r; \quad \text{and } C^2 = \frac{1}{M_\infty^2} + \frac{\gamma - 1}{2} (1 - U^2 - V^2). \quad (2.6)$$

A transformation of the coordinates is subsequently introduced according to

$$\xi = z; \zeta = \frac{B\eta}{1 + B\eta} \quad (2.7)$$

where

$$\eta = r - R_b(z), \quad (2.8)$$

$R_b(z)$ is the local radius of the body, and B is a stretching parameter.

Equation (2.5) becomes

$$\begin{aligned} \left(1 - \frac{U^2}{C^2}\right)\phi_{\xi\xi} - B(1 - \zeta)^2 & \left[2R'_b\left(1 - \frac{U^2}{C^2}\right) + 2\frac{UV}{C^2}\right]\phi_{\zeta\xi} + B^2(1 - \zeta)^4 \\ & \cdot \left[R'_b^2\left(1 - \frac{U^2}{C^2}\right) + \left(1 - \frac{V^2}{C^2}\right) + 2\frac{UV}{C^2}R'_b\right]\phi_{\zeta\zeta} + B(1 - \zeta)^2 \\ & \cdot \left\{ \frac{1}{R_b + \frac{\zeta}{B(1 - \zeta)}} - R''_b\left(1 - \frac{U^2}{C^2}\right) - 2B(1 - \zeta) \right. \\ & \left. \cdot \left[R'_b^2\left(1 - \frac{U^2}{C^2}\right) + \left(1 - \frac{V^2}{C^2}\right) + 2\frac{UV}{C^2}R'_b\right] \right\} \phi_\zeta = 0 \end{aligned} \quad (2.9)$$

with

$$U = 1 + \phi_\xi - R'_b \phi_\zeta B(1 - \zeta)^2 \text{ and } V = \phi_\zeta B(1 - \zeta)^2 \quad (2.10)$$

where R'_b and R''_b are, respectively, the first and second derivatives of $R_b(z)$. The flow field to be considered in the ξ, ζ plane is now $-\infty < \xi < \infty, 0 \leq \zeta \leq 1$.

The boundary condition on the body surface is given by

$$V(\xi, 0) = R'_b(\xi) U(\xi, 0) \quad (2.11)$$

which may be reduced into

$$\phi_\zeta(\xi, \zeta = 0) = \frac{R'_b}{B(1 + R'_b)^2} [1 + \phi_\xi(\xi, \zeta = 0)] \quad (2.12)$$

and

$$\phi = 0 \text{ at } \xi = \pm\infty, \text{ or } \zeta = 1. \quad (2.13)$$

For locations along the ξ -axis where $\zeta = 0$ and $R_b' = 0$, the term ϕ_r/r in Eq. (2.5) is indeterminate. Under this situation, the term ϕ_r/r is replaced by ϕ_{rr} , and terms in Eq. (2.9) are correspondingly modified. Equation (2.9) can now be written as

$$E F \phi_{\zeta\zeta} + H \phi_{\xi\xi} + D \phi_{\xi\xi} + S = 0 \quad (2.14)$$

where

$$\left. \begin{aligned} E &= B^2(1 - \zeta)^4; \\ F &= R_b'^2 \left(1 - \frac{U^2}{C^2}\right) + \left(1 - \frac{V^2}{C^2}\right) + 2 \frac{UV}{C^2} R_b'; \\ H &= -B(1 - \zeta)^2 \left[2R_b' \left(1 - \frac{U^2}{C^2}\right) + 2 \frac{UV}{C^2} \right]; \\ D &= 1 - \frac{U^2}{C^2}; \text{ and} \\ S &= \phi_\zeta B(1 - \zeta)^2 \left[\frac{1}{R_b + \frac{\zeta}{B(1 - \zeta)}} - R_b'' \left(1 - \frac{U^2}{C^2}\right) - 2B(1 - \zeta) F \right]. \end{aligned} \right\} \quad (2.15)$$

Equation (2.14) can be solved by a numerical relaxation scheme. It has been recognized that in solving transonic flow problems by numerical calculations, different finite-difference formulations should be used, depending upon whether the local flow is subsonic or supersonic. For the present problem, variable grid size is used in formulating the finite differences in the ξ -direction while uniform grid size is adopted in the ζ -direction. For the grid point situated at ξ_j and ζ_k , the equivalent finite difference forms of ϕ_ξ , $\phi_{\xi\xi}$, $\phi_{\xi\zeta}$, ϕ_ζ , and $\phi_{\zeta\zeta}$ may be written as

$$\left. \begin{aligned}
 \phi_{\xi} &= \frac{\Delta\xi_1}{\Delta\xi_2(\Delta\xi_1 + \Delta\xi_2)} \phi_{j+1}^k + \frac{\Delta\xi_2 - \Delta\xi_1}{\Delta\xi_1 \cdot \Delta\xi_2} \phi_j^k - \frac{\Delta\xi_2}{\Delta\xi_1(\Delta\xi_1 + \Delta\xi_2)} \phi_{j-1}^k \\
 &= AB1 \phi_{j+1}^k + AB2 \phi_j^k + AB3 \phi_{j-1}^k \\
 \phi_{\xi\xi} &= \frac{2}{\Delta\xi_2(\Delta\xi_1 + \Delta\xi_2)} \phi_{j+1}^k - \frac{2}{\Delta\xi_1 \Delta\xi_2} \phi_j^k + \frac{2}{\Delta\xi_1(\Delta\xi_1 + \Delta\xi_2)} \phi_{j-1}^k \\
 &= BB1 \phi_{j+1}^k + BB2 \phi_j^k + BB3 \phi_{j-1}^k \\
 \phi_{\xi\zeta} &= \frac{1}{2\Delta\xi} \left[AB1 \left(\phi_{j+1}^{k+1} - \phi_{j+1}^{k-1} \right) + AB2 \left(\phi_j^{k+1} - \phi_j^{k-1} \right) + AB3 \left(\phi_{j-1}^{k+1} - \phi_{j-1}^{k-1} \right) \right]
 \end{aligned} \right\} (2.16)$$

for locally subsonic flow,

$$\left. \begin{aligned}
 \phi_{\xi} &= \frac{\Delta\xi_0 + 2\Delta\xi_1}{\Delta\xi_1(\Delta\xi_0 + \Delta\xi_1)} \phi_j^k - \frac{\Delta\xi_1 + \Delta\xi_0}{\Delta\xi_1 \cdot \Delta\xi_0} \phi_{j-1}^k + \frac{\Delta\xi_1}{\Delta\xi_0(\Delta\xi_0 + \Delta\xi_1)} \phi_{j-2}^k \\
 &= AP1 \phi_j^k + AP2 \phi_{j-1}^k + AP3 \phi_{j-2}^k \\
 \phi_{\xi\xi} &= \frac{2}{\Delta\xi_1(\Delta\xi_1 + \Delta\xi_0)} \phi_j^k - \frac{2}{\Delta\xi_0 \Delta\xi_1} \phi_{j-1}^k + \frac{2}{\Delta\xi_0(\Delta\xi_1 + \Delta\xi_0)} \phi_{j-2}^k \\
 &= BP1 \phi_j^k + BP2 \phi_{j-1}^k + BP3 \phi_{j-2}^k \\
 \phi_{\xi\zeta} &= \frac{1}{2\Delta\xi} \left[AP1 \left(\phi_j^{k+1} - \phi_j^{k-1} \right) + AP2 \left(\phi_{j-1}^{k+1} - \phi_{j-1}^{k-1} \right) + AP3 \left(\phi_{j-2}^{k+1} - \phi_{j-2}^{k-1} \right) \right]
 \end{aligned} \right\} (2.17)$$

for locally supersonic flow, and

$$\phi_{\zeta} = \frac{\phi_j^{k+1} - \phi_j^{k-1}}{2\Delta\xi} \text{ and } \phi_{\zeta\zeta} = \frac{\phi_j^{k+1} - 2\phi_j^k + \phi_j^{k-1}}{(\Delta\xi)^2} \quad (2.18)$$

where

$$\Delta\xi_2 = \xi_{j+1} - \xi_j; \quad \Delta\xi_1 = \xi_j - \xi_{j-1}; \quad \Delta\xi_0 = \xi_{j-1} - \xi_{j-2}. \quad (2.19)$$

Equation (2.14) may now be written in finite difference form for the grid point (ξ_j, ζ_k) as

$$\begin{aligned}
& \left(E_F + \frac{H\Delta\zeta}{2} AB2 \right) \phi_j^{k+1} + (-2E_F + \Delta\zeta^2 D BB2) \phi_j^k + \left(E_F - \frac{H\Delta\zeta}{2} AB2 \right) \phi_j^{k-1} \\
& = -\frac{H\Delta\zeta}{2} \left[AB1 \left(\phi_{j+1}^{k+1} - \phi_{j+1}^{k-1} \right) + AB3 \left(\phi_{j-1}^{k+1} - \phi_{j-1}^{k-1} \right) \right] \\
& \quad - \Delta\zeta^2 [D(BB1 \phi_{j+1}^k + BB3 \phi_{j-1}^k) + S]
\end{aligned} \tag{2.20}$$

for subsonic flow, and

$$\begin{aligned}
& \left(E_F + \frac{H\Delta\zeta}{2} AP1 \right) \phi_j^{k+1} + (-2E_F + \Delta\zeta^2 D BP1) \phi_j^k + \left(E_F - \frac{H\Delta\zeta}{2} AP1 \right) \phi_j^{k-1} \\
& = -\frac{H\Delta\zeta}{2} \left[AP2 \left(\phi_{j-1}^{k+1} - \phi_{j-1}^{k-1} \right) + AP3 \left(\phi_{j-2}^{k+1} - \phi_{j-2}^{k-1} \right) \right] \\
& \quad - \Delta\zeta^2 \left[D(BP2 \phi_{j-1}^k + BP3 \phi_{j-2}^k) + S \right]
\end{aligned} \tag{2.21}$$

for supersonic flow. The boundary condition, Eq. (2.12), is specified for all points on the ξ -axis ($\zeta = 0$) by introducing a row of grid points at $\zeta = -\Delta\zeta$ whose value of ϕ (identified as ϕ_j^b) are given by

$$\phi_j^b = \phi_j^{k=2} - 2\Delta\zeta \phi_\zeta(\xi_j, \zeta = 0) \tag{2.22}$$

where $\phi_\zeta(\xi_j, \zeta = 0)$ is computed from Eq. (2.12) with ϕ_ζ again evaluated, depending whether the flow there is supersonic or subsonic.

For the present study, it is also assumed that the boundary conditions at $\xi = \pm\infty$ are actually satisfied at $\xi = -2.0$ and $\xi = 3.0$, respectively. Therefore, the disturbed potential should vanish at $\xi = -2.0$ and $\xi = 3.0$ and also at $\xi = 1$ ($\eta \rightarrow \infty$).

Equations (2.20) or (2.21) may be written for all grid points in the same column and the coefficient matrix for the system of equation of ϕ is tridiagonal. The line relaxation process can be employed for the numerical calculations. An efficient and straightforward method of direct solution of tridiagonal systems has been used to find the ϕ values and the value of

the grid point to account for the boundary condition is updated immediately after the calculations for this column are completed. Calculations are carried out by repeatedly sweeping from upstream toward downstream flow field. The final flow pattern is established when the successive change of ϕ values is less than an arbitrarily small value (e.g., $\epsilon = 3.0 \times 10^{-6}$) for all grid points throughout the field.

The physical and computational planes for the study of the present problem are shown in Fig. 3. Refinement of grid spacings has been applied once for these calculations. This refinement is achieved by dividing each horizontal grid segment into two equal segments and the number of grid points in each row changes from 26 to 51 finally. This scheme of grid point arrangement was used to produce all results of the present study. The stretching parameter B was set to 8 for all results obtained from this series of calculations. It is understood from experience that different values of B would not change the results significantly. Also, for the case of $R_s/R_o = 0.5$, below a free stream Mach number 0.9, over relaxation was used to reduce the computational time without encountering any difficulty in the convergence of the inviscid calculations toward the final solutions. However, for the free stream Mach number of 0.9 or higher, under relaxation is definitely required. On the other hand, for $R_s/R_o = 0$, under relaxation is not needed until free stream Mach number reaches the value of 0.97. A typical set of results of inviscid calculations is shown in Fig. 4 where the pressure coefficients on the equivalent body surface are presented.

3. VISCOUS FLOW ANALYSIS

For a uniform flow approaching the base, it is expected that a turbulent boundary layer grows along the upper wall ahead of the step resulting in a finite viscous layer before the flow separates at the corner. Although the growth of this boundary layer would affect the corresponding inviscid flow field and this effect can be accounted for through the corrections of the displacement effect on the corresponding inviscid body configuration, this influence is disregarded in the present study since it is usually overshadowed by the viscous effects within the separated flow region. However, the presence of a finite viscous layer has influence on the subsequent viscous flow processes of jet mixing, re-compression, reattachment, and flow redevelopment, and this effect must be taken into consideration. The continuous growth of the boundary layer starting from the leading edge on the upper wall can be calculated by any of the more sophisticated methods [59]. It is believed, however, that an integral method of calculation of turbulent boundary layer [60] would be equally adequate for the present problem by employing the inviscid state of flow along the bounding streamline as the guiding stream of the viscous layer. It is thus expected that prior to its separation at the step, an attached boundary layer of the finite thickness is present and compatible to the characteristic Reynolds number of the approaching flow. For convenience, a $1/7$ power law velocity profile is assumed for this viscous layer.

As mentioned in Chapter 1, mixing process occurs along the wake boundary after the flow separates from the corner; the shear layer grows and the dividing streamline is energized. Subsequently, the flow will undergo a recompression process until the dividing streamline stagnates

on the lower wall (sting). A wall boundary layer redevelops afterward and eventually the pressure decreases toward the free stream value asymptotically. In order to study this problem, the individual flow components must be analyzed so that the effect of each component toward the establishment of the overall flow field can be identified and ascertained.

3.1 QUASI-CONSTANT PRESSURE JET MIXING PROCESS

It is known that for a supersonic flow passing over a backward facing step, a free turbulent jet mixing process occurs under an essentially constant pressure condition after the flow separates from the wall. For the present problem, since the pressure field of the mixing process is determined from the freestream flow condition from the boundary layer concept, it is obvious that the guiding inviscid flow would not have the same velocity and the mixing process would not be under a truly constant pressure condition. Furthermore, the existence of an initial boundary layer would upset the similarity requirement even under a constant pressure flow condition. It is thus expected that the existing turbulent jet mixing is a non-similar problem. An analysis by Brink and Chow [61] on the non-similar jet mixing process with pressure gradient but without initial boundary layer has shown that a locally similar mixing process can adequately describe this non-similar mixing flow. For the present problem, it is assumed that the jet mixing flow can be described by a quasi-constant pressure jet mixing process; namely, that at each section along the path of the jet mixing region, the velocity profile can be derived from a constant pressure mixing analysis starting from the same origin with the same initial profile (e.g., the same power law profile). A constant pressure, isoenergetic turbulent jet mixing process is

shown schematically in Fig. 5 where a system of coordinates X, Y is chosen to coincide with the equivalent body profile. The initial velocity profile is given by

$$\begin{aligned}\phi_1 &= \zeta_1^{1/7} \text{ for } \zeta_1 < 1 \\ \phi_1 &= 1 \quad \text{for } \zeta_1 \geq 1\end{aligned}\tag{3.1}$$

where $\zeta_1 = y/\delta_1$, $\phi = u/u_e$, and δ_1 is the thickness of initial boundary layer. Since the turbulence level within the wall viscous layer is generally much less than that within the free turbulent mixing flow, it is anticipated that the major mixing activities occur along the dividing streamline and the condition within the upper part of the initial viscous layer is essentially unchanged until the mixing effects reach there. This upper edge of the mixing region is identified by ζ_m ($\zeta_m = y_m/\delta_1$). Therefore, the analysis of mixing can be divided into two parts. One covers the region where the mixing effect has not reached the upper edge of the initial viscous layer ($\zeta_m < 1$) and another deals with the region further downstream where the mixing effect has spread throughout the initial viscous layer ($\zeta_m > 1$). A linear velocity profile is assumed for these mixing regions. From the continuity and momentum principle, one obtains for such a mixing region

$$\int_0^{y_m} \rho u r dy = \int_{y_d}^{y_m} \rho u r dy\tag{3.2}$$

and

$$\int_0^{y_m} \rho u^2 r dy = \int_{y_d - \delta_b}^{y_m} \rho u^2 r dy\tag{3.3}$$

where $r = R_b + y \cos \theta_b$.

For isoenergetic flow, the density can be related with velocity through

$$\frac{\rho}{\rho_e} = \frac{1 - C_e^2}{1 - C_e^2 \phi^2}. \quad (3.4)$$

Equations (3.2) and (3.3) can be written as

$$R_o \int_0^{\zeta_m} \frac{1 - C_e^2}{1 - C_e^2 \phi^2} \phi \, d\zeta_1 + \delta_1 \int_0^{\zeta_m} \frac{1 - C_e^2}{1 - C_e^2 \phi^2} \phi \, \zeta_1 \, d\zeta_1 = \\ R_b \int_{\zeta_d}^{\zeta_m} \frac{1 - C_e^2}{1 - C_e^2 \phi^2} \phi \, d\zeta_1 + \delta_1 \cos \theta_b \int_{\zeta_d}^{\zeta_m} \frac{1 - C_e^2}{1 - C_e^2 \phi^2} \phi \, \zeta_1 \, d\zeta_1 \quad (3.5)$$

and

$$R_o \int_0^{\zeta_m} \frac{1 - C_e^2}{1 - C_e^2 \phi^2} \phi^2 \, d\zeta_1 + \delta_1 \int_0^{\zeta_m} \frac{1 - C_e^2}{1 - C_e^2 \phi^2} \phi^2 \, \zeta_1 \, d\zeta_1 = \\ R_b \int_{(y_d - \delta_b)/\delta_1}^{\zeta_m} \frac{1 - C_e^2}{1 - C_e^2 \phi^2} \phi^2 \, d\zeta_1 + \delta_1 \cos \theta_b \int_{(y_d - \delta_b)/\delta_1}^{\zeta_m} \\ \cdot \frac{1 - C_e^2}{1 - C_e^2 \phi^2} \phi^2 \, \zeta_1 \, d\zeta_1. \quad (3.6)$$

For a linear velocity profile, the following relations can be obtained after some mathematical manipulations:

$$\left(\frac{\delta_a + \delta_b}{\delta_1} \right)^2 \frac{\cos \theta_b}{C_m} \left[\frac{1}{2} \ln \frac{(1 + C_m)(1 - C_d)}{(1 - C_m)(1 + C_d)} + C_d - C_m \right] + \left(\frac{\delta_a + \delta_b}{\delta_1} \right) \\ \cdot \frac{R_o}{\delta_1} \frac{1}{2} \ln \frac{1 - C_d^2}{1 - C_m^2} - \frac{C_e C_m}{1 - C_e^2} \left[\frac{R_o}{\delta_1} I_1(\zeta_m) + I_2(\zeta_m) \right] = 0 \quad (3.7)$$

$$\frac{\delta_b}{\delta_a} = \frac{\phi_d}{\phi_m - \phi_d}, \quad (3.8)$$

and

$$\left(\frac{\delta_a + \delta_b}{\delta_1} \right)^2 \frac{\cos \theta_b}{2c_m^2} \left[\ln \frac{1}{1 - c_m^2} - c_m^2 \right] + \left(\frac{\delta_a + \delta_b}{\delta_1} \right) \cdot \frac{R_\ell}{\delta_1} \\ \cdot \left[\frac{1}{2c_m} \ln \frac{1 + c_m}{1 - c_m} - 1 \right] - \frac{c_e^2}{1 - c_e^2} \left[\frac{R_o}{\delta_1} I_3(\zeta_m) + I_4(\zeta_m) \right] = 0 \quad (3.9)$$

where $R_\ell = R_b + (y_d - \delta_b) \cos \theta_b$,

$$\phi_m = \frac{u_m}{u_e} = \zeta_m^{1/7},$$

$$I_1(\zeta_m) = \int_0^{\zeta_m} \frac{1 - c_e^2}{1 - c_e^2 \phi_1^2} \phi_1 \, d\zeta_1,$$

$$I_2(\zeta_m) = \int_0^{\zeta_m} \frac{1 - c_e^2}{1 - c_e^2 \phi_1^2} \phi_1 \zeta_1 \, d\zeta_1,$$

$$I_3(\zeta_m) = \int_0^{\zeta_m} \frac{1 - c_e^2}{1 - c_e^2 \phi_1^2} \phi_1^2 \, d\zeta_1, \text{ and}$$

$$I_4(\zeta_m) = \int_0^{\zeta_m} \frac{1 - c_e^2}{1 - c_e^2 \phi_1^2} \phi_1^2 \zeta_1 \, d\zeta_1$$

for $\zeta_m \leq 1$, and

$$\left(\frac{\delta_a + \delta_b}{\delta_1} \right)^2 \frac{\cos \theta_b}{c_e} \left[\frac{1}{2} \ln \frac{(1 + c_e)(1 - c_d)}{(1 - c_e)(1 + c_d)} - c_e + c_d \right] + \left(\frac{\delta_a + \delta_b}{\delta_1} \right) \\ \cdot \frac{R_\ell}{\delta_1} \frac{1}{2} \ln \frac{1 - c_d^2}{1 - c_e^2} - \frac{c_e^2}{1 - c_e^2} \left[\frac{R_o}{\delta_1} I_1 - I_1(1) + I_2(1) + \frac{R_o}{\delta_1} (\zeta_m - 1) \right. \\ \left. + \frac{1}{2} (\zeta_m^2 - 1) \right] = 0 \quad (3.10)$$

$$\frac{\delta_b}{\delta_a} = \frac{\phi_d}{1 - \phi_d}, \quad (3.11)$$

and

$$\begin{aligned} & \left(\frac{\delta_a + \delta_b}{\delta_1} \right)^2 \cos \theta_b \frac{1}{2C_e^2} \left[\ln \frac{1}{1 - C_e^2} - C_e^2 \right] + \left(\frac{\delta_a + \delta_b}{\delta_1} \right) \frac{R_\ell}{\delta_1} \\ & \cdot \left[\frac{1}{2C_e} \ln \frac{1 + C_e}{1 - C_e} - 1 \right] - \frac{C_e^2}{1 - C_e^2} \left[\frac{R_o}{\delta_1} I_3^{(1)} + I_4^{(1)} \right. \\ & \left. + \frac{R_o}{\delta_1} (\zeta_m - 1) + \frac{1}{2} (\zeta_m^2 - 1) \right] = 0 \end{aligned} \quad (3.12)$$

for $\zeta_m > 1$. The set of equations (i.e., Eqs. (3.7), (3.8), and (3.9) or Eqs. (3.10), (3.11), and (3.12)) can be solved simultaneously to give ϕ_d , δ_a , δ_b for $\zeta_m \leq 1$ and $\zeta_m \geq 1$, respectively, once ζ_m is known. It is necessary to relate the physical location for the specific value of ζ_m and the corresponding velocity profile. If one assumes that the slope of the linear profile matches the maximum slope of a fully developed error function profile [62], i.e.,

$$\left. \frac{\partial \phi}{\partial \eta} \right|_{\eta=0} \approx \frac{1}{\sqrt{\pi}} \quad (3.13)$$

with $\eta = \sigma(y/x)$ where σ is spread parameter of similar jet mixing flows, one obtains the corresponding location along the mixing region given by

$$\frac{x}{\delta_1} = \frac{\sigma}{\sqrt{\pi}} \frac{1}{\phi_m} \frac{\delta_a + \delta_b}{\delta_1} \quad (3.14)$$

for $\zeta_m \leq 1$, and

$$\frac{x}{\delta_1} = \frac{\sigma}{\sqrt{\pi}} \frac{\delta_a + \delta_b}{\delta_1} \quad (3.15)$$

for $\zeta_m > 1$.

Since the guiding inviscid flow condition is initially unknown, the correct location for a specific ζ_m value and the corresponding velocity profile must be found by iterative process. It can also be shown that the shear stress along the dividing streamline is given by

$$\frac{\tau_d}{\rho_e u_e^2} = \frac{1}{R_d} \frac{d}{dx} \int_{y_d - \delta_b}^{y_d} \frac{\rho}{\rho_e} \left(\frac{u}{u_e} \right)^2 r dy. \quad (3.16)$$

One readily obtains from Eq. (3.16)

$$\begin{aligned} \frac{\tau_d}{\rho_e u_e^2} &= \frac{1}{R_d} \frac{1 - C_e^2}{C_e^2} \frac{d}{dx} \delta_b \left[R_l \left(\frac{1}{2C_d} \ln \frac{1 + C_d}{1 - C_d} - 1 \right) \right. \\ &\quad \left. - \frac{\delta_b \cos \theta_b}{2} \left(\frac{1}{C_d^2} \ln (1 - C_d^2) + 1 \right) \right]. \end{aligned} \quad (3.17)$$

The displacement y_d relative to the equivalent body boundary and the transverse velocity component of the dividing streamline are also given by

$$\frac{y_d}{\delta_1} = \zeta_m - \frac{\delta_a}{\delta_1} \text{ and } \frac{dy_d}{dx} = \frac{v_d}{u_d}. \quad (3.18)$$

The eddy diffusivity relating the shear stress and the velocity gradient is evaluated according to

$$\frac{\varepsilon}{u_e \delta_a} = \frac{\tau_d}{\rho u_e^2} \frac{1 - C_d^2}{1 - C_e^2} \frac{\delta_b}{\phi_d \delta_a}. \quad (3.19)$$

The value of σ is 12 for present analysis. Calculations with other σ values ($\sigma = 10, 11, 13, 14$) have also been carried out for comparison purposes.

3.2 RECOMPRESSION AND REATTACHMENT

Near the end of the wake, the flow realigns itself to the original flow direction, thereby initiating a recompression process. The pressure is impressed by the freestream condition of the already established corresponding inviscid flow field and the flow within the viscous region copes with this continuously increasing in pressure mainly at the expense of its kinetic energy. The portion of the flow which does not possess enough kinetic energy is forced to turn back to form a recirculatory wake flow and the rest of the flow will proceed downstream.

For a system of curvilinear coordinates, x, y within the meridian plane, the conservational principles written in time averaged quantities for the dissipative flow region can be expressed (also see Fig. 6) as [43]

$$\frac{\partial(\rho u r)}{\partial x} + \frac{\partial}{\partial y} \left[\rho v r \left(1 - \frac{y}{R} \right) \right] = 0 \quad (3.20)$$

which is the equation of continuity, and

$$\begin{aligned} \frac{\partial(\rho u^2 r)}{\partial x} + \frac{\partial}{\partial y} \left[\rho u v r \left(1 - \frac{y}{R} \right) \right] - \frac{\rho u v r}{R} &= -r \frac{\partial P}{\partial x} + \frac{\partial}{\partial y} \\ \cdot \left[r \tau_{yx} \left(1 - \frac{y}{R} \right) \right] - \frac{\tau_{xy} r}{R} \end{aligned} \quad (3.21)$$

which is the x -momentum equation where $r = r_c(x) + y \cos \theta_c(x)$ and $dr_c/dx = \sin \theta_c(x)$, r_c being the radius of the base of the coordinate system and R is the radius of curvature of the curvilinear x -axis. It is understood that the effect of the normal viscous stress has been disregarded. In the present study, the x -axis is selected to assume a straight line trajectory which is aligned with the freestream flow direction but located at the dividing streamline at the end of the mixing

region. The governing equations for this recompression process can be greatly simplified by letting $R \rightarrow \infty$. Under this situation, Eqs. (3.20) and (3.21) become

$$\frac{\partial(\rho u r)}{\partial x} + \frac{\partial(\rho v r)}{\partial y} = 0 \quad (3.22)$$

and

$$\frac{\partial(\rho u^2 r)}{\partial x} + \frac{\partial(\rho u v r)}{\partial y} = -r \frac{\partial p}{\partial x} + \frac{\partial}{\partial y} (r \tau_{yx}) \quad (3.23)$$

with $r = r_c + y \cos \theta_c$, and $dr_c/dx = -\sin \theta_c$, where θ_c is now a positive valued constant angle.

With the initial conditions provided by the quasi-constant pressure jet mixing analysis, the recompression region can be studied within the framework of the boundary layer concept. As aforementioned, the shear layer is divided into two regions along the dividing streamline, namely, the upper viscous layer and the lower viscous layer, including the backflow. Referring to Fig. 6 where the thickness of shear layers are also shown, integration of continuity equation (Eq. (3.22)) across the upper viscous layer would yield

$$\tan \beta_e = \frac{v_e}{u_e} = \frac{dy_a}{dx} - \frac{1}{R_d + \delta_a \cos \theta_c} \frac{1}{\rho_e u_e} \frac{d}{dx} \rho_e u_e \int_{y_d}^{y_a} \frac{\rho}{\rho_e} \frac{u}{u_e} r dy \quad (3.24)$$

where β_e is the streamline angle at the edge of the viscous layer with respect to the x-axis. For the lower layer, similar consideration would lead to

$$\rho_d u_d \int_{y_d - \delta_b}^{y_d} \frac{\rho}{\rho_d} \frac{u}{u_d} r dy = \rho_b u_b \int_{R_s}^{R_s + h_b} \frac{\rho}{\rho_b} \frac{u}{u_b} y_w dy_w. \quad (3.25)$$

Also, integration of the momentum relationship (Eq. (3.23)) would yield

$$\begin{aligned}
 R_d \tau_d = & \frac{d}{dx} \rho_e u_e^2 \int_{y_d}^{y_a} \frac{\rho}{\rho_e} \frac{u}{u_e} r \left(1 - \frac{u}{u_e} \right) dy - \rho_e u_e \int_{y_d}^{y_a} \frac{\rho}{\rho_e} \frac{u}{u_e} r dy \\
 & \cdot \frac{du_e}{dx} - (R_d - y_d \cos \theta_c) \frac{d}{dx} P_e \int_{y_d}^{y_a} \frac{P}{P_e} dy - \cos \theta_c \frac{d}{dx} P_e \\
 & \cdot \int_{y_d}^{y_a} \frac{P}{P_e} y dy + P_e (R_d + \delta_a \cos \theta_c) \frac{dy_a}{dx} - P_d R_d \frac{dy_d}{dx} \quad (3.26)
 \end{aligned}$$

for the viscous layer above the dividing streamline and

$$\begin{aligned}
 R_d \tau_d = & \frac{d}{dx} \rho_d u_d^2 \int_{y_d - \delta_b}^{y_d} \frac{\rho}{\rho_d} \frac{u^2}{u_d^2} r dy + \delta_b \left(R_d - \frac{\delta_b}{2} \cos \theta_c \right) \frac{dP_d}{dx} \\
 & + \cos \theta_c \left[\frac{d}{dx} \rho_b u_b^2 \int_{R_s}^{R_s + h_b} \frac{\rho}{\rho_b} \frac{u^2}{u_b^2} y_w dy_w + \frac{h_b}{2} (2R_s + h_b) \frac{dP_w}{dx} \right] \\
 & \quad (3.27)
 \end{aligned}$$

for the viscous layer below the dividing streamline where the wall shear stress associated with the backflow wall boundary layer has been neglected.

In the present analysis, it has been assumed from the boundary layer concept that $P_e = P_d = P_w$. It is also assumed that the velocity profile follows a polynomial of the form given by

$$\begin{aligned}
 \phi = \frac{u}{u_e} = & \phi_d + s \zeta_a + [3(1 - \phi_d) - 2s] \zeta_a^2 + [s - 2(1 - \phi_d)] \\
 & \cdot \zeta_a^3 \quad (0 \leq \zeta_a \leq 1) \quad (3.28)
 \end{aligned}$$

for the viscous layer above the dividing streamline where

$$\phi_d = \frac{u_d}{u_e}, \quad s = \left. \frac{\partial \phi}{\partial \zeta_a} \right|_d, \quad \zeta_a = \frac{y - y_d}{\delta_a};$$

a linear velocity profile given by

$$\phi = \frac{u}{u_e} = \phi_d \zeta_\ell \quad (0 \leq \zeta_\ell \leq 1) \quad (3.29)$$

for the forward flow of the viscous layer below the dividing streamline

where

$$\zeta_\ell = \frac{y - y_d + \delta_b}{\delta_b}$$

and

$$\phi = \frac{u}{u_e} = -\phi_b \cos \frac{\pi}{2} \zeta_b \quad (0 \leq \zeta_b \leq 1) \quad (3.30)$$

for the reverse flow where $\phi_b = u_b/u_e$, and $\zeta_b = (y_w - R_s)/h_b$.

It is further assumed that the slope parameter s can be coupled [40, 45, 46, 48, 57] with ϕ_d through

$$s = g \phi_d \quad (3.31)$$

where g is a constant to be evaluated from the condition at the end section of the mixing region by

$$g = \frac{s_m}{\phi_{dm}} \quad (3.32)$$

where the subscript m refers to the end section of mixing region. Such a coupling would assure that both s and ϕ_d would vanish together at the point of reattachment.

It is understood that due to the existence of the lower wall, an additional wall boundary layer exists within the reverse flow and the profile would not have the shape given by Eq. (3.30). However, if one assumes that a cosine profile also describes the reverse wall boundary layer flow, the profile as given by Eq. (3.30) would yield the same mass

and momentum flux as the actual reverse flow with boundary layer as long as h_b and ϕ_b are the same. The remaining difference is the small wall shear stress which is usually neglected.

For isoenergetic flows, the density ratios can be found through the velocity ratios given by

$$\frac{\rho}{\rho_d} = \frac{1 - C_d^2}{1 - C_d^2 \left(\frac{\phi}{\phi_d} \right)^2} \text{ and } \frac{\rho}{\rho_b} = \frac{1 - C_b^2}{1 - C_b^2 \left(\frac{\phi}{\phi_b} \right)^2} \quad (3.33)$$

where $\phi_d = u_d/u_e = C_d/C_e$, and $\phi_b = u_b/u_e = C_b/C_e$.

Upon substituting Eq. (3.33) and after some mathematical manipulations, Eqs. (3.24) through (3.27) can be written as

$$\begin{aligned} & [(R_d + \delta_a \cos \theta_c) - (1 - C_e^2)(R_d F1 + 2\delta_a \cos \theta_c F2)] \frac{dy_a}{dx} \\ & + (1 - C_e^2)[(R_d F1 + 2\delta_a \cos \theta_c F2) - \delta_a \cos \theta_c F1] \frac{dy_d}{dx} \\ & - (1 - C_e^2) \delta_a (R_d F3 + \delta_a \cos \theta_c F4) \frac{d\phi}{dx} \\ & - \delta_a \left[\left(\frac{1}{C_e} - \frac{3\gamma - 1}{\gamma - 1} C_e \right) (R_d F1 + \delta_a \cos \theta_c F2) \right. \\ & \left. + 2C_e (1 - C_e^2) (R_d F5 + \delta_a \cos \theta_c F6) \right] \frac{dC_e}{dx} = \tan \beta_e (R_d + \delta_a \cos \theta_c) \\ & - \delta_a \sin \theta_c (1 - C_e^2) F1 \end{aligned} \quad (3.34)$$

$$\begin{aligned}
& C_d \delta_b \cos \theta_c F13 \frac{dy_d}{dx} + \delta_b C_e \{ (R_d - \delta_b \cos \theta_c) F13 + \delta_b \cos \theta_c F14 \\
& + 2C_d^2 [(R_d - \delta_b \cos \theta_c) F17 + \delta_b \cos \theta_c F18] \} \frac{d\phi_d}{dx} \\
& + C_d [(R_d - 2\delta_b \cos \theta_c) F13 + 2\delta_b \cos \theta_c F14] \frac{d\delta_b}{dx} \\
& - C_b (2h_b F16 + R_s F15) \frac{dh_b}{dx} - h_b C_e [h_b F16 + R_s F15 + 2C_b^2 \\
& \cdot (h_b F20 + R_s F19)] \frac{d\phi_b}{dx} - \left\{ h_b \phi_b [h_b F16 + R_s F15 + 2C_b^2 \right. \\
& \left. \cdot (h_b F20 + R_s F19)] - \delta_b \phi_d \{ (R_d - \delta_b \cos \theta_c) F13 \right. \\
& \left. + \delta_b \cos \theta_c F14 + 2C_d^2 [(R_d - \delta_b \cos \theta_c) F17 + \delta_b \cos \theta_c F18] \} \right\} \\
& \cdot \frac{dC_e}{dx} = C_d \delta_b \sin \theta_c F13. \tag{3.35}
\end{aligned}$$

$$\begin{aligned}
& (R_d F7 + 2\delta_a \cos \theta_c F8) \frac{dy_a}{dx} + [\delta_a \cos \theta_c F7 - (R_d F7 + 2\delta_a \cos \theta_c F8)] \\
& \cdot \frac{dy_d}{dx} + \delta_a (R_d F9 + \delta_a \cos \theta_c F10) \frac{d\phi_d}{dx} + \frac{\delta_a}{C_e} \\
& \cdot \left[\frac{2}{1 - C_e^2} \left(1 - \frac{2\gamma - 1}{\gamma - 1} C_e^2 \right) (R_d F7 + \delta_a \cos \theta_c F8) \right. \\
& - (R_d F1 + \delta_a \cos \theta_c F2) + 2C_e^2 (R_d F11 + \delta_a \cos \theta_c F12) \\
& \left. + \frac{1}{1 - C_e^2} \left(R_d + \frac{1}{2} \delta_a \cos \theta_c \right) \right] \frac{dC_e}{dx} = \frac{R_d \tau_d}{\rho_e u_e^2} \frac{1}{1 - C_e^2} + \delta_a \sin \theta_c F7 \tag{3.36}
\end{aligned}$$

$$\begin{aligned}
& \delta_b \frac{P_e}{P_{\infty}} C_d^2 \cos \theta_c F21 \frac{dy_d}{dx} + 2\delta_b \frac{P_e}{P_{\infty}} C_e C_d \{(R_d - \delta_b \cos \theta_c) F21 \\
& + \delta_b \cos \theta_c F22 + C_d^2 [(R_d - \delta_b \cos \theta_c) F25 + \delta_b \cos \theta_c F26]\} \\
& \cdot \frac{d\phi_d}{dx} + \frac{P_e}{P_{\infty}} C_d^2 [(R_d - 2\delta_b \cos \theta_c) F21 + \delta_b \cos \theta_c F22] \frac{d\delta_b}{dx} \\
& + \frac{P_e}{P_{\infty}} C_b^2 [R_s F23 + 2h_b F24] \cos \theta_c \frac{dh_b}{dx} + \frac{P_e}{P_{\infty}} 2h_b C_b C_e \cos \theta_c \\
& \cdot [R_s F23 + h_b F24 + C_b^2 (R_s F27 + h_b F28)] \frac{d\phi_b}{dx} \\
& + \left\{ 2 \frac{P_e}{P_{\infty}} \left[\delta_b C_d \phi_d \{(R_d - \delta_b \cos \theta_c) F21 + \delta_b \cos \theta_c F22 + C_d^2 \right. \right. \\
& \cdot [(R_d - \delta_b \cos \theta_c) F25 + \delta_b \cos \theta_c F26]\} + \cos \theta_c h_b C_b \phi_b \\
& \cdot \{R_s F23 + h_b F24 + C_b^2 (R_s F27 + h_b F28)\} \left. \right] - \frac{2\gamma}{\gamma - 1} \\
& \cdot \left[\frac{\gamma - 1}{2\gamma} \{R_d \delta_b - \frac{\delta_b^2}{2} \cos \theta_c + \frac{h_b}{2} (2R_s + h_b) \cos \theta_c \} \right. \\
& + \delta_b C_d^2 [(R_d - \delta_b \cos \theta_c) F21 + \delta_b \cos \theta_c F22] \\
& + h_b C_b^2 \cos \theta_c (R_s F23 + h_b F24) \left. \right] C_e (1 - C_e^2)^{1/\gamma-1} \Big\} \\
& \cdot \frac{dC_e}{dx} = \frac{R_d \tau_d}{\rho_e u_e^2} (1 - C_e^2)^{1/\gamma-1} C_e^2 + \delta_b \sin \theta_c \frac{P_e}{P_{\infty}} C_d^2 F21 \quad (3.37)
\end{aligned}$$

where F1 through F28 stand for integrals associated with the viscous layer (the detailed list of these integrals is given in the APPENDIX) which can only be evaluated by the numerical integration method.

In addition, it is assumed that the geometry of the wake has a locally triangular shape which can be expressed by

$$\frac{dh_b}{dx} = \frac{h_b}{\delta_b} \frac{d\delta_b}{dx} . \quad (3.38)$$

Such an assumption would assure that the wake centerline and dividing streamline shall pass through the point of reattachment together on the lower wall at the end of the wake (see Fig. 7). Also, the geometrical relationship $dr_c/dx = -\sin \theta_c$ can be written as

$$-\cos \theta_c \frac{dy_d}{dx} + \cos \theta_c \frac{d\delta_b}{dx} + \frac{dh_b}{dx} = -\sin \theta_c . \quad (3.39)$$

Equations (3.35), (3.37), (3.38), and (3.39) can be combined to give

$$\begin{aligned} & \left[\delta_b \frac{P_e}{P_{\infty}} C_d^2 \cos \theta_c F21 + \frac{CF5 CF11}{CF7} + \frac{\delta_b \cos \theta_c}{h_b + \delta_b \cos \theta_c} CF14 \right] \frac{dy_d}{dx} \\ & + \left[2\delta_b \frac{P_e}{P_{\infty}} C_e C_d CF3 + \frac{CF6 CF11}{CF7} \right] \frac{d\phi_d}{dx} \\ & + \left[2 \frac{P_e}{P_{\infty}} (\delta_b C_d \phi_d CF3 + h_b \cos \theta_c C_b \phi_b CF4) - \frac{2\gamma}{\gamma - 1} \right. \\ & \cdot \left. \left(\frac{\gamma - 1}{2\gamma} CF12 + CF13 \right) C_e (1 - C_e^2)^{1/\gamma-1} - \frac{CF8 CF11}{CF7} \right] \frac{dC_e}{dx} = \\ & \frac{R_d \tau_d}{\rho_e u_e^2} (1 - C_e^2)^{1/\gamma-1} C_e^2 + \delta_b \sin \theta_c \frac{P_e}{P_{\infty}} C_d^2 F21 \\ & + \frac{CF9 CF11}{CF7} + \frac{\delta_b \sin \theta_c}{h_b + \delta_b \cos \theta_c} CF14 \end{aligned} \quad (3.40)$$

where $CF1 = (R_d - \delta_b \cos \theta_c) F13 + \delta_b \cos \theta_c F14 + 2C_d^2$
 $\cdot [(R_d - \delta_b \cos \theta_c) F17 + \delta_b \cos \theta_c F18]$

$$CF2 = R_s F15 + h_b F16 + 2C_b^2 (R_s F19 + h_b F20)$$

$$CF3 = (R_d - \delta_b \cos \theta_c) F21 + \delta_b \cos \theta_c F22 + C_d^2$$

 $\cdot [(R_d - \delta_b \cos \theta_c) F25 + \delta_b \cos \theta_c F26]$

$$\begin{aligned}
CF4 &= R_s F23 + h_b F24 + C_b^2 (R_s F27 + h_b F28) \\
CF5 &= C_d \delta_b \cos \theta_c F13 \\
CF6 &= C_e \delta_b CF1 \\
CF7 &= h_b C_e CF2 \\
CF8 &= h_b \phi_b CF2 - \delta_b \phi_d CF1 \\
CF9 &= C_d \delta_b \sin \theta_c F13 \\
CF10 &= C_d [(R_d - 2\delta_b \cos \theta_c) F13 + 2\delta_b \cos \theta_c F14] \\
&\quad - C_b (h_b/\delta_b) (R_s F15 + 2h_b F16) \\
CF11 &= 2h_b \cos \theta_c (P_e/P_{\infty}) C_b C_e CF4 \\
CF12 &= R_d \delta_b - (\delta_b^2/2) \cos \theta_c + (h_b/2) \cos \theta_c (2R_s + h_b) \\
CF13 &= \delta_b C_d^2 [(R_d - \delta_b \cos \theta_c) F21 + \delta_b \cos \theta_c F22] \\
&\quad + h_b \cos \theta_c C_b^2 (R_s F23 + h_b F24) \\
CF14 &= (P_e/P_{\infty}) \{ C_d^2 [(R_d - 2\delta_b \cos \theta_c) F21 + 2\delta_b \cos \theta_c F22] \\
&\quad + (h_b/\delta_b) \cos \theta_c C_b^2 (R_s F23 + 2h_b F24) \} + (CF10 CF11/CF7)
\end{aligned}$$

Equations (3.34), (3.35), (3.36), (3.38), (3.39), and (3.40) form a system of first order simultaneous differential equations.

The shear stress along the dividing streamline which appears in Eqs. (3.36) and (3.40) will be evaluated from an eddy diffusivity formulation, i.e.,

$$\frac{\tau_d}{\rho_e u_e^2} = \left. \frac{\varepsilon(x)}{u_e \delta_a} \frac{\rho}{\rho_e} \frac{\partial \phi}{\partial \zeta_a} \right|_d \quad (3.41)$$

where $\varepsilon(x)$ is the average eddy viscosity over the thickness of the upper viscous layer within the recompression region. The information of eddy viscosity along the dividing streamline within the recompression region is scarcely available even when the flow is incompressible. For the present study, the eddy viscosity has been evaluated by [46].

$$\frac{\varepsilon}{\varepsilon_m} = \frac{u_e}{u_{em}} \left(\frac{\delta_a}{\delta_{am}} \right)^2 \left(\frac{\ell_m + x_r}{\ell_m} \right)$$

where ℓ_m refers to the length of the mixing region, and x_r measures the length along the recompression flow process.

It should be noted that the guiding inviscid flow condition at the edge of the viscous layer is furnished from the already established corresponding inviscid flow field depending upon the location of the edge of the viscous layer, and the value of the freestream Crocco number is thus a function of $(R_d + \delta_a \cos \theta_c)$ which describes the spread of the viscous layer. It is found from numerical calculations that the term dC_e/dx in the system of equations varies slowly throughout this region. Consequently, this term can be left at right-hand side of these equations as a known quantity which can be evaluated from the previous steps of integration. In this way, iteration can be completely avoided (except at the initial step of recompression) and the numerical calculations can be considerably simplified.

The foregoing system of differential equations (Eq. (3.34), (3.35), (3.36), (3.38), (3.39), and (3.40)) describe the variation of δ_a , y_d , ϕ_d , ϕ_b , δ_b , and h_b throughout this recompression flow process. These values can be established through numerical integration with the initial condition provided by the preceding jet mixing process.

3.3 REDEVELOPMENT OF FLOW

After the flow reattachment, the viscous layer further undergoes a process of redevelopment while the pressure rises continuously until a plateau is reached. Thereafter, the pressure is reduced toward that of

the original approaching flow level asymptotically until the fully rehabilitated state is reached at far downstream positions. In the study of the corresponding flow problems within the supersonic flow regime [42,43], the flow redevelopment was interpreted as a process of relaxation of the pressure difference across the viscous layer. It has been found that the concept of relaxation of pressure difference can indeed be adopted to predict the base pressure and to describe many special features associated with axisymmetric flows (e.g., effect of sting, overshoot in static pressure on the sting). It has been also shown that upon adopting such an interpretation, the fully rehabilitated state is a saddle-point singularity of the system of equations which provides the closure condition for the Chapman-Korst model. For the present study, the major difficulty in the calculation of flow redevelopment after reattachment lies in the non-equilibrium nature of the turbulence structure which is uniquely different from both the wall or free turbulent types of flows. Nevertheless, the inviscid flow field is already specified for this region and the problem of redevelopment of viscous flow is more or less of the parabolic nature. More detailed experimental investigations are needed before additional progress can be made in this aspect of the problem.

4. METHOD OF CALCULATIONS

For a specific flow condition where the Mach number of the approaching flow and the step geometry (e.g., sting-body radius ratio) are given, the usual purpose of performing such calculations would be the determination of the flow field corresponding to a specific momentum thickness ratio* of the boundary layer at the step compatible with the characteristic Reynolds number of the flow. It has been found that to achieve such a purpose, many sets of inviscid flow calculations with different Sh values must be performed through an iterative procedure and the costs of producing such results are prohibitively high. Instead, one is forced to determine the correct initial momentum thickness ratio of the boundary layer of the flow at the step with a specific value of the shape parameter Sh. For convenience, the momentum thickness ratio of the boundary layer at the step is calculated from the initial boundary layer thickness with the free stream condition furnished by the already established inviscid flow field through

$$\frac{\delta_1^{**}}{H} = \frac{\delta_1}{H} \int_0^1 \frac{1 - C_e^2}{1 - C_e^2 \phi_1^2} \phi_1 (1 - \phi_1) \left(1 + \frac{H}{R_o} \frac{\delta_1}{H} \zeta_1 \right) d\zeta_1 . \quad (4.1)$$

Here, $\phi_1 = (\zeta_1)^{1/7}$ for $\zeta_1 \leq 1$, and $\phi_1 = 1$ for $\zeta_1 \geq 1$. For detailed calculation of the transonic or high subsonic Mach number flow past a backward facing step in axisymmetric configuration, one begins with the selection of a value of the shape parameter Sh and proceeds to calculate the corresponding inviscid flow with the given information. A typical set of results obtained from such calculations of the inviscid flow field is shown in Fig. 4 where the surface pressure coefficient on the equivalent body is presented. A sharp change from decreasing to increasing

*Strictly speaking, the build-up of this initial boundary layer at the step relies on the flow on the upper wall. For a given upper wall length, it is thus a problem to be solved by successive approximations.

pressure occurs at the section of minimum C_p within the wake region. It suggests that the recompression process shall begin from this section and the length of the quasi-constant pressure jet mixing region can be determined.

The flow conditions at this section as a result of jet mixing, such as values of ϕ_d , δ_a/H , and δ_b/H , may be obtained from the quasi-constant pressure mixing analysis with a selected initial boundary layer thickness in conjunction with the information obtained from inviscid flow calculations. The streamline direction β_e at the edge of the mixing region at this section may also be found. A slanted system of coordinates x, y is chosen for the study of the subsequent recompression process that both β_e and y_d at the end of mixing are zero within this coordinate system.

The results obtained from the previous jet mixing analysis are tacitly taken as the initial conditions for the recompression process. As the system of equations (Eqs. (3.34), (3.35), (3.36), (3.38), (3.39), and (3.40)) is integrated numerically step-by-step toward the point of reattachment, it is found that different values of initial boundary layer thickness would produce widely different and divergent values of dividing streamline velocity. As shown in Fig. 8, for larger values of $\delta_1^{**}/H, \phi_d$ is reduced drastically and will vanish before the lower wall is reached; while for slightly smaller values of δ_1^{**}/H , ϕ_d will eventually increase. This phenomenon suggests that the point of reattachment behaves as a saddle point singularity for the system of equations describing the flow. Ideally, the point of reattachment can be reached by repeatedly performing the calculations with intermediate δ_1^{**}/H values between two different branches of integration paths. However, for the present flow problem, the calculation of third or second digit after the decimal point for

the initial momentum thickness ratio of the boundary layer will be good enough for the engineering purpose if one is not interested in the detailed pressure distribution up to the point of reattachment. The available results would provide a rough estimation of the base drag. Calculations with different shape parameters Sh can be carried out similarly and the graph of base pressure coefficients as a function of initial momentum thickness with specific sting radius can also be constructed which will be presented in the next chapter.

5. RESULTS AND DISCUSSION

Upon employing the flow relations presented in the previous chapters for the individual flow processes, calculations can be made for the specific cases of flow. Since the viscous flow processes are guided by the inviscid flow established from numerical solution of the full potential equation, it is important to determine the inviscid flow field accurately. Figure 9 shows the effect of refinement of grid spacings for the flow case of $M_\infty = 0.75$, $Sh = 0.135$ with $R_s/R_o = 0.5$. It is obvious that there is no significant difference in the surface pressure coefficient on the equivalent body when the grid spacings are successively refined. It seems that it is adequate to employ the inviscid results after the refinement of grid spacings has been applied once.

The inviscid calculations have been made in wide ranges of Sh values in order to investigate its effect on the surface pressure coefficient. Figure 10 shows the effect of Sh values on the pressure at the upper corner of the step with different Mach numbers at vanishing sting radius ratio. It is obvious that the pressure at the step decreases with increasing Sh value which corresponds to shorter equivalent body. Also, for certain Sh values, the pressure at the step decreases with increasing Mach number within the range of Mach number calculated (this trend may be reversed when the Mach number is less than but close to unity). Figure 11 shows the effect of presence of sting to the pressure at the step with different Sh values for the free stream Mach number of 0.75. It shows that the pressure at the step decreases with increasing sting radius ratio for all calculated Sh values. This is indeed the effect of axisymmetric geometry.

When the viscous flow analyses are combined into the considerations, the effect of the initial boundary layer momentum thickness with different Mach numbers for vanishing sting radius ratio is illustrated in Fig. 12. Generally speaking, the pressure at the step is lower for smaller momentum thickness ratio. The small value of momentum thickness corresponds to the flow condition of higher Reynolds number. Therefore, this figure reflects the Reynolds number influence on the pressure at the step. It is natural to expect that the viscous flow with higher Reynolds number can cope with stronger recompression. Nevertheless, it should be noted that doubling the momentum thickness would correspond to a tremendous reduction in the Reynolds number. It also shows that the Reynolds number has little influence under flow conditions of fairly thick initial boundary layer. For a fixed initial momentum thickness, cases of higher approaching flow Mach number produce longer wake regions and higher values of C_p at the step; this phenomenon will be discussed some more later.

The effect of sting radius ratio on the pressure at the step for freestream Mach number of 0.75 is shown in Fig. 13. It shows that a smaller sting radius results in higher pressure at the step, while larger sting radius would produce lower pressures at the step. Also, for a fixed initial momentum thickness, a smaller sting radius would have a longer wake so that the turbulent exchange process will transport momentum more effectively that the viscous layer can cope with a stronger recompression process. However, this mechanism is effective only when sting radius ratio is close to unity. Figure 14 further illustrates that the pressure at the step decreases as sting radius ratio increases and this can be easily explained by the effect of axisymmetry. Also, it shows that the pressure at the step is reduced with decreasing initial momentum thickness ratios.

If one implies from the boundary layer concept that the pressure at the step is the base pressure, Fig. 15 presents the comparison of base pressure coefficients with several available experimental data. For experiments carried out under transonic flow conditions, a tunnel must have a perforated test section with an auxiliary pumping system to attenuate the reflected shocks and expansion waves originated from the model. Since transonic facility is much more elaborate and expensive, there is rather meager amount of the consistent and reliable experimental data. Koh [63] obtained the base pressure data by using a long cylindrical body model extended from far upstream in the Boeing transonic and supersonic wind tunnel to eliminate the support interference. Merz [64] obtained the base pressure data with similar cylindrical model but under a constant pressure boundary condition (open jet test section). No specific momentum thickness is reported by Koh in his tests. Merz reported in his tests that the momentum thickness ratio δ_1^*/H varies from 0.06 for $M_\infty = 0.27$ to 0.05 for $M_\infty = 0.8$.

Figure 15 shows that the pressure at the step is much higher than the base pressure reported from experiments. For higher approaching subsonic flow Mach numbers, the pressure at the step may approach that of the free stream even though the base pressure may be reduced. This is obviously true when the approaching flow is sonic ($M = 1$). Under this situation, the Mach number at the step is also sonic while the base is impressed by a lower pressure resulting from a Prandtl-Meyer expansion. Therefore, the pressure at the step is inadequate to be taken as the base pressure under these situations. Since the experimental pressure data were taken from the base of the model body rather than from the step, it is necessary to identify a characteristic wake pressure from the theoretical calculations as the base pressure. Since the recirculating

flow will sweep by the face of the base, the static pressure of the backflow at the end of mixing C_{pbm} may be selected for this purpose. It was originally suggested [1] that the stagnation pressure of the backflow at this section be taken as the base pressure. Since the backflow velocity is usually small, the present selection would not significantly change the results at lower free stream Mach numbers, and yields better results at high subsonic free stream Mach numbers. Figure 16 presents the so defined base pressure coefficient C_{pb} as a function of Mach number for zero sting radius ratio. It may be observed that C_{pb} decreases with decreasing initial momentum thickness which, again, indicates the effect of higher Reynolds number. The comparison of C_{pb} with experimental base pressure data is shown in Fig. 17. Much better agreement, especially in demonstrating the transonic drag rise, leads one to conclude that C_{pbm} may be taken as the base pressure under this high subsonic Mach number or transonic Mach number flow conditions.

Figures 18 and 19 present the pressure distributions on the sting (for $R_s/R_o = 0$, there is no sting and it can be considered as the center-line of the wake) within the wake region with two different momentum thickness ratios at $M_\infty = 0.75$ for two different sting radius ratios, respectively. It can be observed that the pressure at the point of reattachment is already above the approaching free stream value. This is mainly due to the fact that the edge of the viscous layer is located within the influence of the inviscid stagnation point even though axisymmetric geometry would generally induce stronger pressure rise during recompression. This phenomenon was also observed in the two-dimensional flow past wedges of small wedge angles [48].

Variations of pressure, stagnation pressure of the dividing streamline and the backflow are shown in Figs. 20, 23, 26, and 29 for various Mach numbers, sting radius ratios, and initial momentum thickness ratios. Figures 21, 24, 27, and 30 present the dividing streamline velocity and maximum reverse flow velocity and Figs. 22, 25, 28, and 31 show the geometry of the wake region for these different flow cases. These provide a rather detailed comparison of the flow properties within the wake region. It is generally observed that the dimensionless velocity of dividing streamline is energized in the mixing region, decreases in the recompression region, and finally vanishes at the reattachment point. While these property values may vary from one case to another, they all show consistent behavior compatible to the adopted flow model, and the influences from each flow mechanism can be extracted from detailed comparison of these results. It should be mentioned that the backflow upstream of the recompression region has not been considered and presented within these figures, since there is no such a need in the process of calculations of the present problem (as a result of assumption of a semi-dead wake region). It may be estimated from continuity principle if the need should arise, since the dynamic effect of this backflow within the essentially constant pressure region would be negligibly small. Also, the apparent unsMOOTHNESS exhibited by some of the curves presented within these figures is the inherent result of component analysis when two different components are joined together.

In the quasi-constant pressure jet mixing analysis, an empirical parameter σ , the turbulent mixing spread parameter, has been introduced to facilitate the calculation of the mixing process. Originally, σ is a similarity parameter for plane mixing flows which are inversely proportional to the rate of spread of mixing layer and is adopted as a parameter for the present non-similar flow situation. For incompressible flow, the value $\sigma = 12$ is generally used and this seems to be a proper value for conditions which correspond to the mixing between a uniform stream and a quiescent fluid. However, there is no adequate information provided for the axisymmetric case. Tanner [66] suggested that the angle between the wall from which the flow separates and the wall on which the flow reattaches has a great influence on the value of σ . It has been observed that, for fully developed compressible turbulent mixing flows, the mixing zone width varies linearly with the x-coordinate although the rate of spread depends upon the Mach number. It implies that at constant Mach number, σ is also constant. Experimental investigations have shown that there is a trend for σ to increase with increasing Mach number. Tanner also reviewed several relationships between σ and Mach number suggested by many investigators. Because of lacking extensive experimental results, it is difficult to establish the correct relationships between σ and Mach number. In order to assess the influence of σ in the present investigation, different values of σ have been employed to carry out the calculations. Figure 32 presents the influence of σ to the initial momentum thickness compatible to a certain set of inviscid calculations (constant Sh value). For a specific inviscid flow field, smaller σ values lead to larger initial momentum thickness ratios. This phenomenon can also be illustrated in Fig. 33. Large σ values yield higher pressure ratios

at the step for a given geometry and approaching flow conditions as a result of ineffective transfer of momentum across the viscous layer. Figure 34 presents the influence of σ on the pressure distribution on the sting for the freestream Mach number of 0.75 and $R_s/R_o = 0.5$. It can be seen that σ has an influence on the pressure distribution in the whole wake region.

For the purpose of comparison, calculations of corresponding inviscid body geometry with $m = 2$ have also been carried out. Figure 35 presents the variation of pressure at the step with respect to the initial momentum thickness ratios for different Mach numbers with zero sting radius ratio. The curves are similar to that of $m = 3$. However, the level of pressure coefficient is much lower and decreases more quickly when initial momentum thickness decreases. This can be observed from Fig. 36. Even when one recognizes that the pressure at the step is not the base pressure, good agreement with the base pressure data is observed when C_p step under this condition ($m = 2$) is employed and is shown in Fig. 37. Figure 38 presents the comparison between different inviscid pressure fields with a specific Sh value obtained from $m = 2$ and $m = 3$ calculations, respectively. For the case of $m = 2$, the pressure at the step is lower and the mixing region is relatively short. This also can be seen from Fig. 39 where the dimensionless velocity of dividing streamline of these two cases is presented. The dividing streamline velocity reaches a higher value at the end of the mixing region for the case of $m = 3$ due to relatively long mixing region. Figure 40 presents the comparison of the pressure distribution at the centerline of the wake region between cases of $m = 2$ and $m = 3$. It is obvious that the pressure within the wake and the pressure at the point of reattachment for the case of $m = 2$ is much lower than that of the case with $m = 3$. In addition, the case

of $m = 2$ would yield also shorter wake region as shown in Fig. 41. Since consistent and reliable experimental data are not yet available, it is not possible to decide which m value is preferable to simulate the actual flow condition.

As mentioned in section 3.3, after the flow reattachment, the flow further undergoes redevelopment process while the pressure rises continuously until a plateau is reached. Thereafter, the pressure is reduced toward that of the original approaching flow level asymptotically and the fully rehabilitated state is reached at far downstream positions. However, the study of flow redevelopment is not yet possible as it is hampered by the extremely complex nature of the flow as well as the non-equilibrium turbulence structure in this region. Figure 42 shows the pressure distribution downstream of reattachment for a specific case of calculations by tracing the streamline starting at the edge of the viscous layer at the section of reattachment. This simple tracing qualitatively illustrates the complex nature of pressure distribution after the flow reattachment.

It should be noted that the results reported thus far can only be regarded as the first approximation to the solution of the problem [58]. The corresponding inviscid body geometry compatible with the established viscous flow with a finite Reynolds number will be different from what originally has been assumed (Eq. (2.1)) which corresponds to the limiting case of infinite Reynolds number. The profile of the equivalent body for the case of finite Reynolds number should be at a distance away from the dividing streamline which is approximately equal to the "local displacement thickness" of the viscous layer above

the dividing streamline, and it would not coincide with the sting downstream of the wake. Since the inviscid flow field is established through the finite difference calculations, it is possible to include this correction of the effect of finite Reynolds number into the consideration. However, it is cumbersome to apply to the present analysis because different velocity profiles have been assumed for the quasi-constant pressure jet mixing region and recompression region, respectively. Also, redevelopment of flow must be analyzed before such additional improvements can be made. However, it is expected that the present analysis as a first approximation will yield close prediction of the base pressure of this problem.

For the two-dimensional supersonic flow case, it is possible to show rigorously that the fully rehabilitated state is a saddle point singularity. It is not feasible, however, to show in the present calculations that the point of reattachment is a saddle point singularity. This saddle point behavior can only be illustrated through numerical calculations. Although the real flow does not reveal any sensitive characteristics, as associated with a saddle point, the validity of this mathematical behavior should be judged only by the merits of its ultimate results when compared with experimental data. It is well known, however, that as long as one adopts the Navier-Stokes equation to describe the steady viscous flow, meanwhile demanding continuous solution to this equation, saddle point singularity or singularity of other types may inherently occur.

6. CONCLUSIONS

It has been shown from calculations that the overall flow pattern of separated flows is established as a result of interaction between the viscous and inviscid streams, and the solution of this problem can be obtained only by simultaneously considering the influence from both streams. The present theoretical analysis is effective in dealing with the axisymmetric transonic turbulent separated flows by performing the finite difference and integral calculation procedures with a minimum of empirical information. The results of this analysis show reasonable agreement with the available experimental data. Although the adoption of the form of a spatial variation of eddy viscosity is based on speculation, fortunately, this theoretical analysis has provided a reasonable prediction of flow field as well as the base pressure and has turned out to be a workable scheme for the present situation. However, extensive and reliable experimental data with the transonic flow regime are needed for determining proper values of the parameter σ for mixing and parameter m for the corresponding inviscid body geometry. Also, more detailed experiments must be carried out to provide the information of turbulence structure in the redevelopment region so as to facilitate the development of a model for analysis of this flow component.

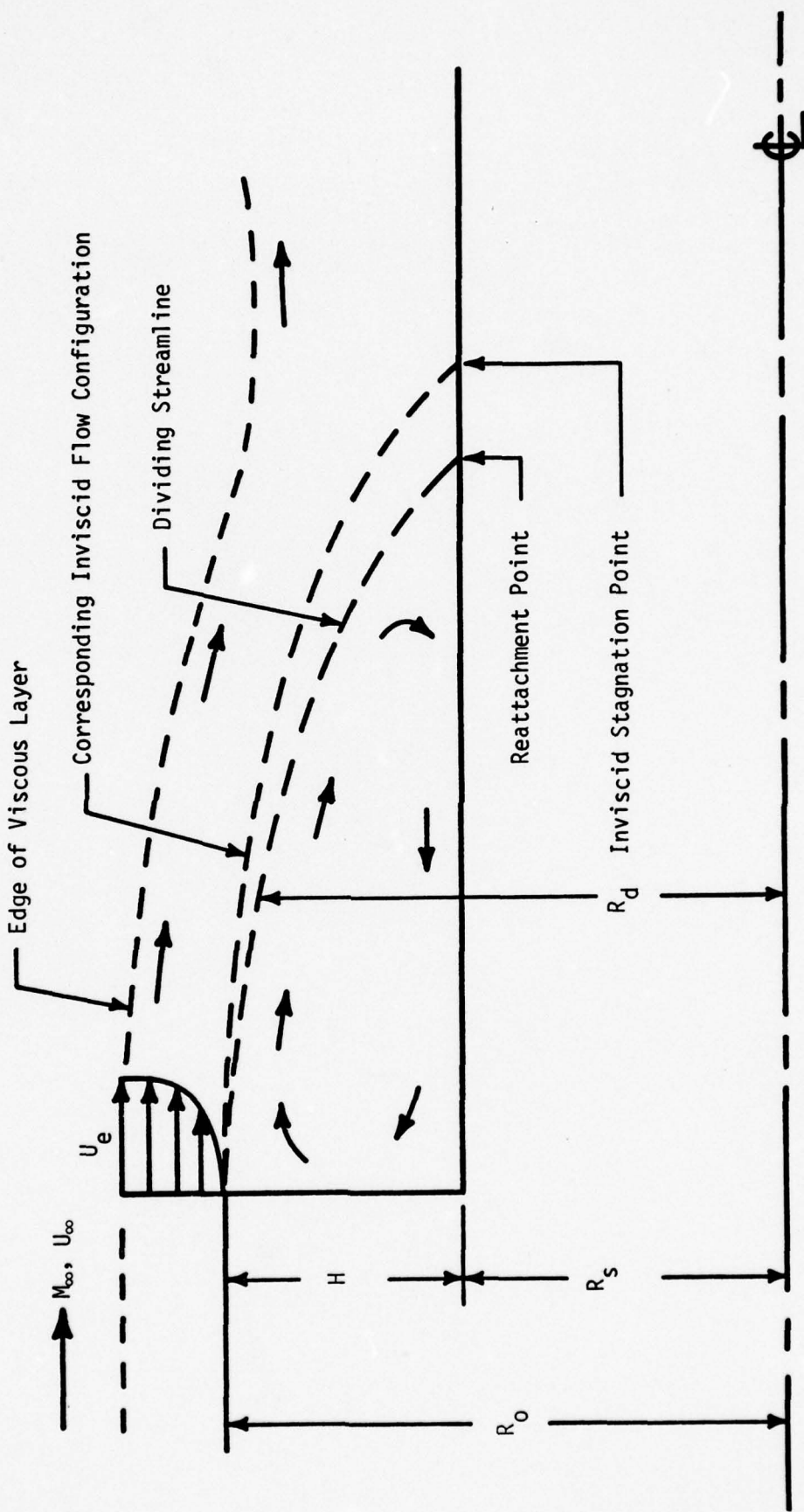


Figure 1 Transonic Flow past an Axisymmetric Backward Facing Step

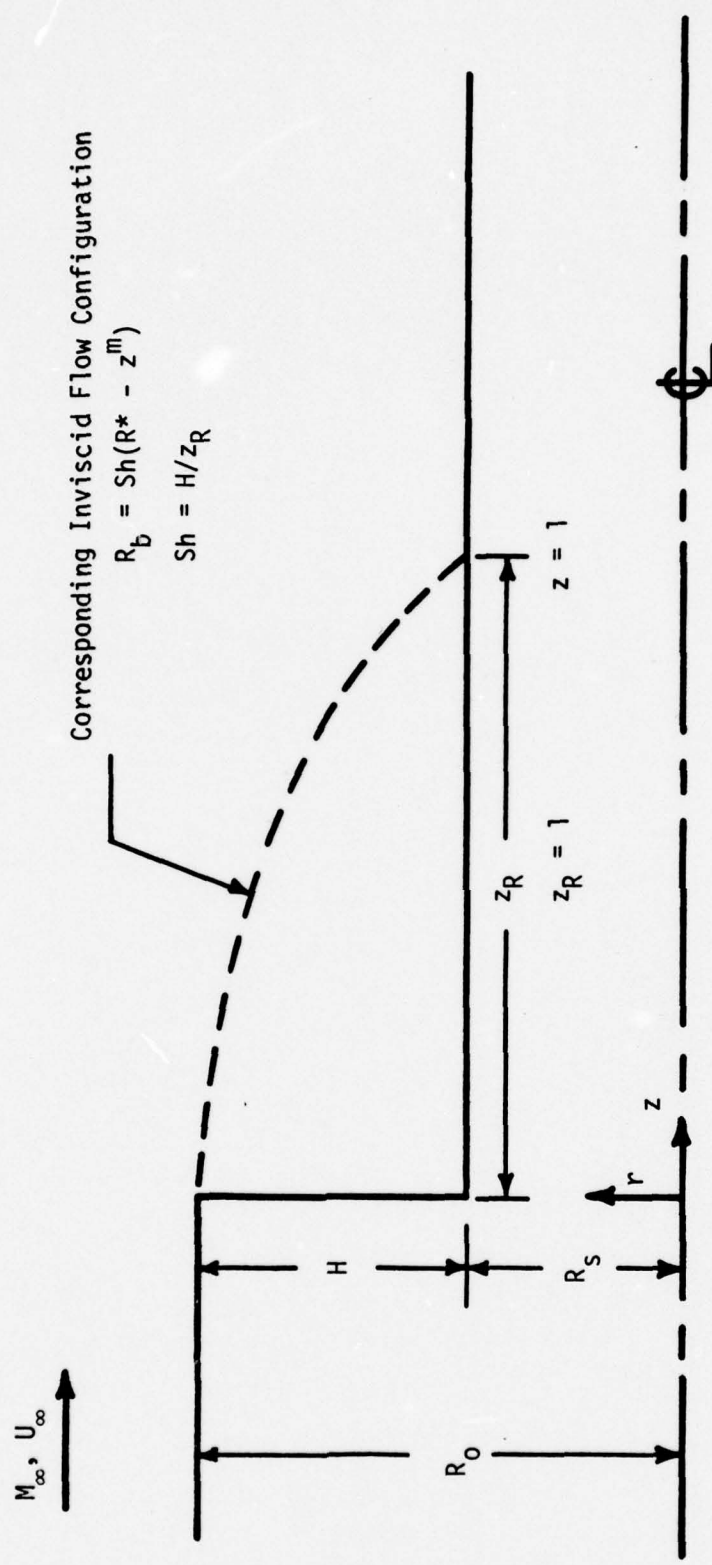


Figure 2 Corresponding Inviscid Flow Configuration

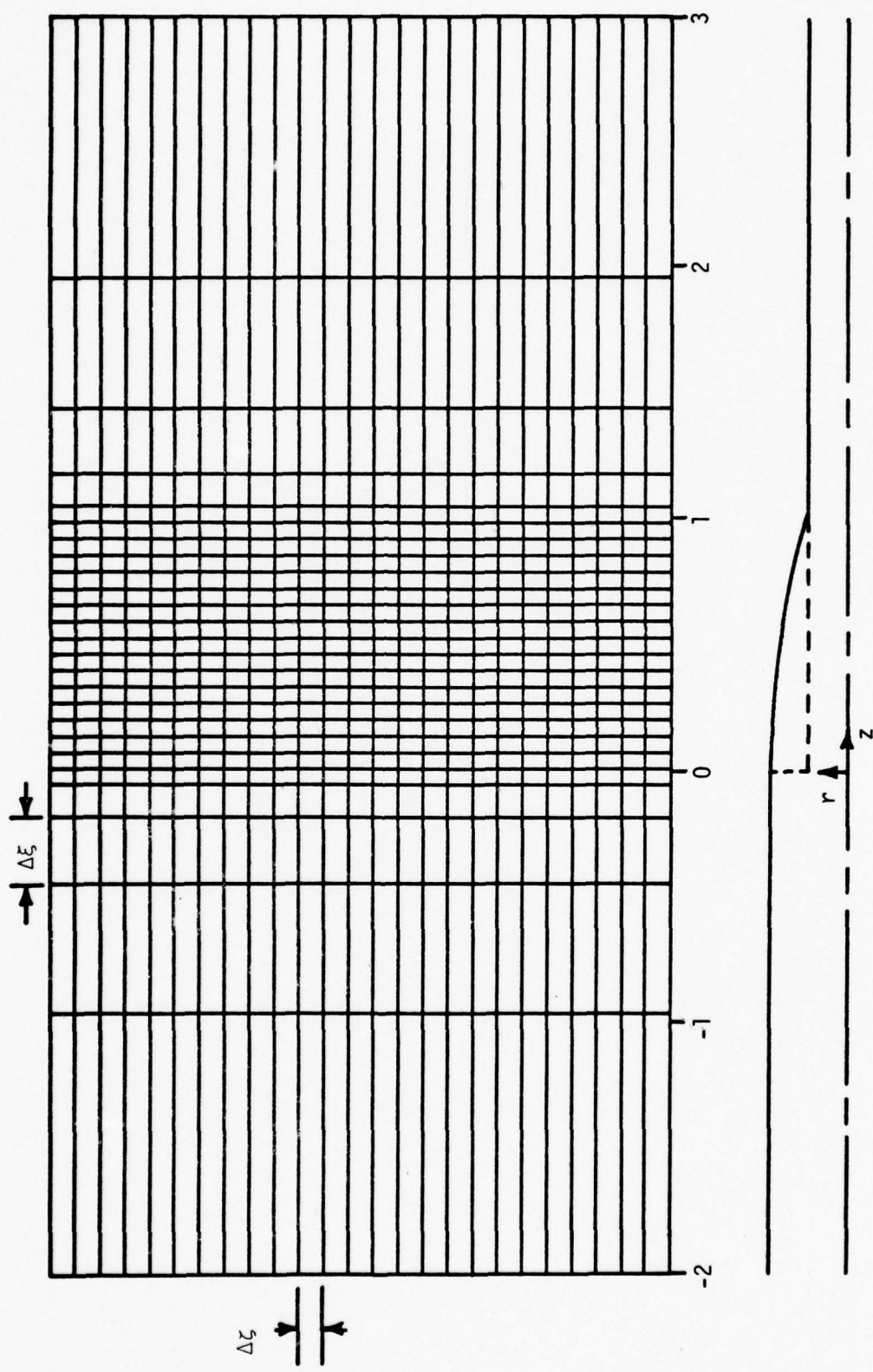


Figure 3 Computational Plane with Coarse Mesh in Relation to Actual Body

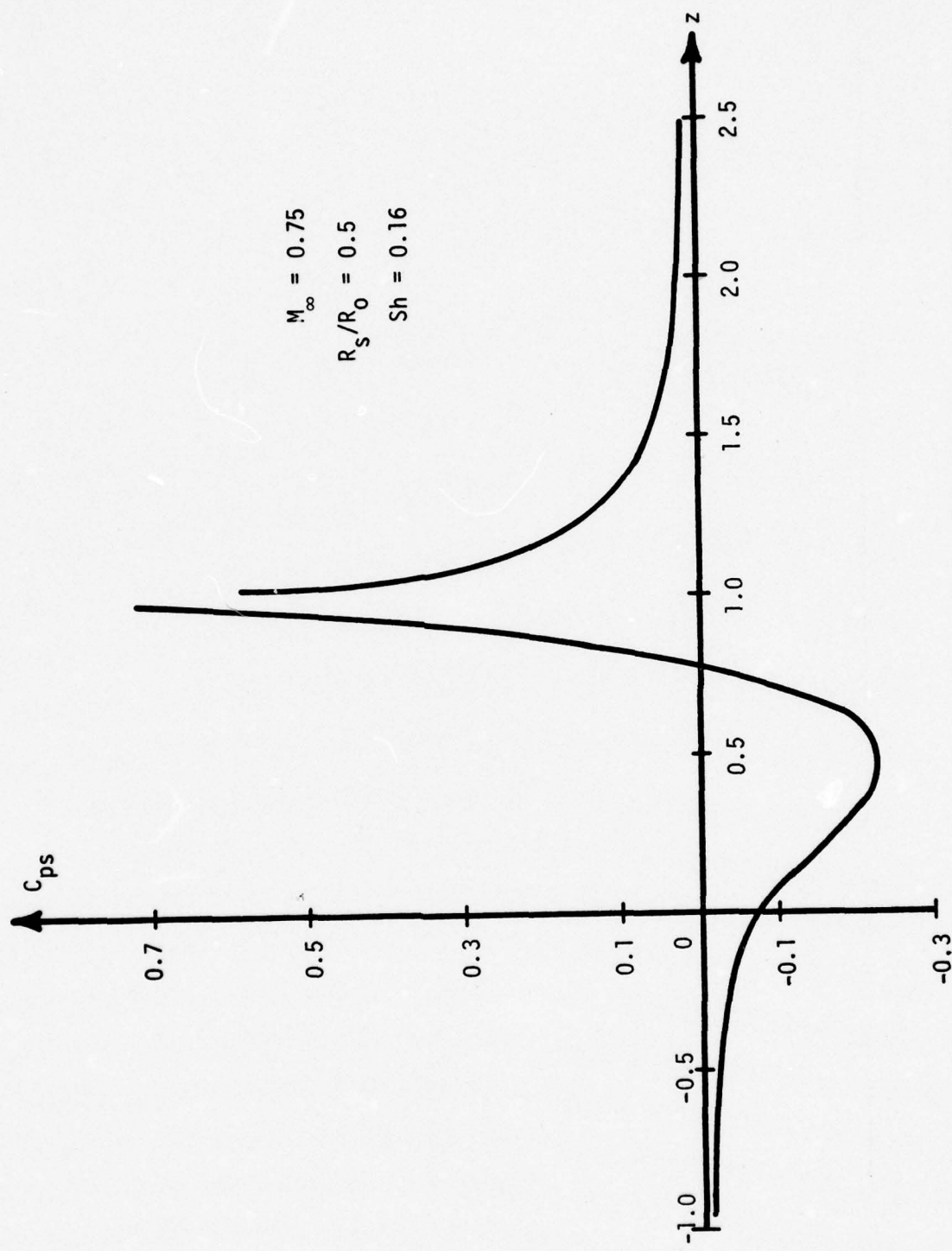


Figure 4 Surface Pressure Coefficient on Equivalent Body

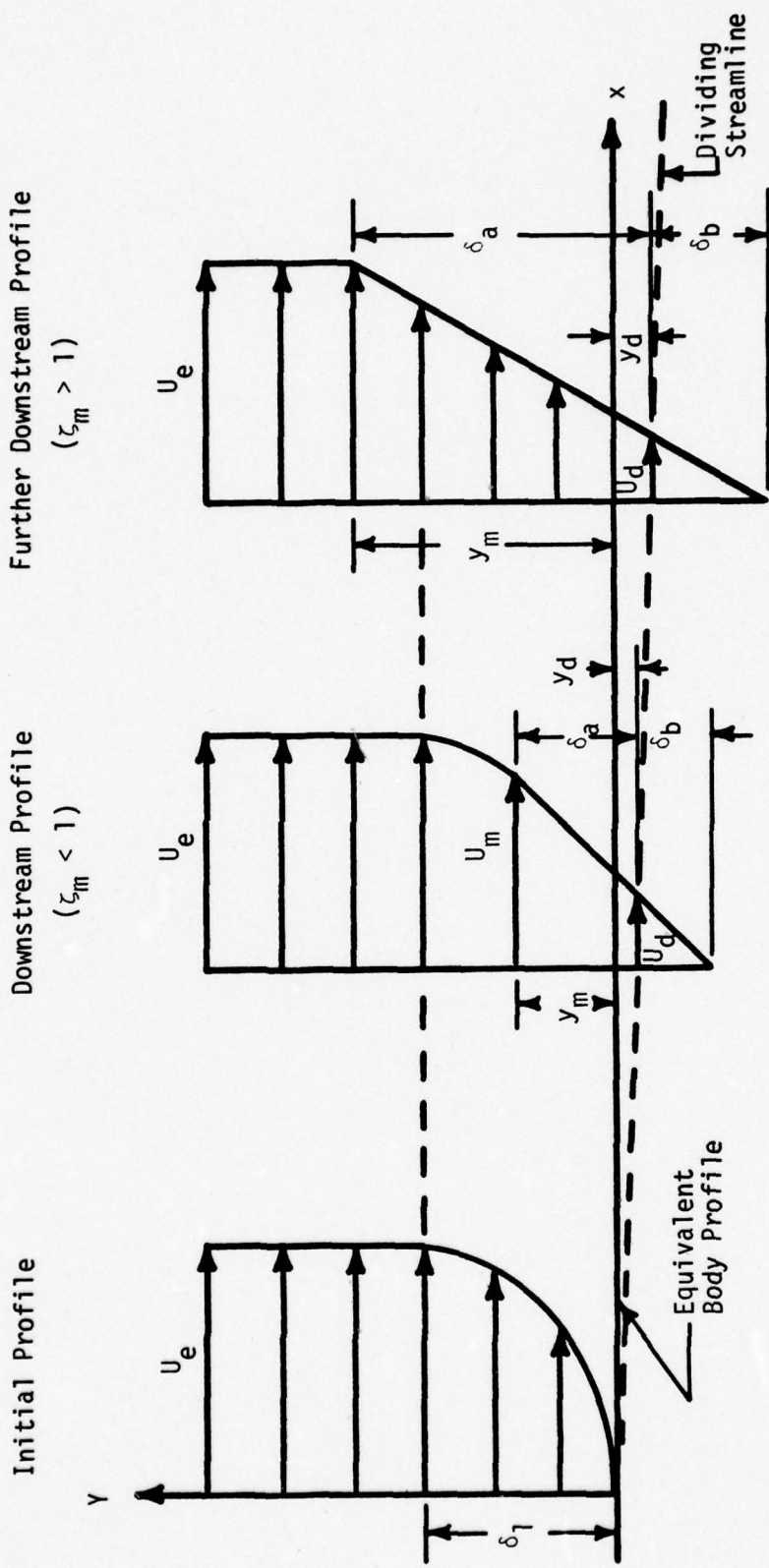


Figure 5 Constant Pressure Turbulent Jet Mixing with Initial Boundary Layer

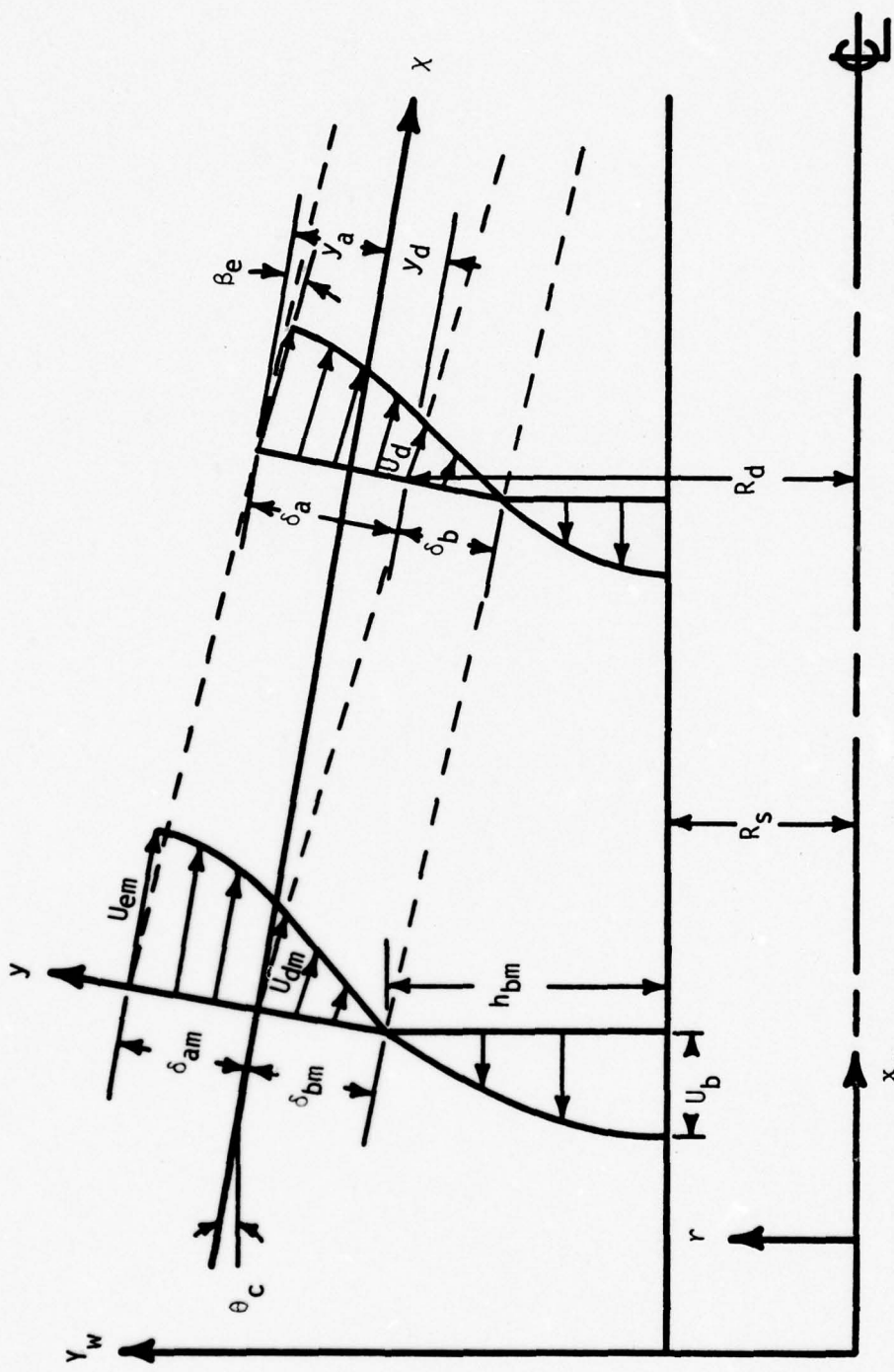


Figure 6 Flow within the Recompression Region

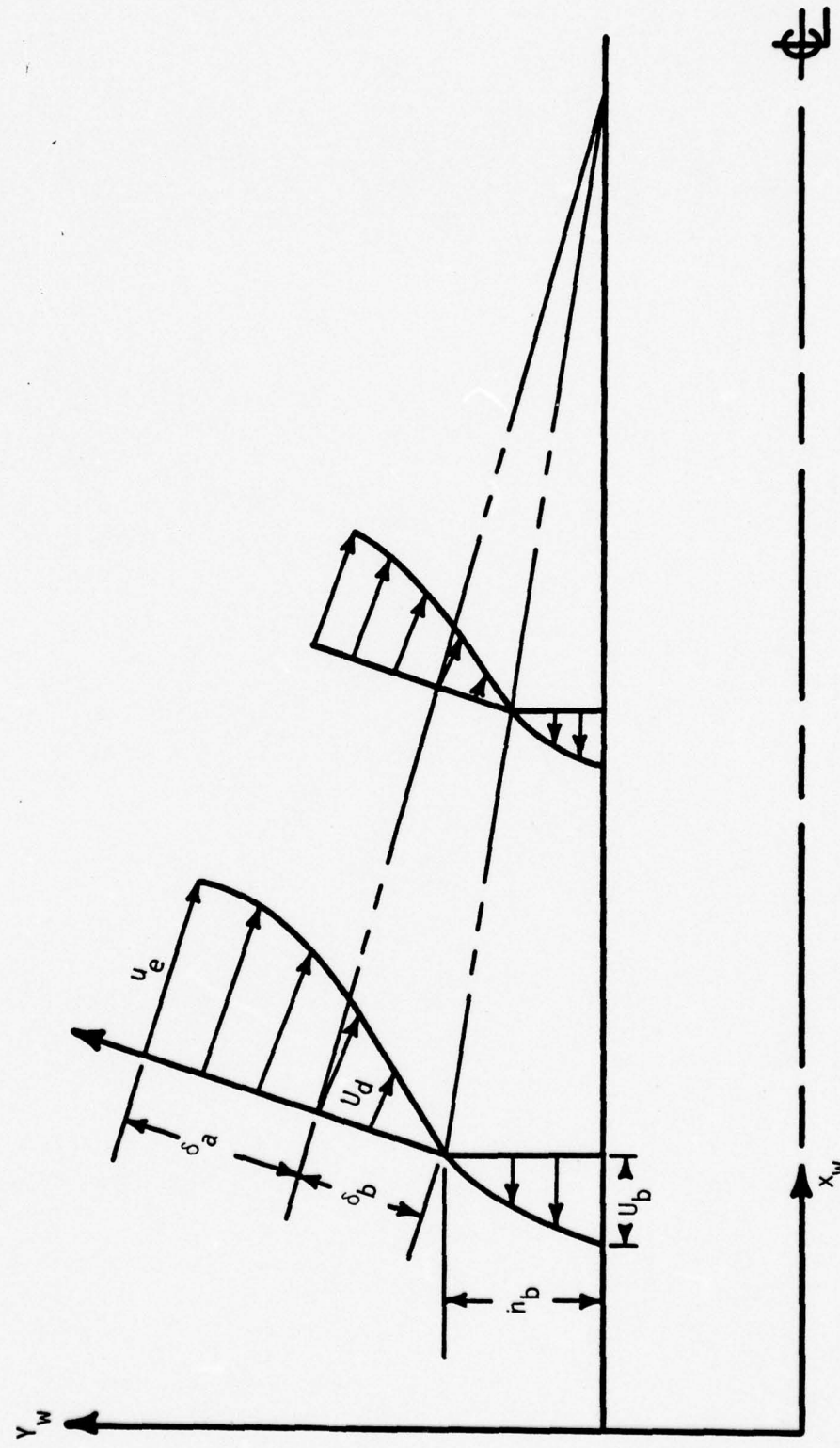


Figure 7 The Locally Triangular Flow Geometry

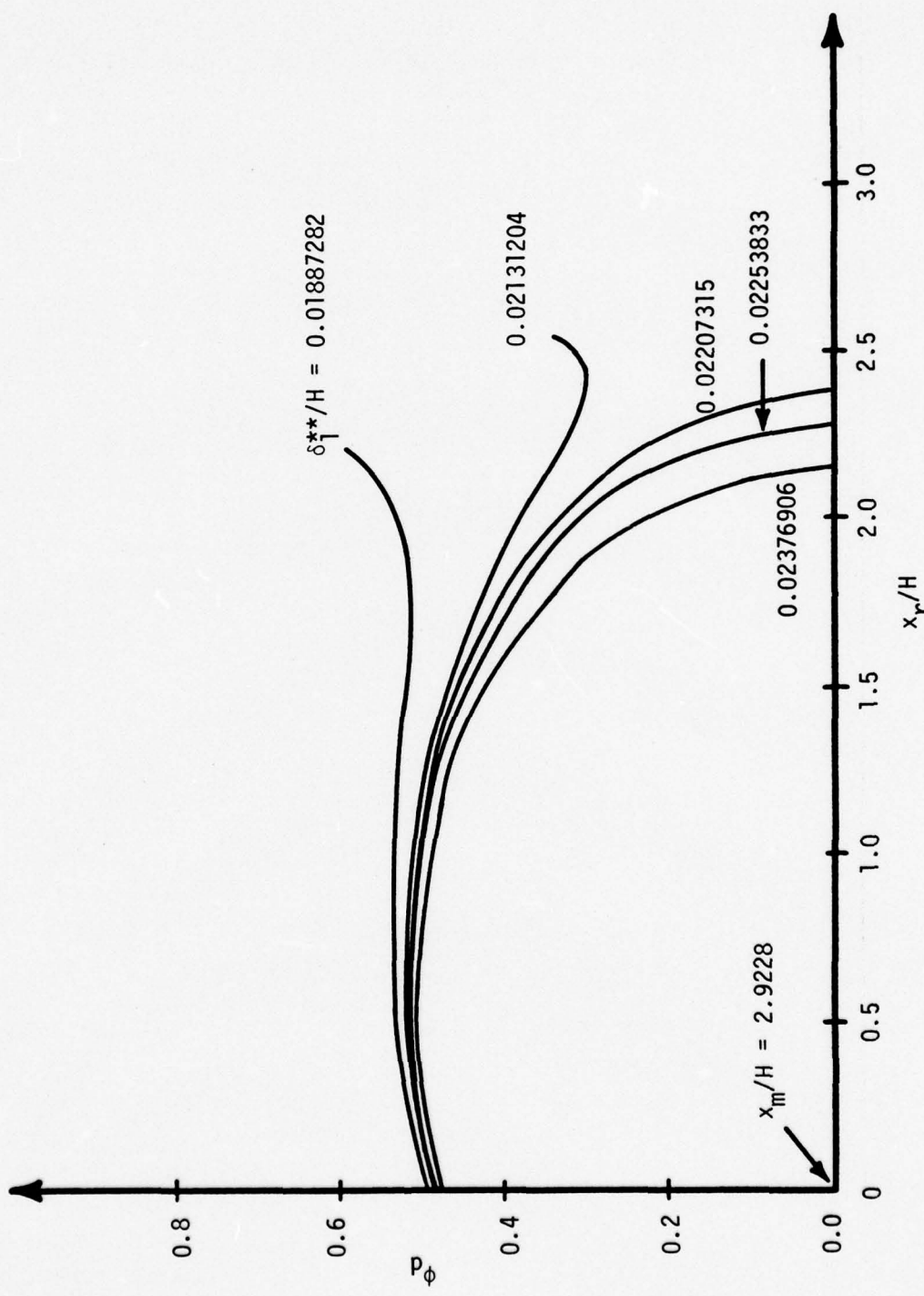


Figure 8 Saddle Point Behavior at Reattachment Point

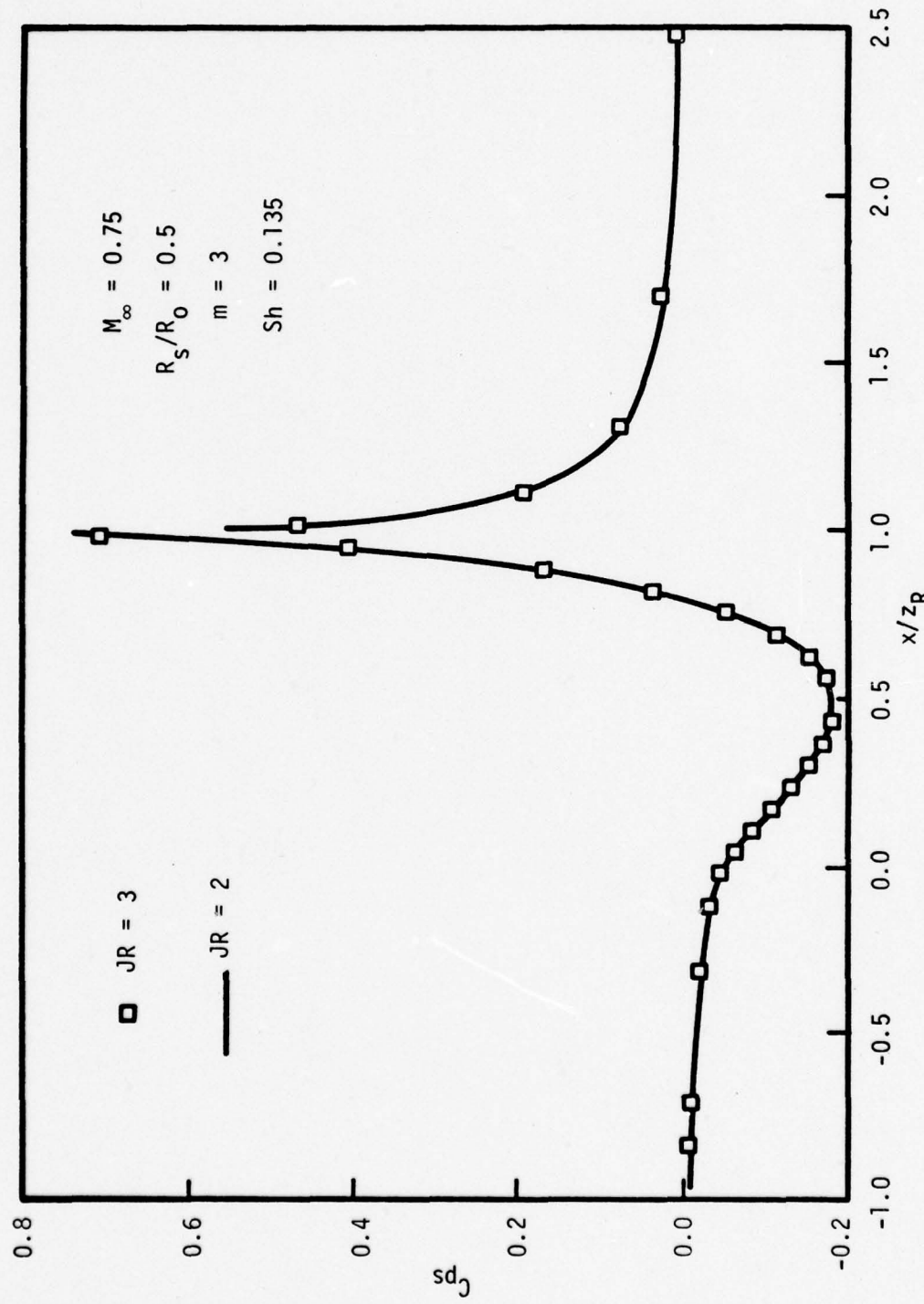


Figure 9 Comparison of Pressure Distribution on Equivalent Body for $JR = 2$ and $JR = 3$

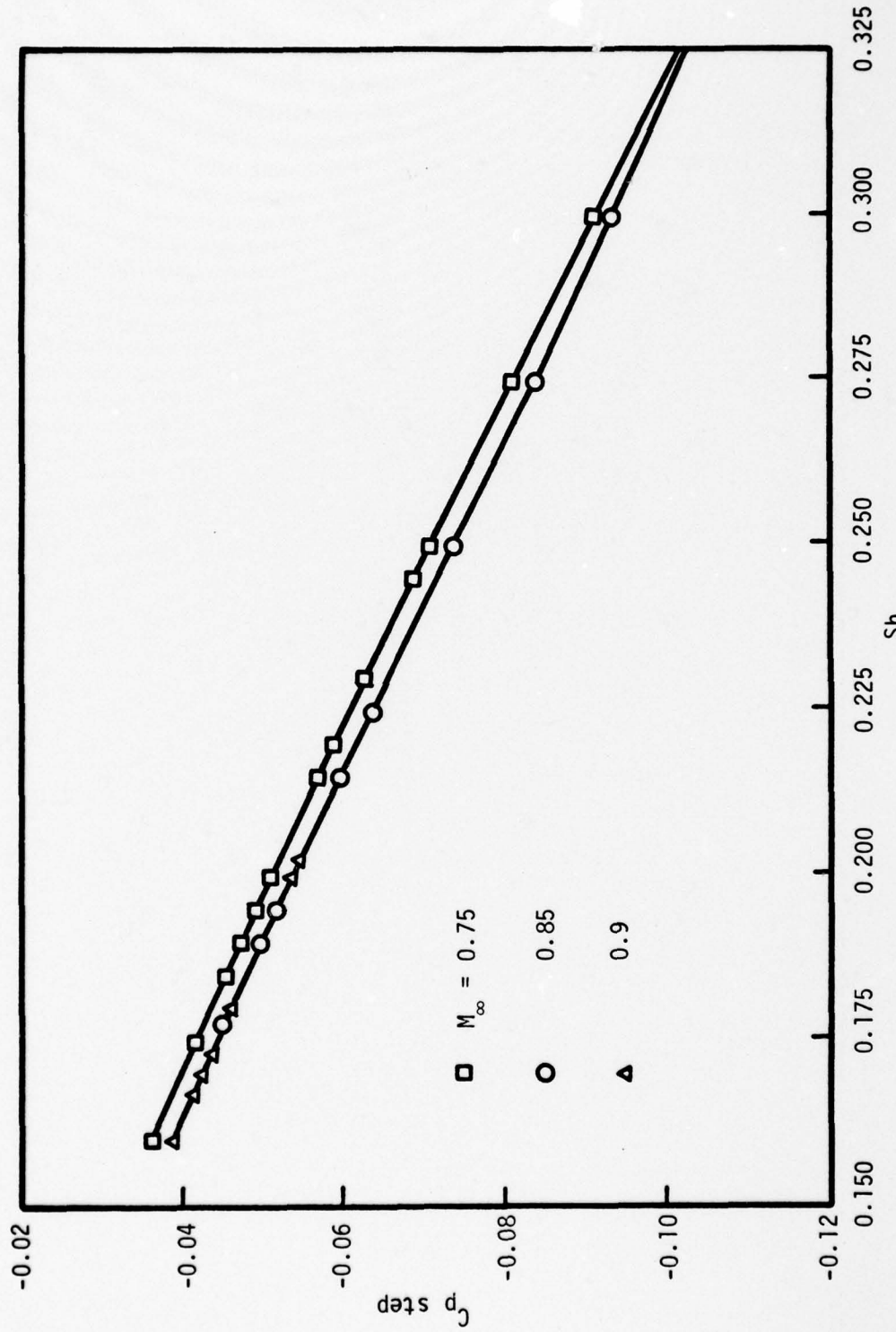


Figure 10 Variation of C_p step vs Sh as a Function of Freestream Mach Number for zero Sting Radius Ratio (Inviscid Flow)

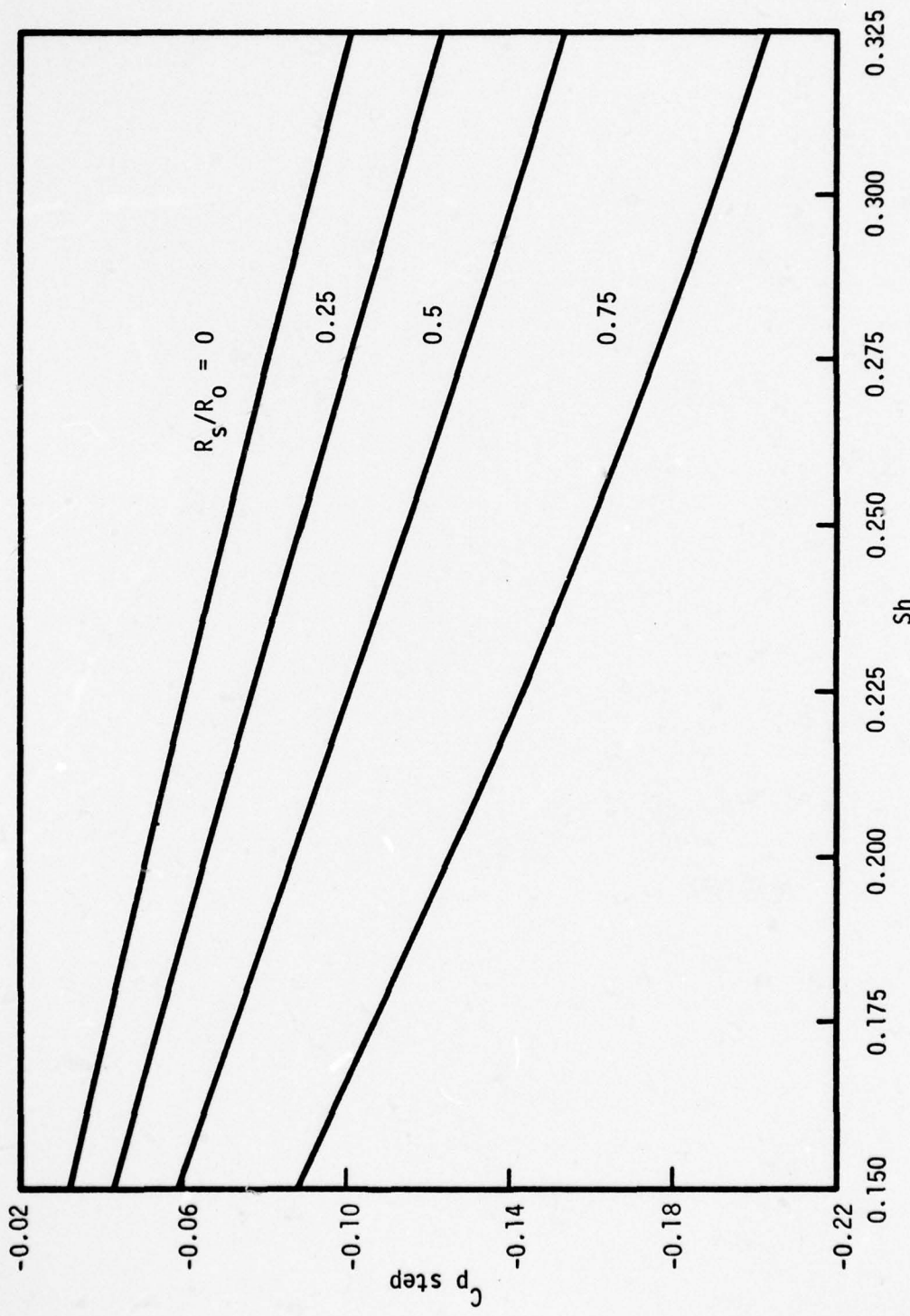


Figure 11 Variation of C_p step vs Sh as a Function of
String Radius Ratio for $M_\infty = 0.75$ (Inviscid Flow)

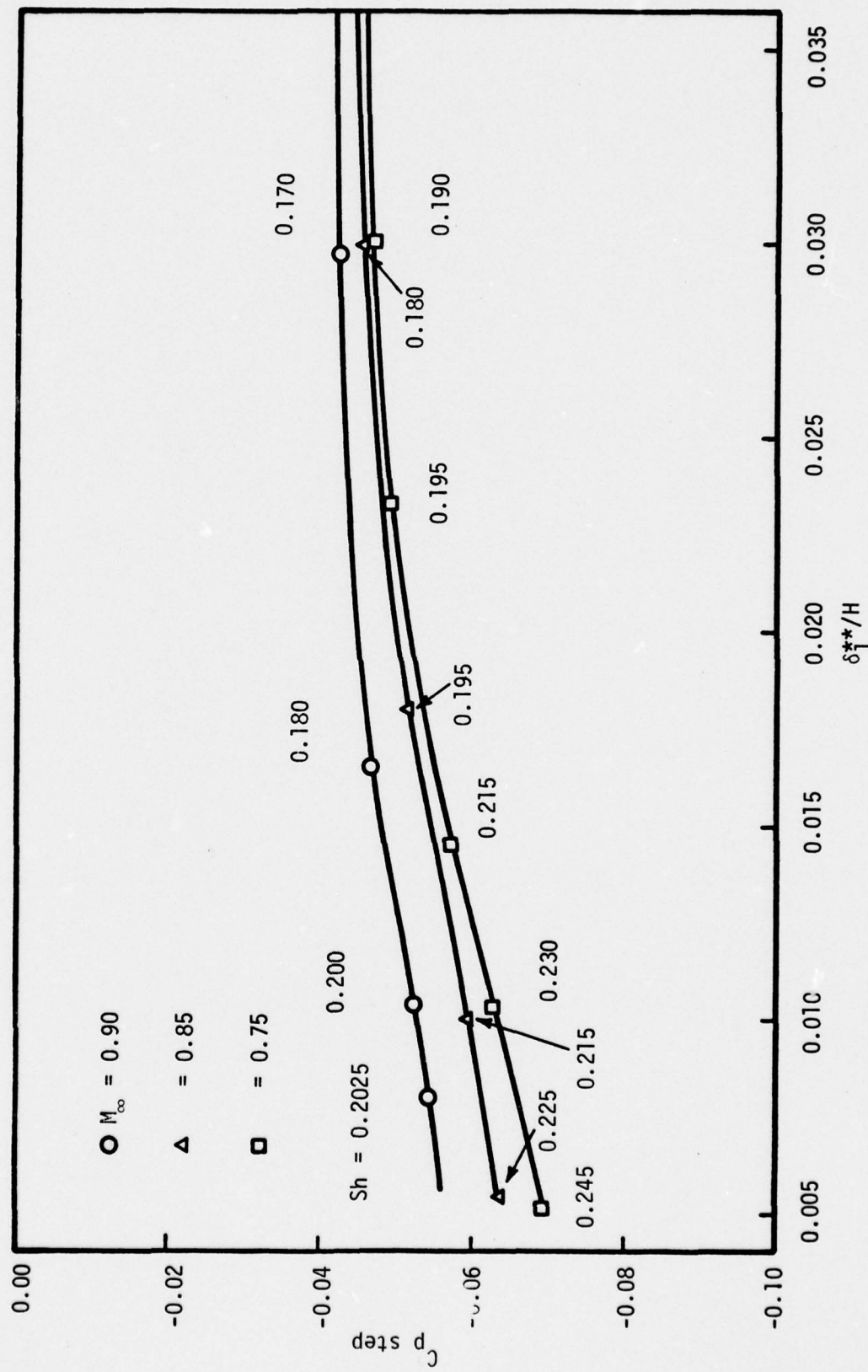


Figure 12 Variation of C_p step with the Initial Momentum Thickness as a Function of Mach Number for zero Sting Radius

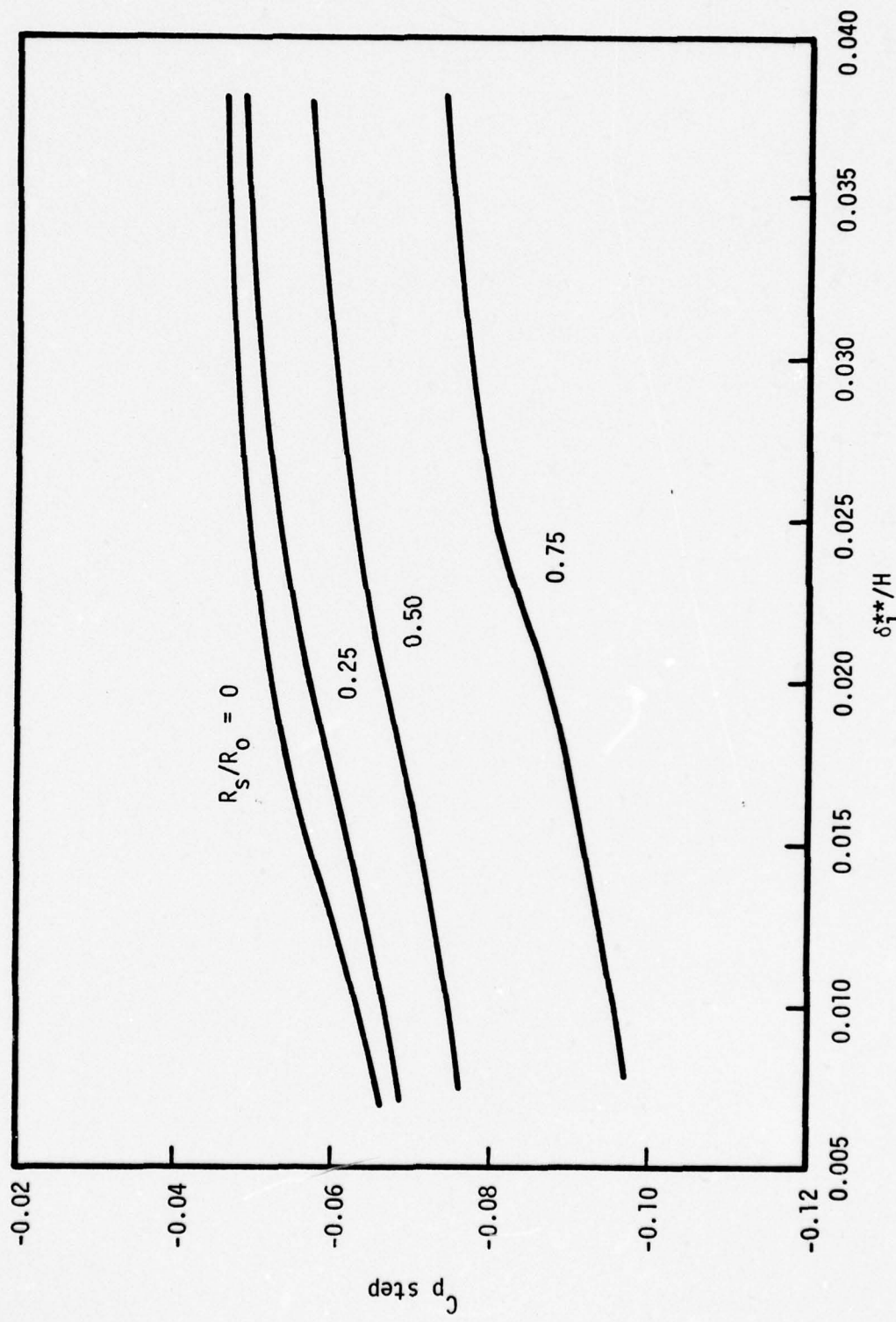


Figure 13 Variation of C_p step with Initial Momentum Thickness
as a Function of Sting Radius Ratio for $M_\infty = 0.75$

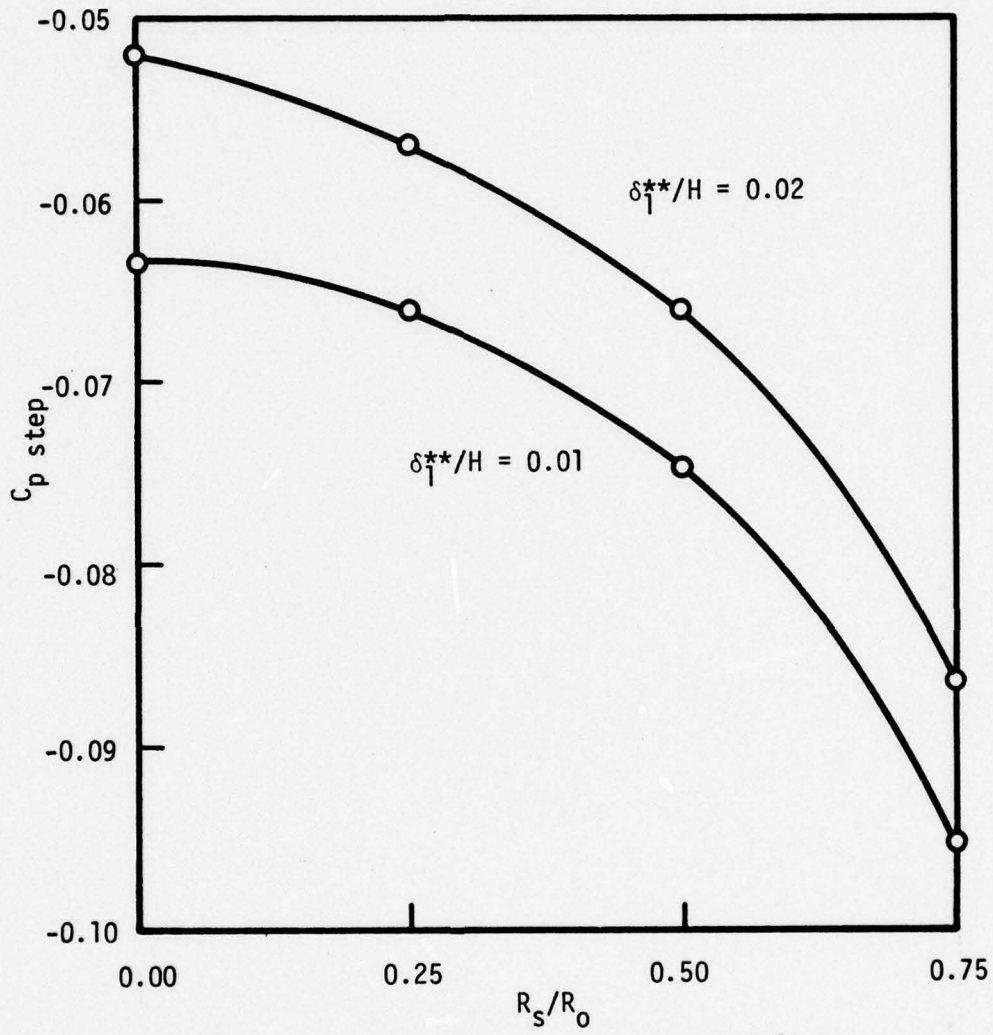


Figure 14 Variation of C_p step vs Sting Radius
Ratio as a Function of δ_1^{**}/H for $M_\infty = 0.75$
($m = 3$ and $\sigma = 12$)

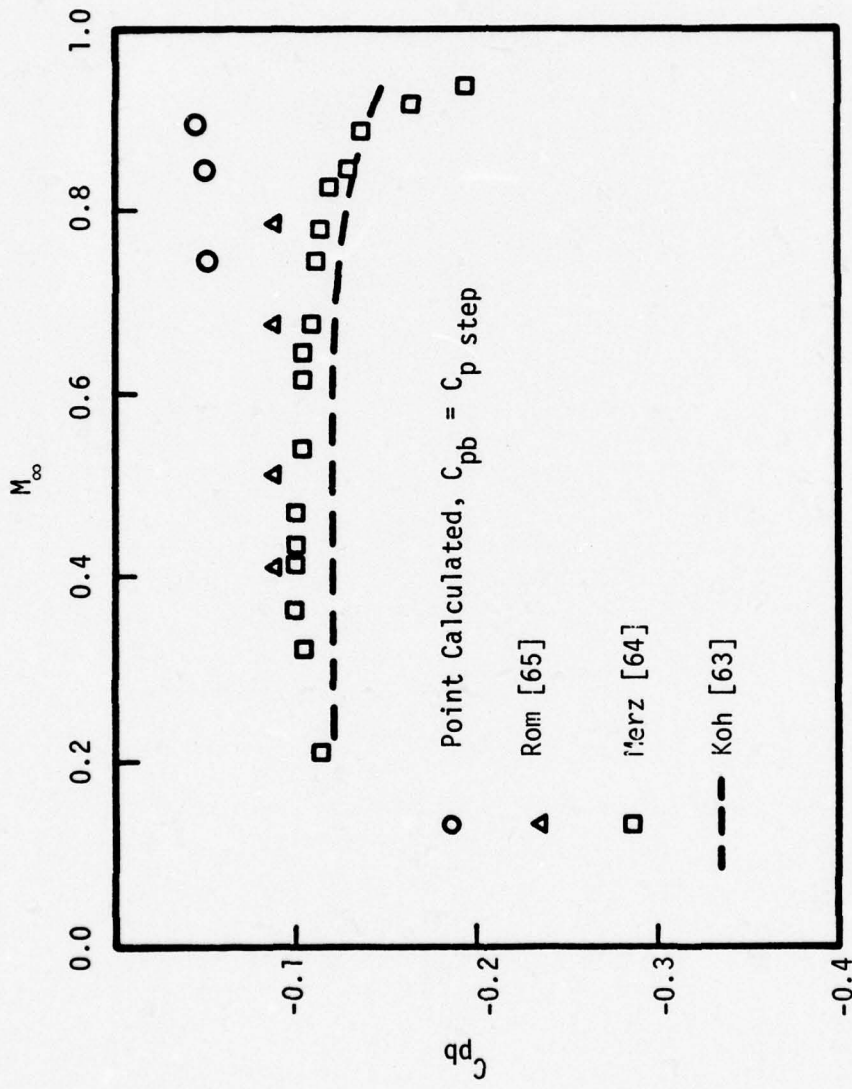


Figure 15 Comparison of Base Pressure with Experimental Data for Zero Sting Radius Ratio

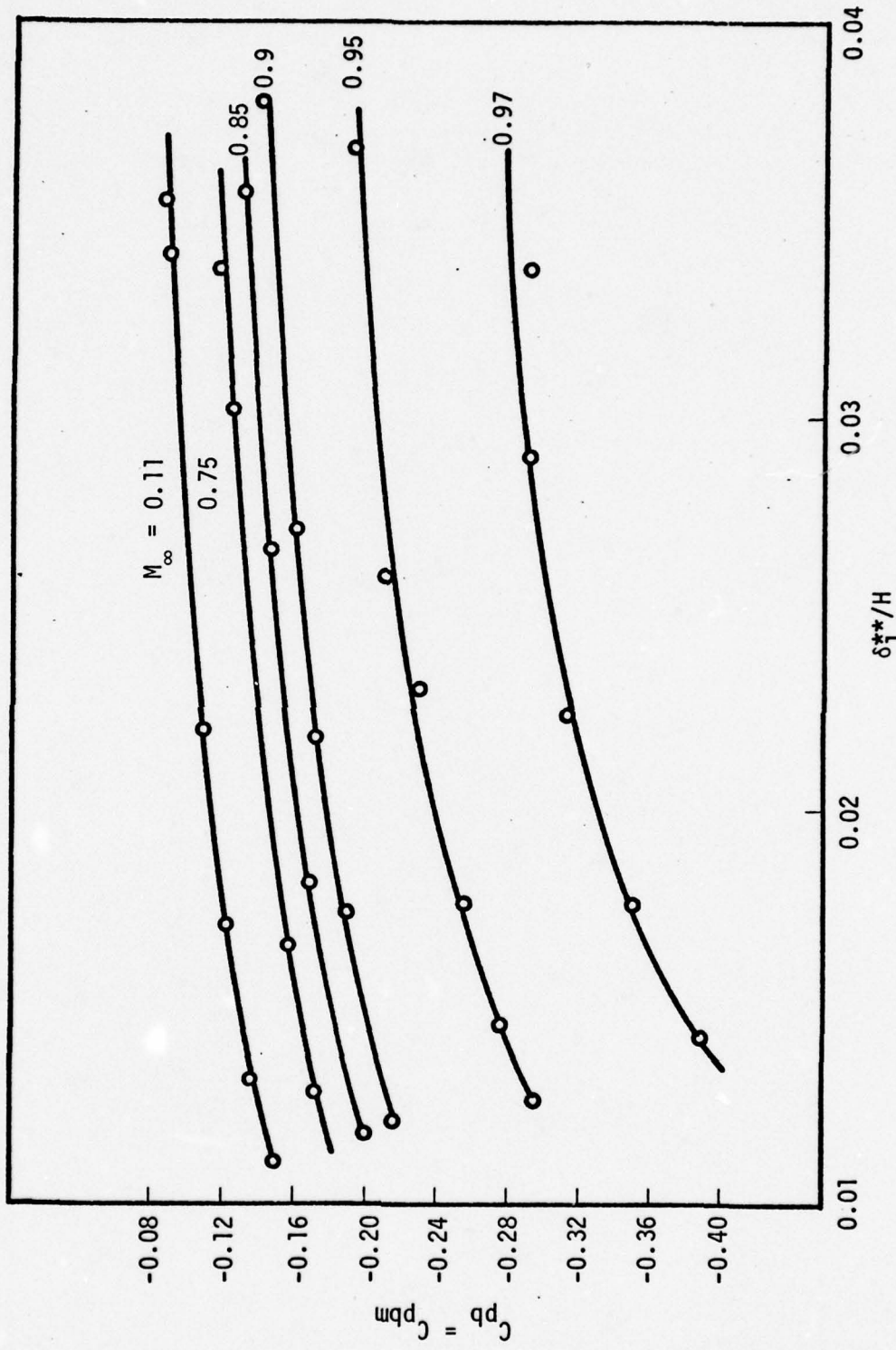


Figure 16 Variation of C_{pbm} vs δ_1^{**}/H as a Function of Mach Number for Zero Stagnation Radius Ratio ($m = 3$ and $\sigma = 12$)

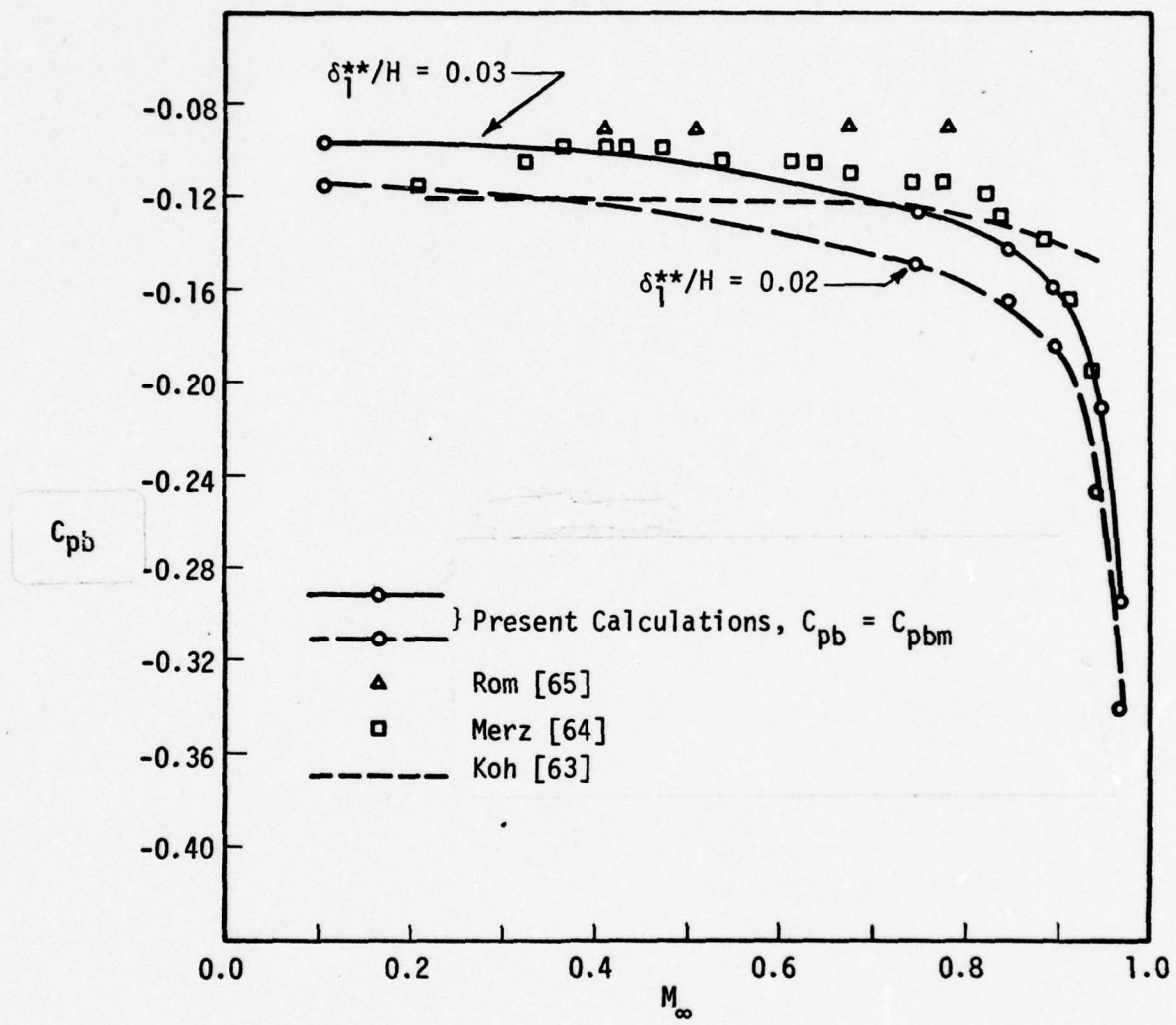


Figure 17 Comparison of Base Pressure with Experimental Data for Zero Sting Radius Ratio

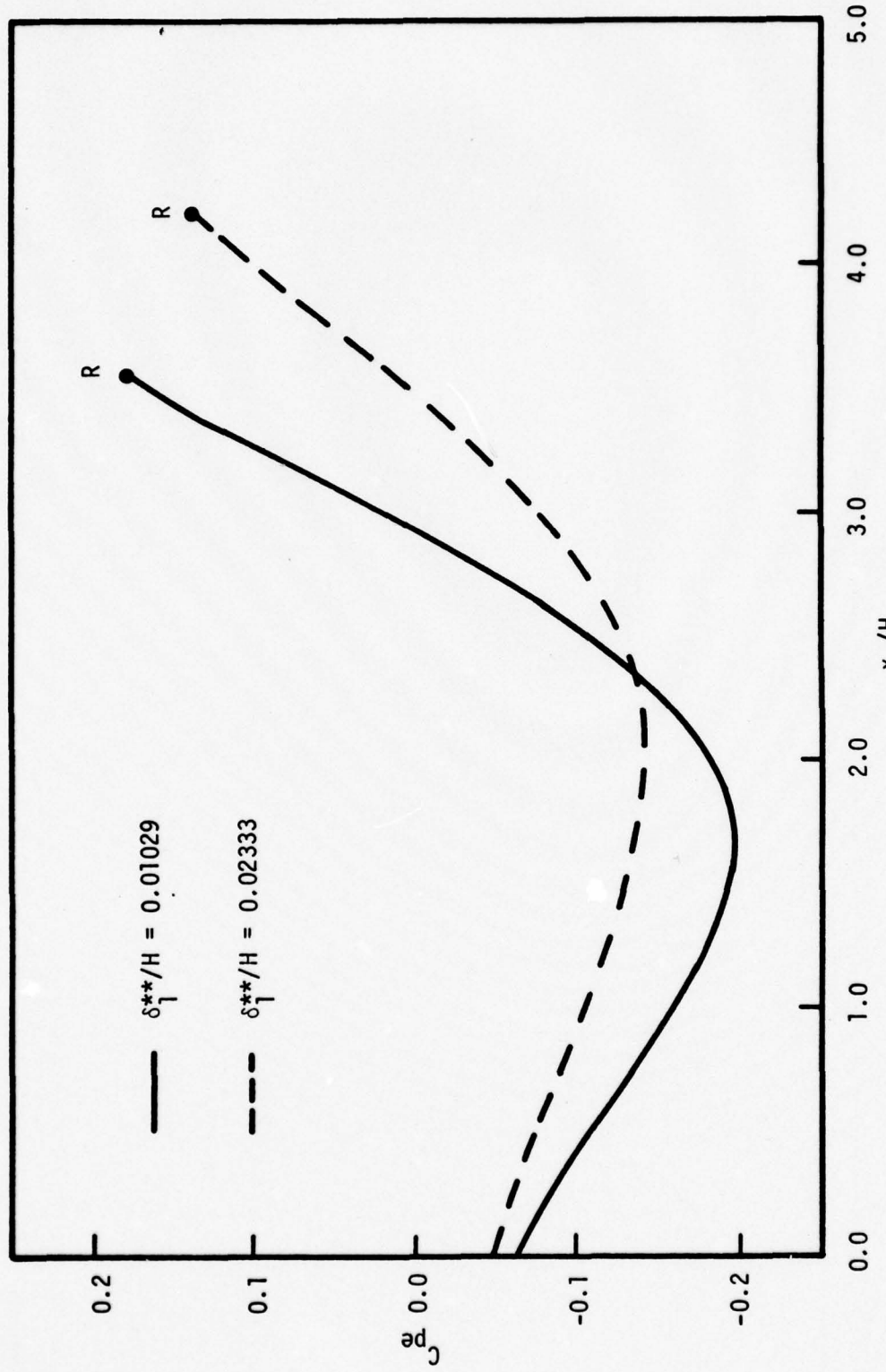


Figure 18 Wall Pressure Distribution as a Function of Initial Momentum Thickness for $M_\infty = 0.75$, $R_s/R_o = 0$ ($m = 3$ and $\sigma = 12$)

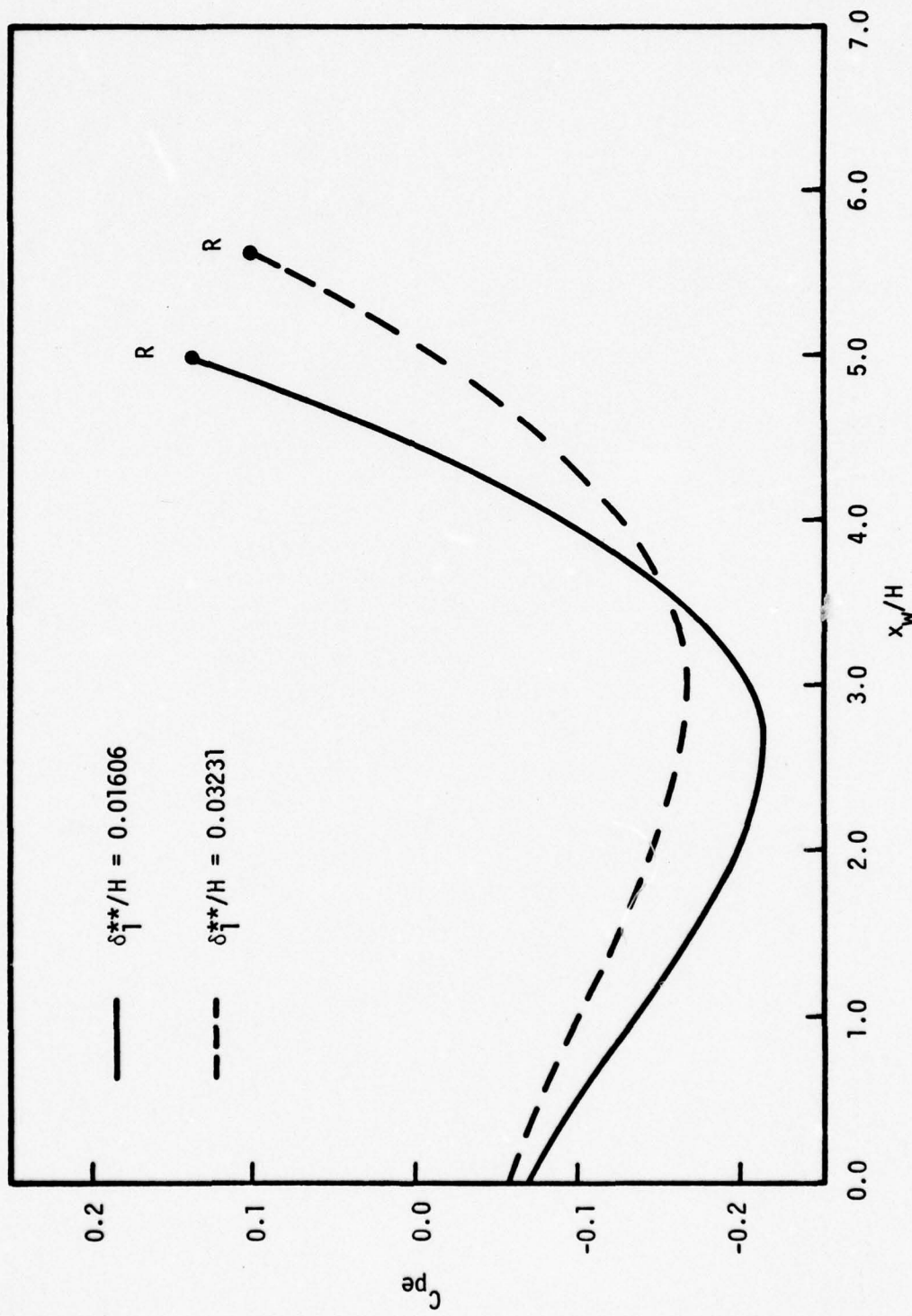


Figure 19 Wall Pressure Distribution as a Function of Initial Momentum Thickness for $M_\infty = 0.75$, $R_s/R_\infty = 0.5$ ($m = 3$ and $\sigma = 12$)

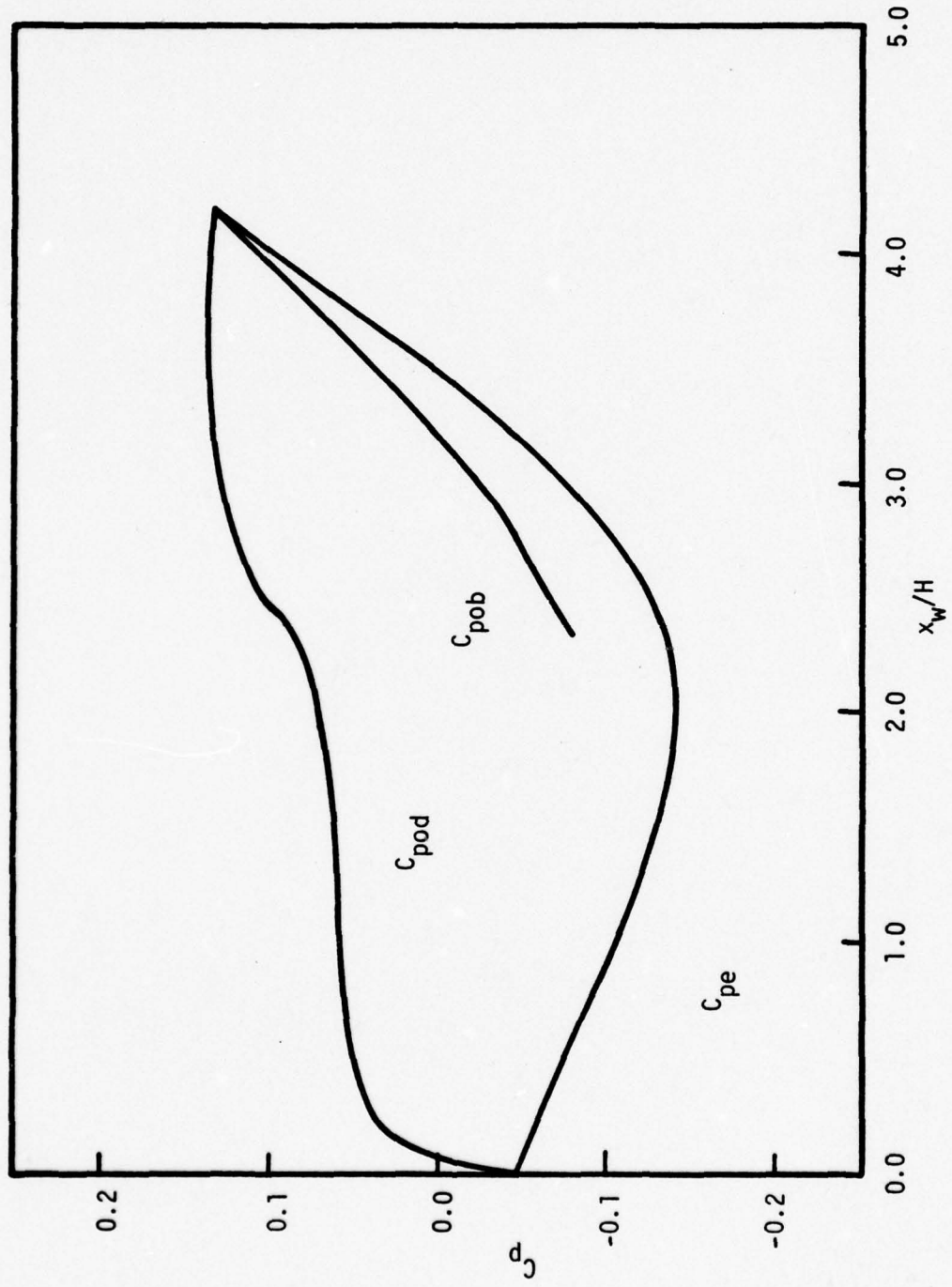


Figure 20 Pressure Distribution in the Wake Region for
 $M_\infty = 0.75$, $R_s/R_o = 0$, $\delta_1^{**}/H = 0.02333$ ($m = 3$ and $\sigma = 12$)

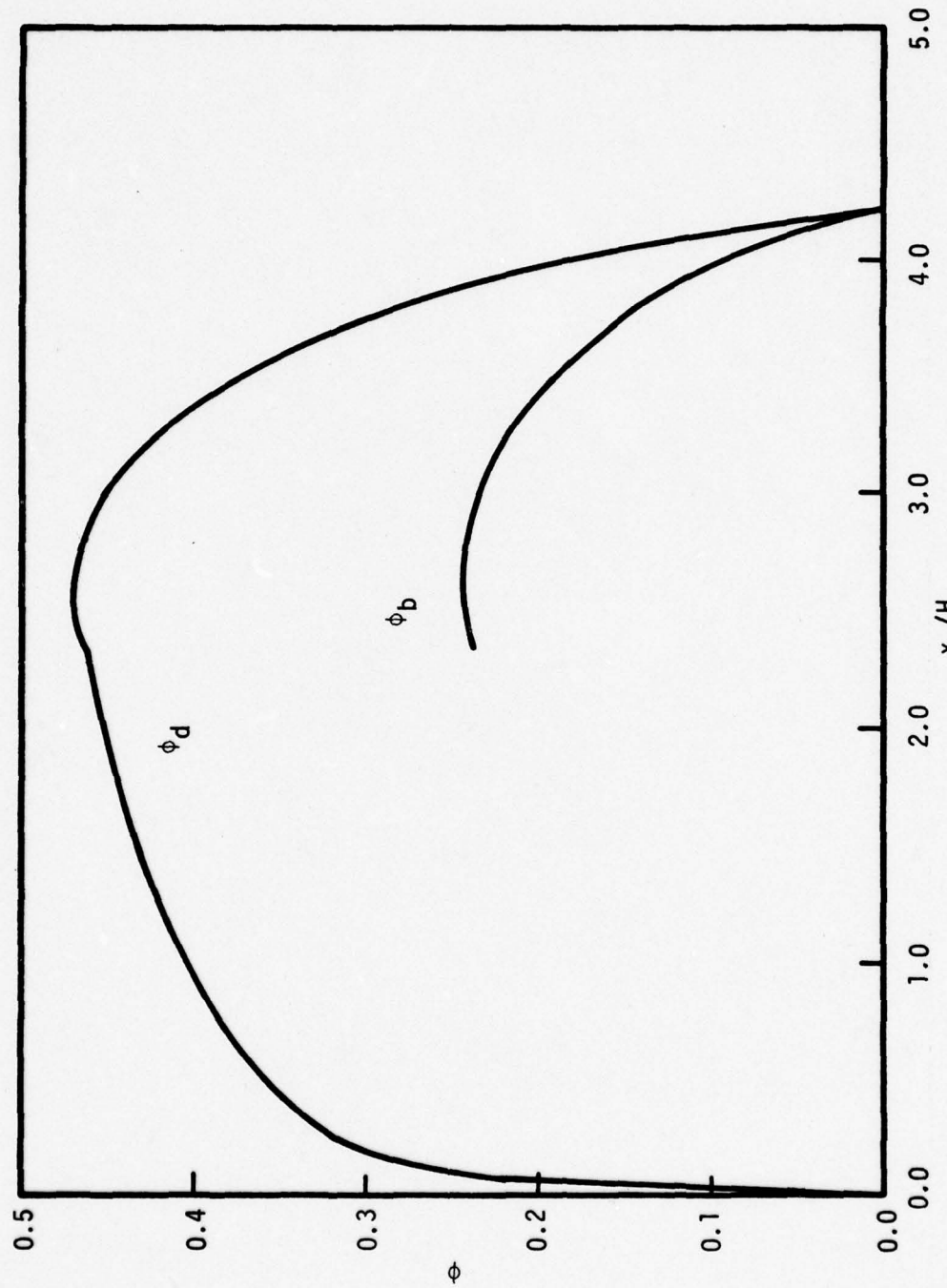


Figure 21 ϕ_d, ϕ_b in the Wake Region for $M_\infty = 0.75$,
 $R_s/R_o = 0$, $\delta_1^{**}/H = 0.02333$ ($m = 3$ and $\sigma = 12$)

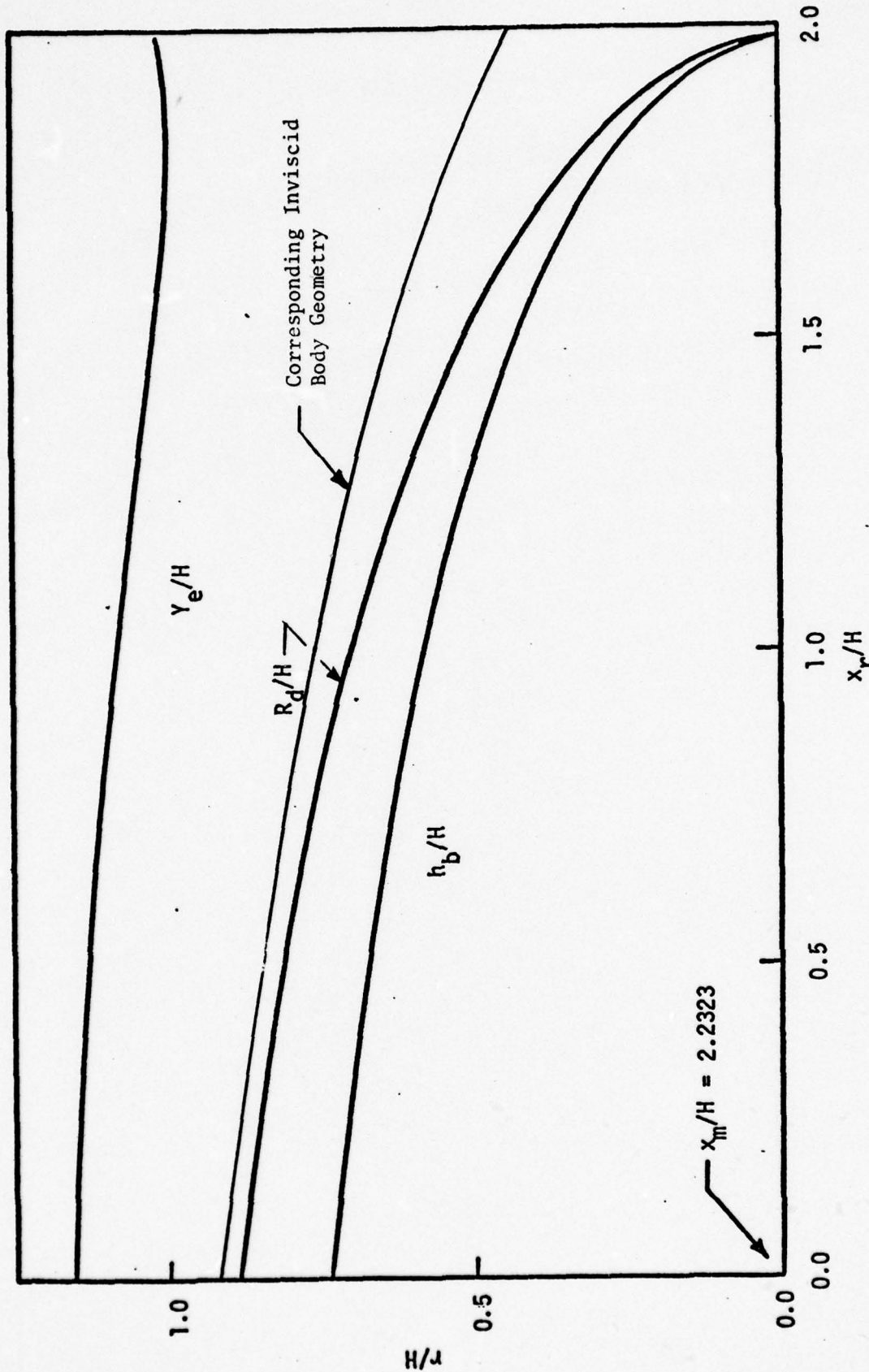


Figure 22 Geometry of the Wake Region for $M_{\infty} = 0.75$, $R_s/R_o = 0$, $\delta_1^{**}/H = 0.2333$, $SH = 0.195$ ($m = 0.195$ and $\sigma = 12$)

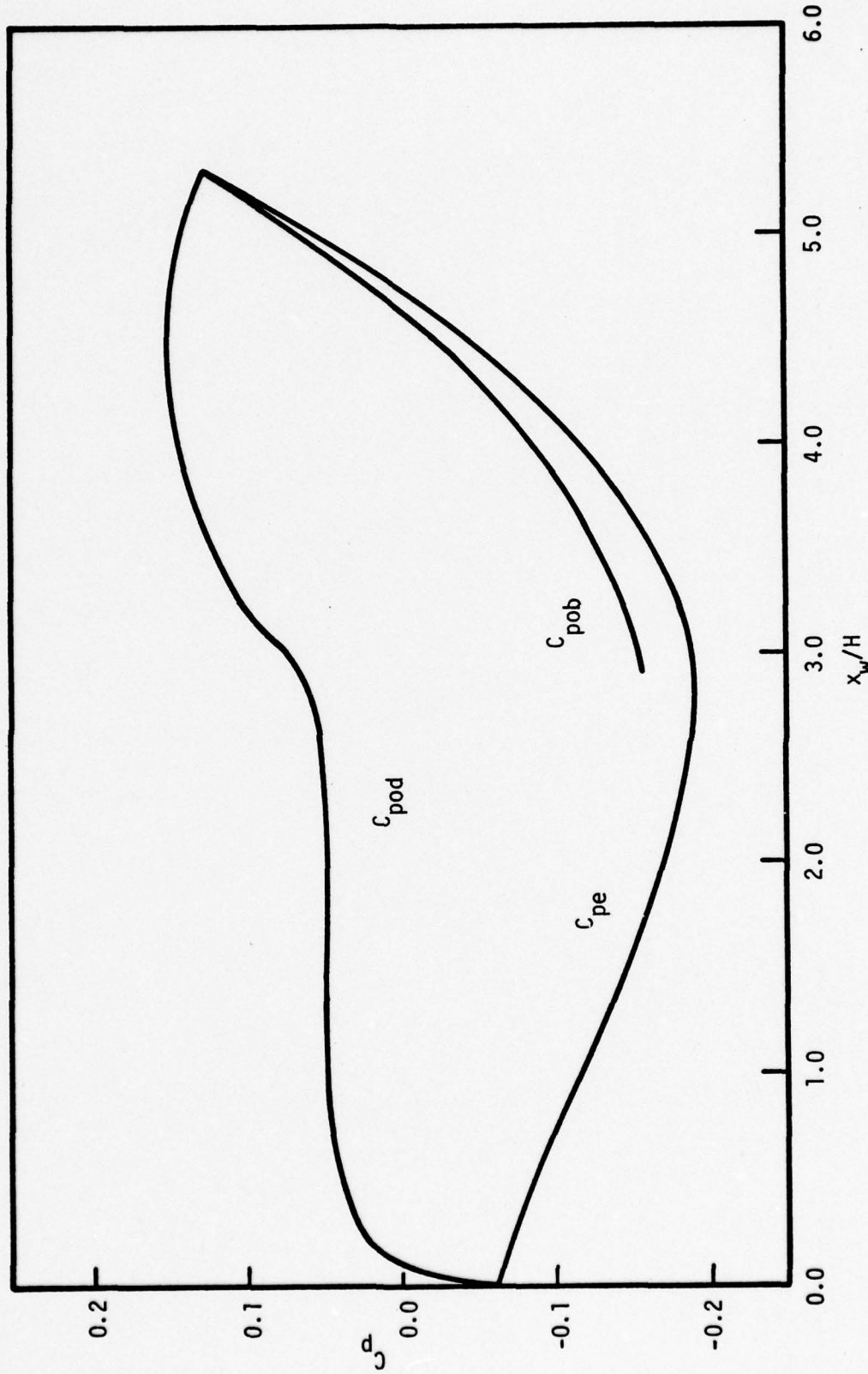


Figure 23 Pressure Distribution in the Wake Region for $M_\infty = 0.75$,
 $R_s/R_0 = 0.5$, $\delta^{**}/H = 0.02207$ ($m = 3$ and $\sigma = 12^\circ$)

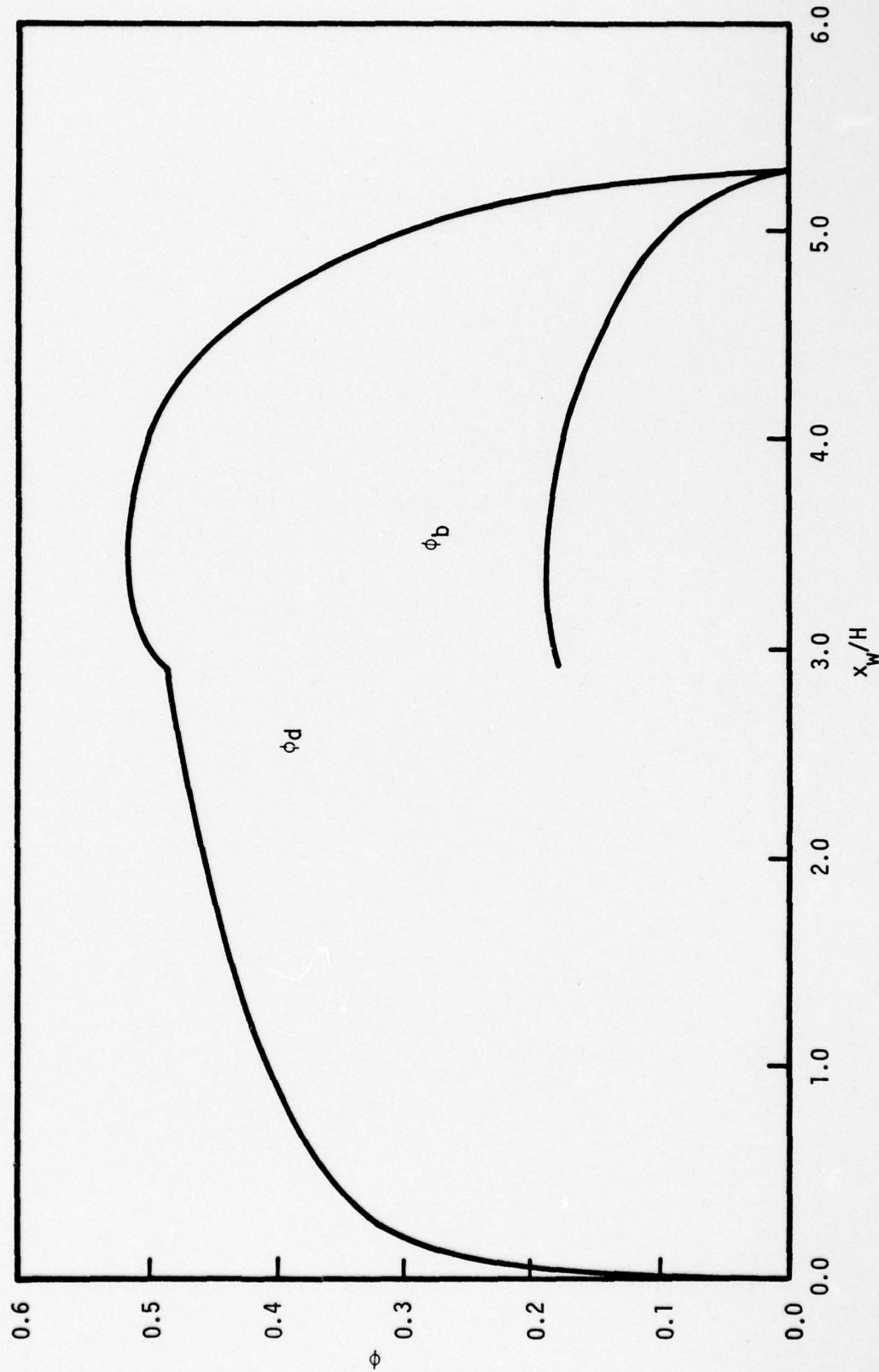


Figure 24 ϕ_d^*, ϕ_b in the Wake Region for $M_\infty = 0.75$, $R_s/R_o = 0.5$, $\delta_1^{**}/H = 0.02207$ ($m = 3$ and $\sigma = 12$)

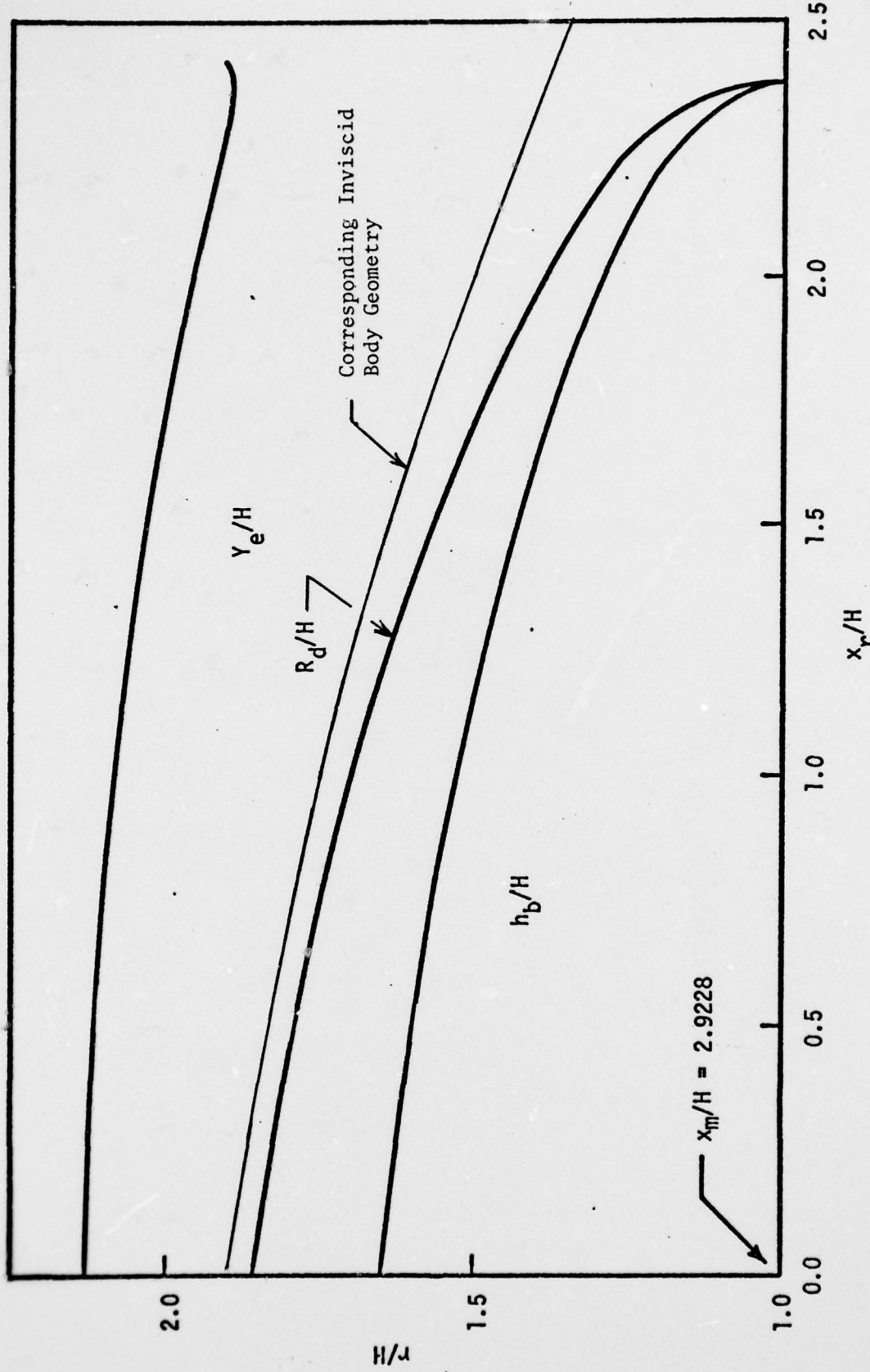


Figure 25 Geometry of the Wake Region for $M_\infty = 0.75$, $R_s/R_o = 0.5$,
 $\delta^{**}/H = 0.02207$, $SH = 0.16$ ($m = 3$ and $\sigma = 12$)

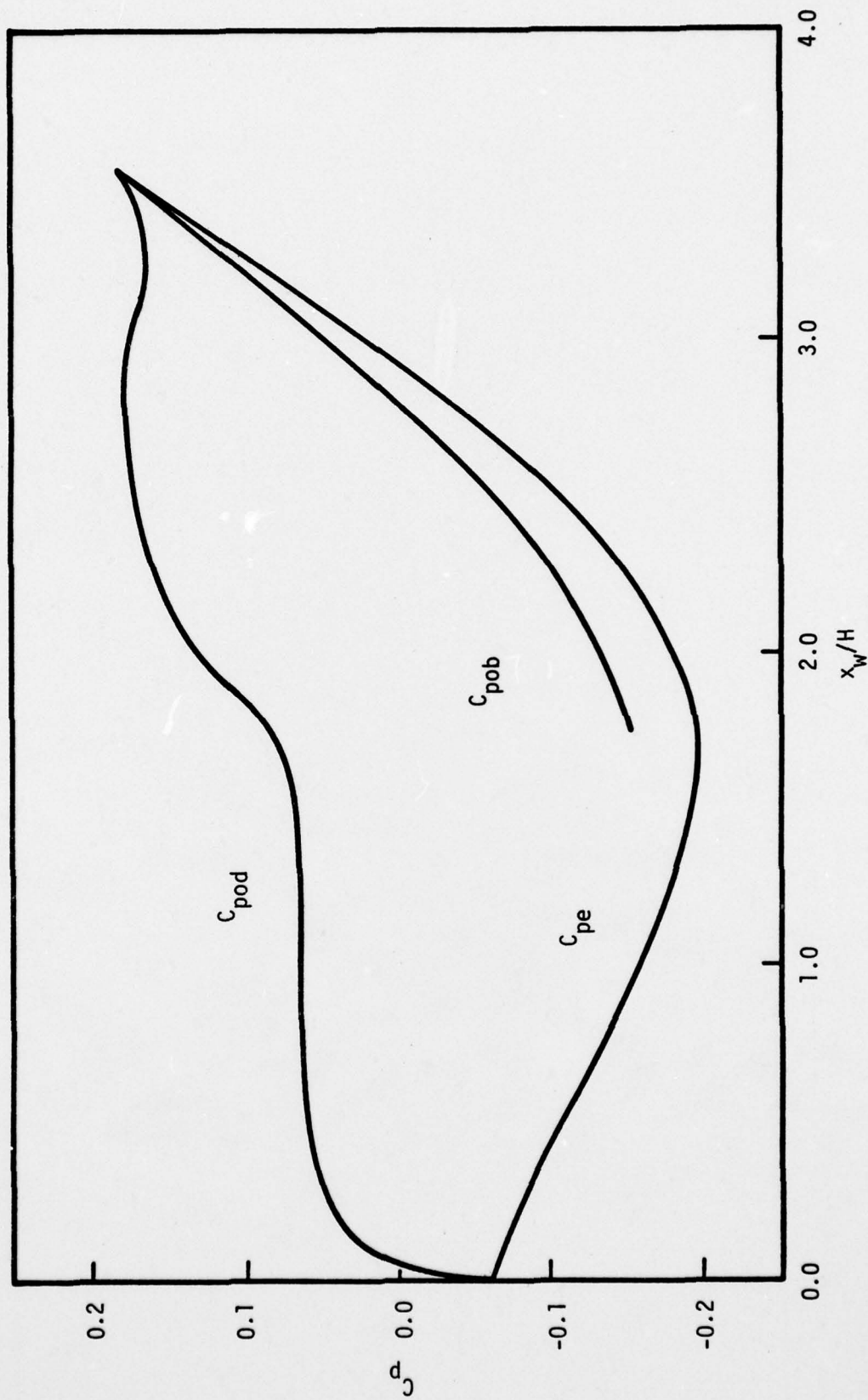


Figure 26 Pressure Distribution in the Wake Region for
 $M_\infty = 0.75$, $R_s/R_o = 0$, $\delta_1^{**}/H = 0.01029$ ($m = 3$ and $\sigma = 12$)

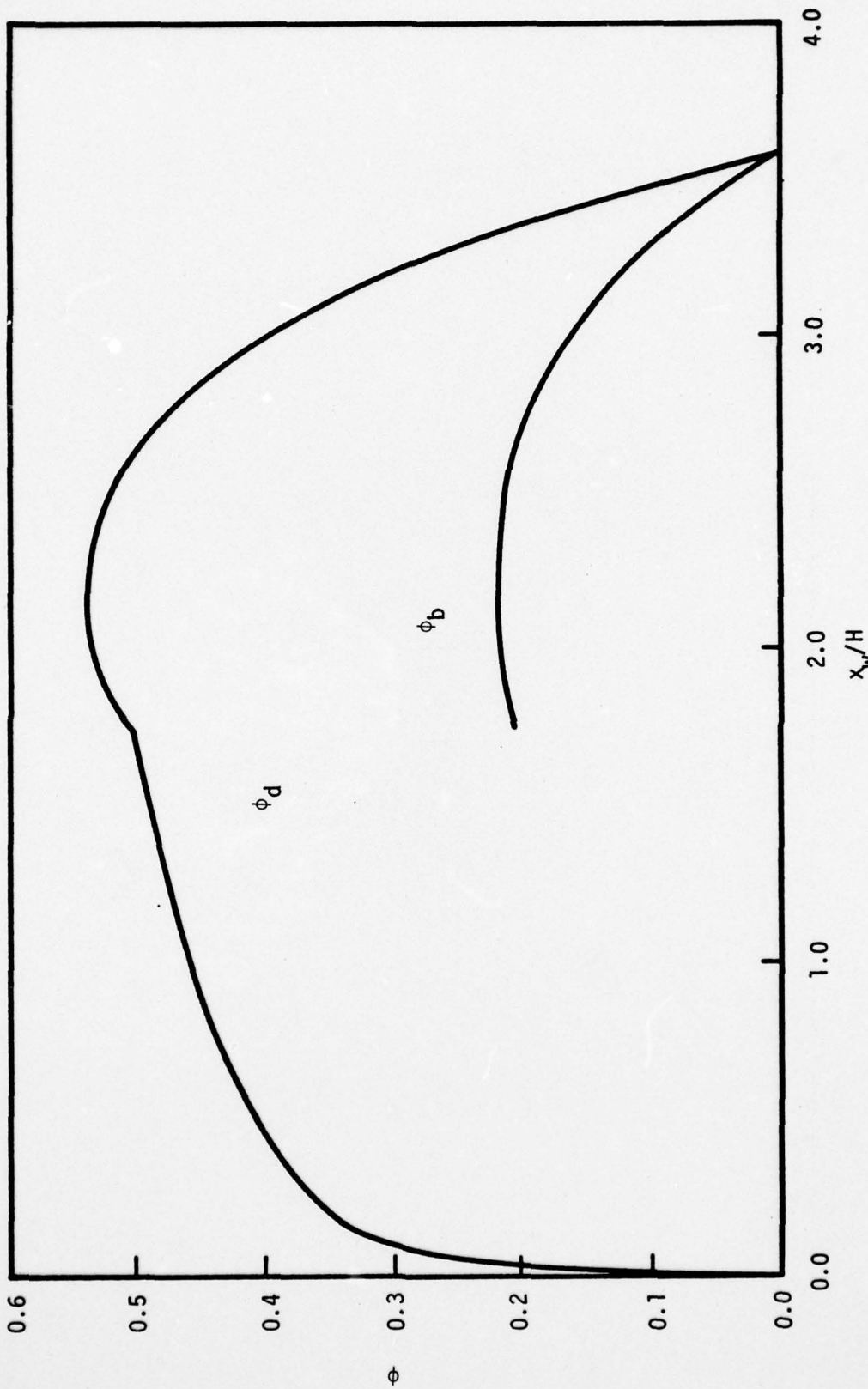


Figure 27 ϕ_d , ϕ_b in the Wake Region for $M_\infty = 0.75$, $R_s/R_0 = 0$,
 $\delta_1^{**}/H = 0.01029$ ($m = 3$ and $\sigma = 12$)

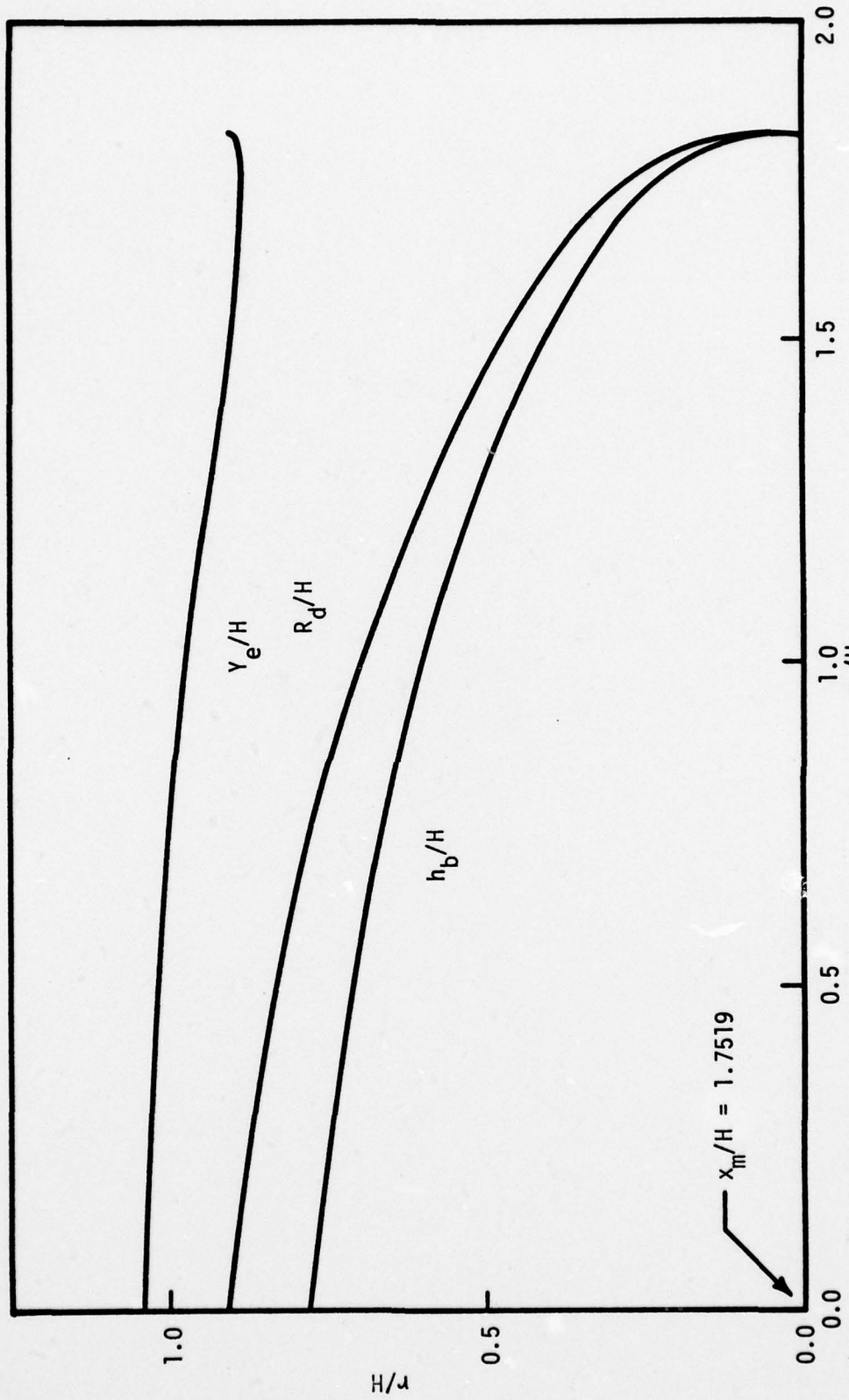


Figure 28 Geometry of Wake Region for $M_\infty = 0.75$, $R_s/R_o = 0$,
 $\delta_1^{**}/H = 0.01029$ ($m = 3$ and $\sigma = 12$)

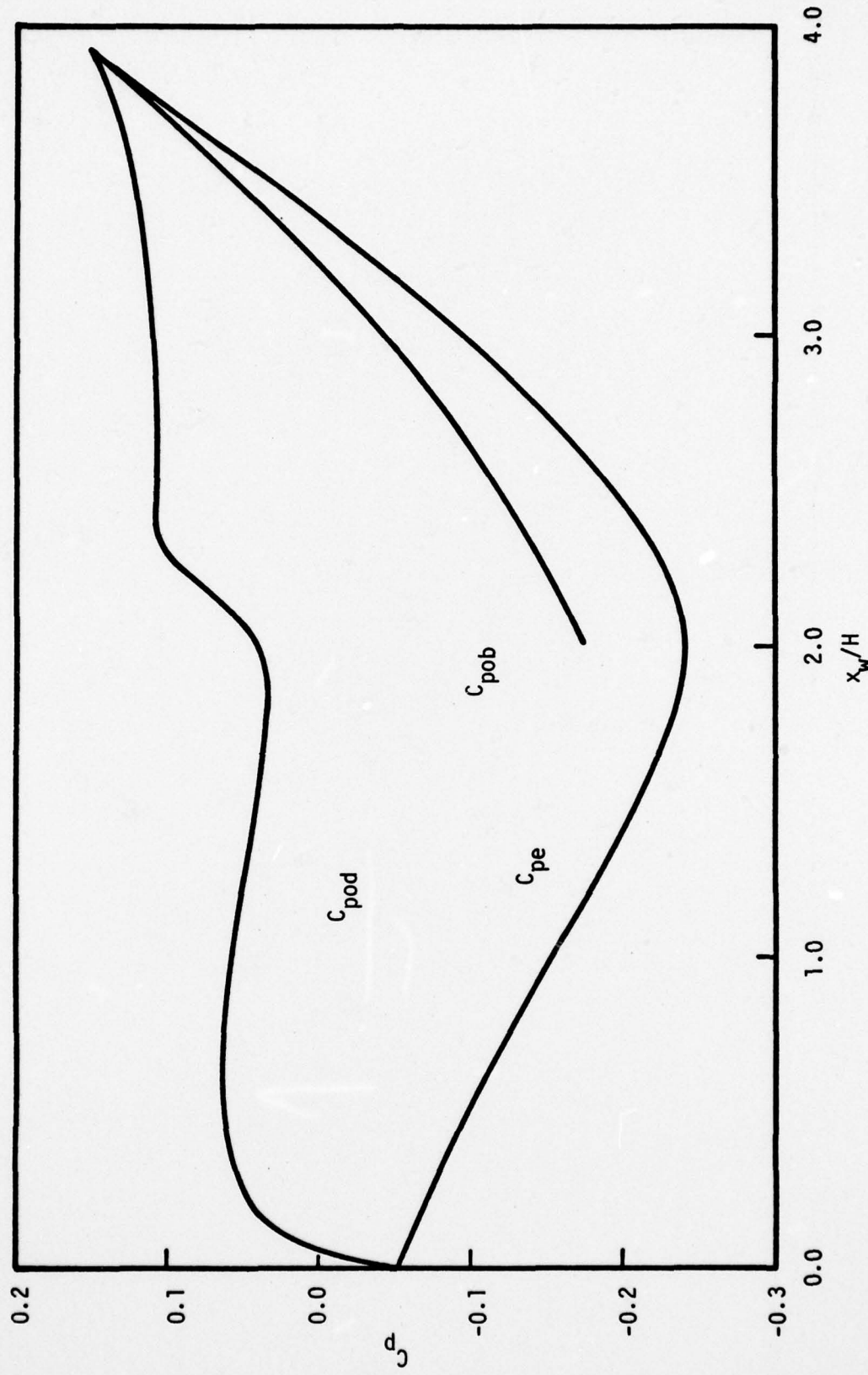


Figure 29 Pressure Distribution in the Wake Region for
 $M_\infty = 0.9$, $R_s/R_o = 0$, $\delta_1^{**}/H = 0.01018$ ($m = 3$ and $\sigma = 12$)

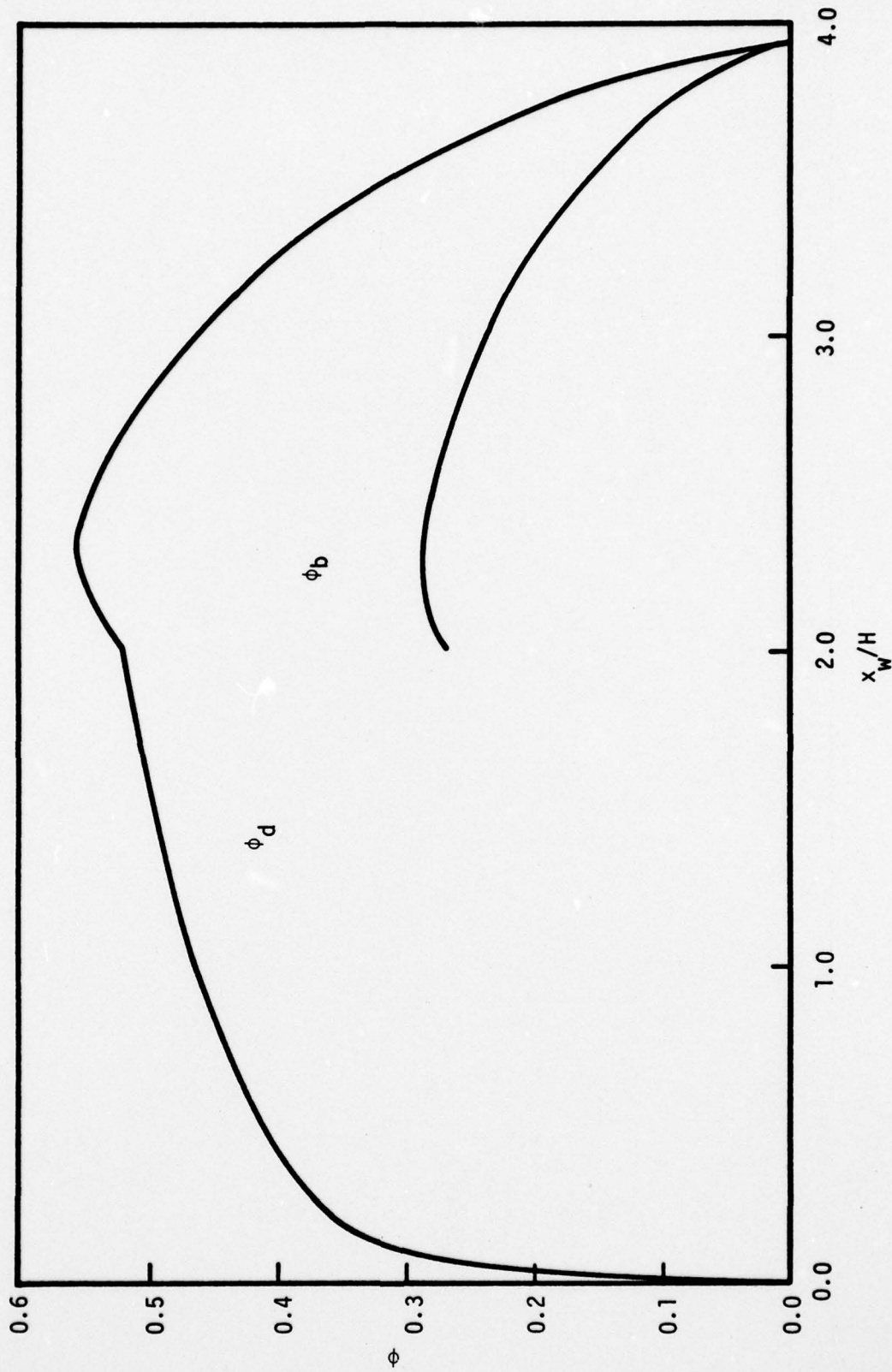


Figure 30 ϕ_d, ϕ_b in the Wake Region for $M_\infty = 0.9, R_s/R_0 = 0,$
 $\delta^{**}/H = 0.01018$ ($m = 3$ and $\sigma = 12$)

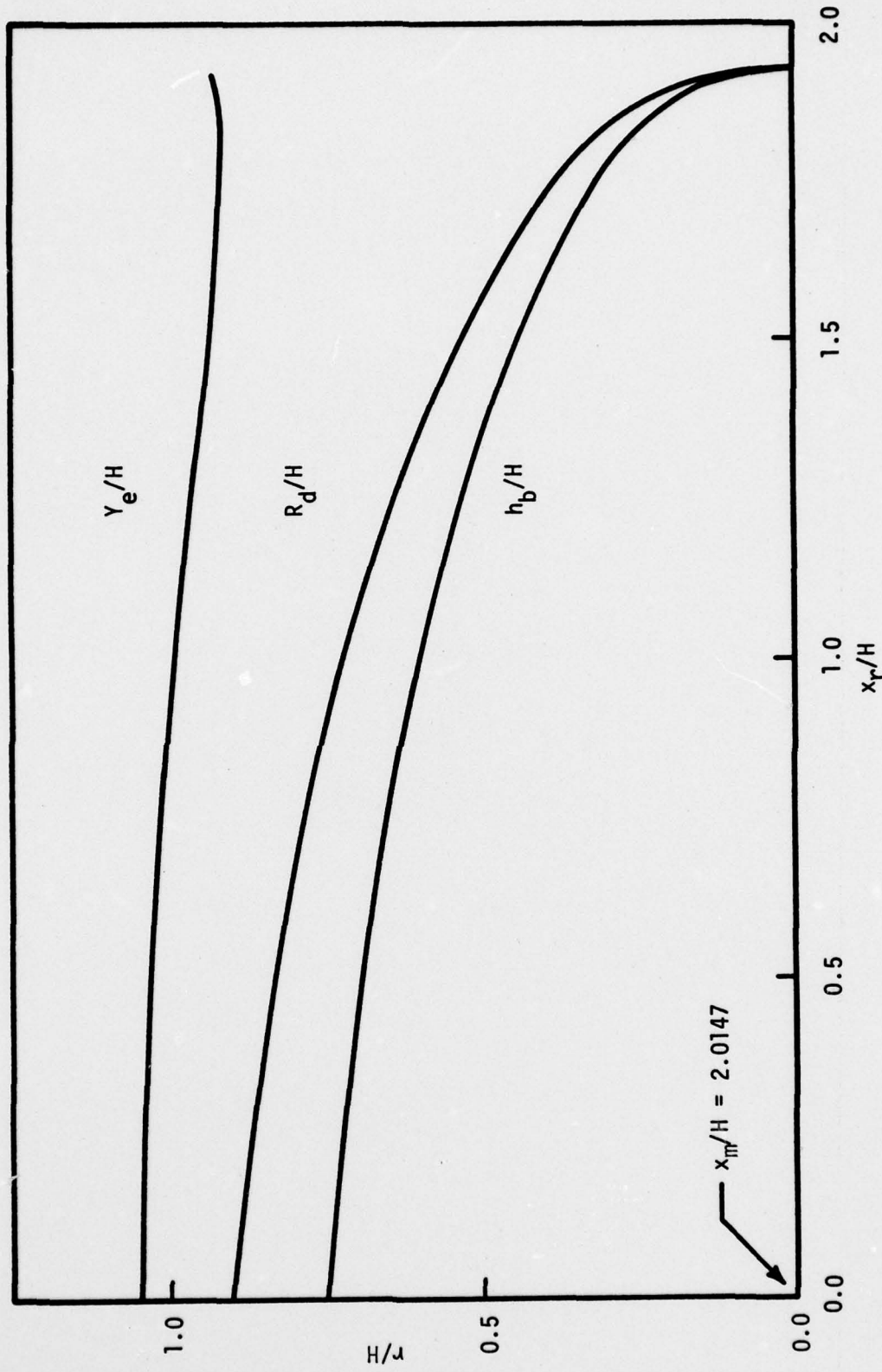


Figure 31 Geometry of the Wake Region for $M_\infty = 0.9$,
 $R_s/R_0 = 0$, $\delta_1^{**}/H = 0.01018$ ($m = 3$ and $\sigma = 12$)

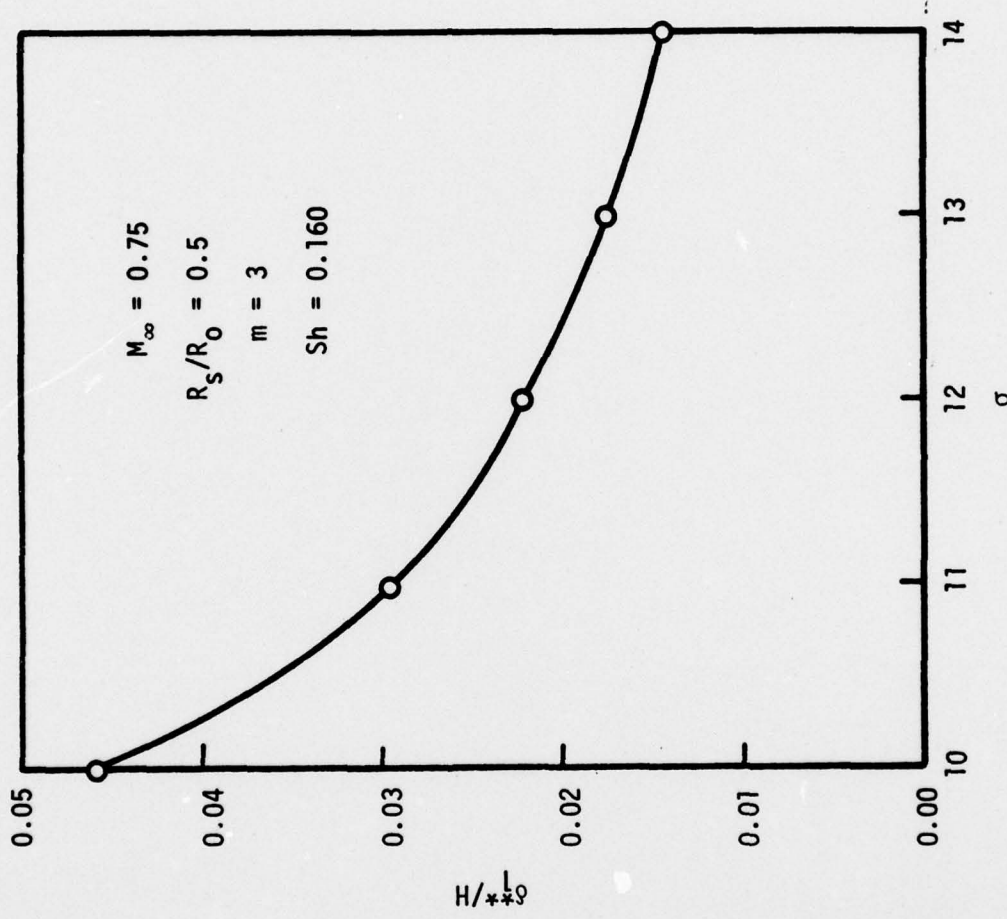


Figure 32 Variation of H_1^{**}/H vs σ for Constant Sh

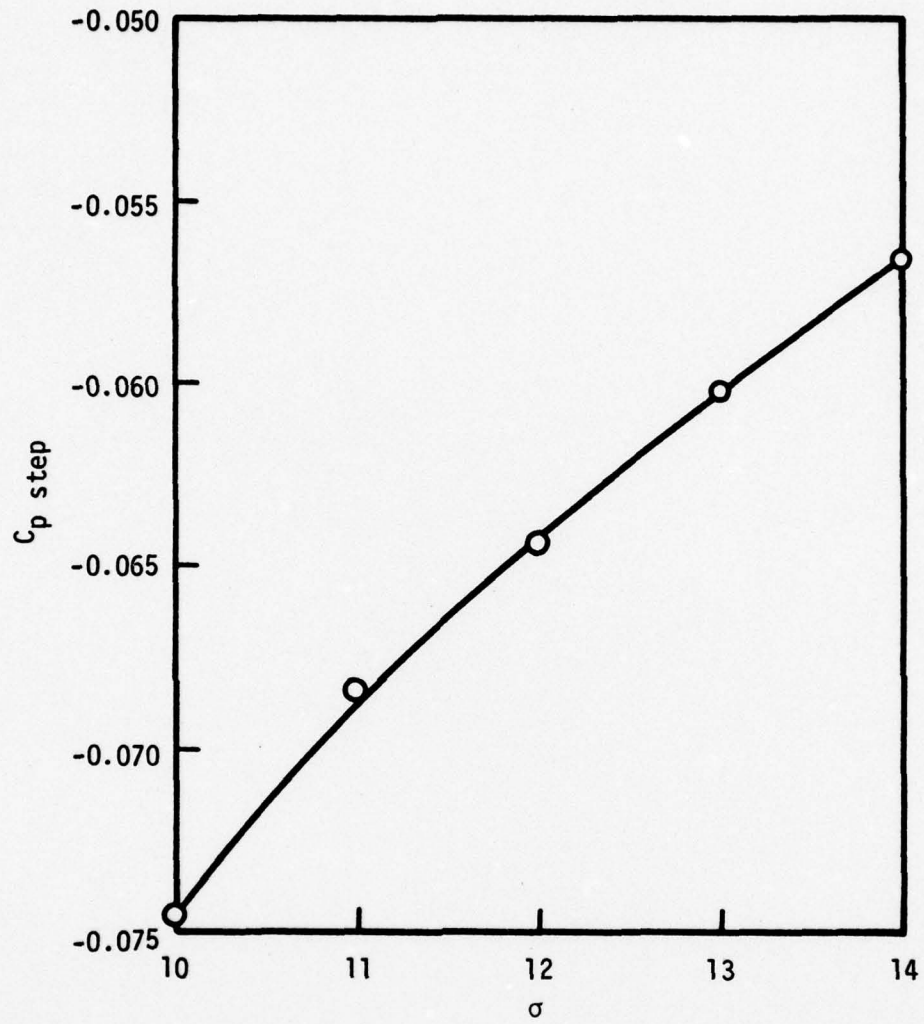


Figure 33 Variation of $C_{p \text{ step}}$ vs σ for
 $M_\infty = 0.75$, $R_s/R_o = 0.5$, and $\delta_1^{**}/H = 0.022$

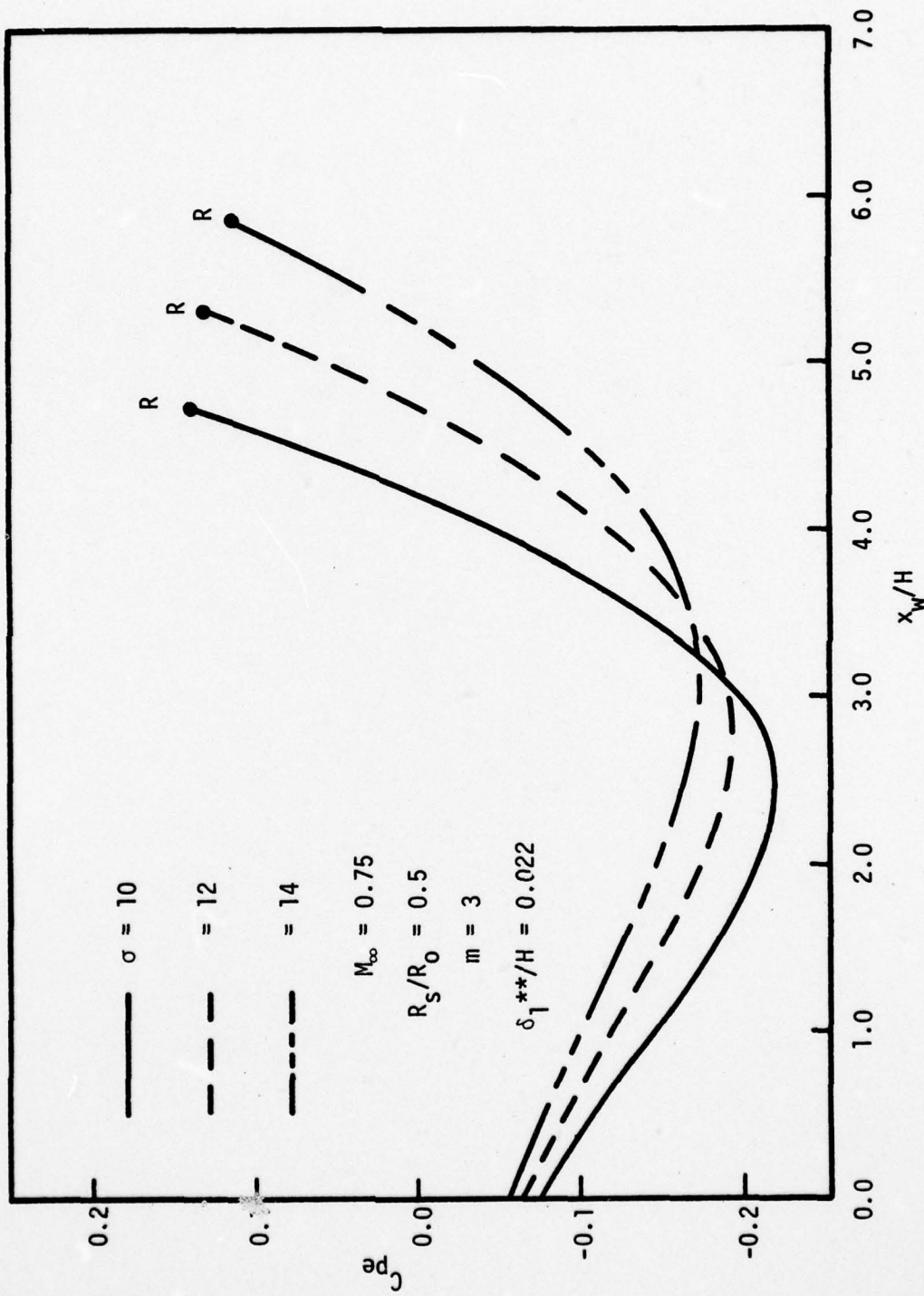


Figure 34 Pressure Distributions in the Wake Region as a Function of σ

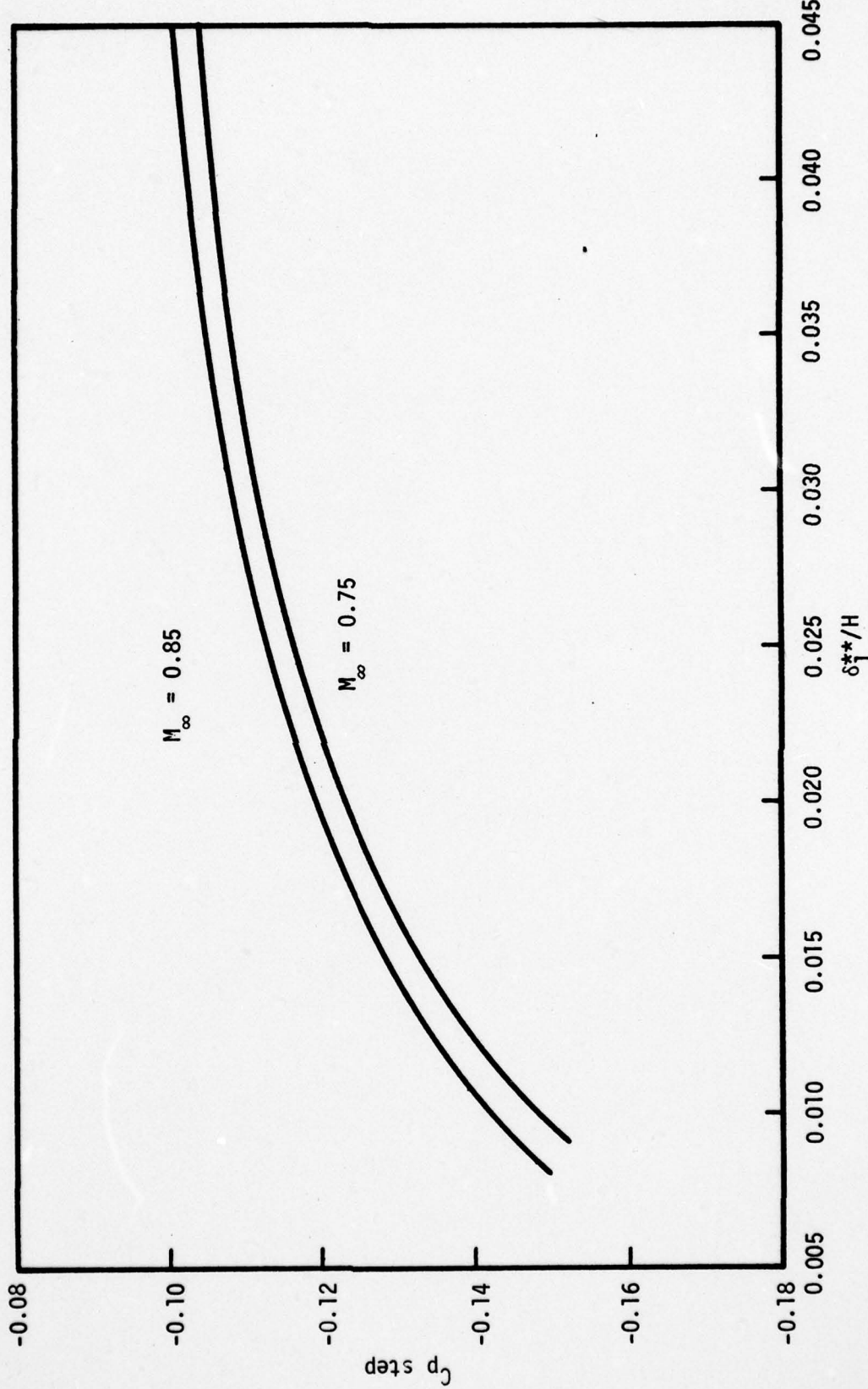


Figure 35 Variation of C_p step vs δ_1^{**}/H as a Function of Mach Number for Zero String Radius Ratio ($m = 2$ and $\sigma = 12$)

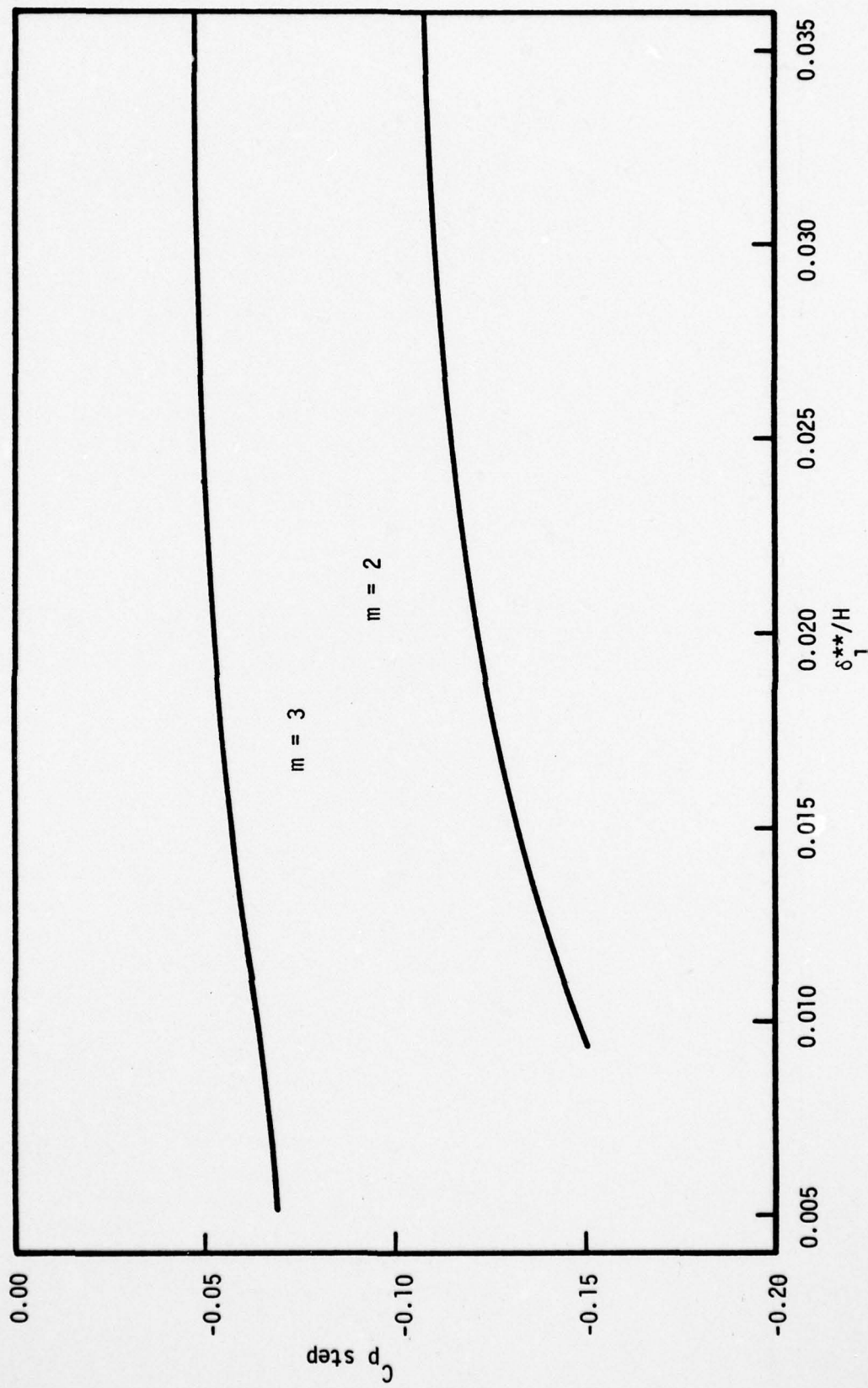


Figure 36 Comparison of C_p step vs δ_1^{**}/H for $m = 3$ and $m = 2$
for $M_\infty = 0.75$, $R_s/R_0 = 0$ and $\sigma = 12$

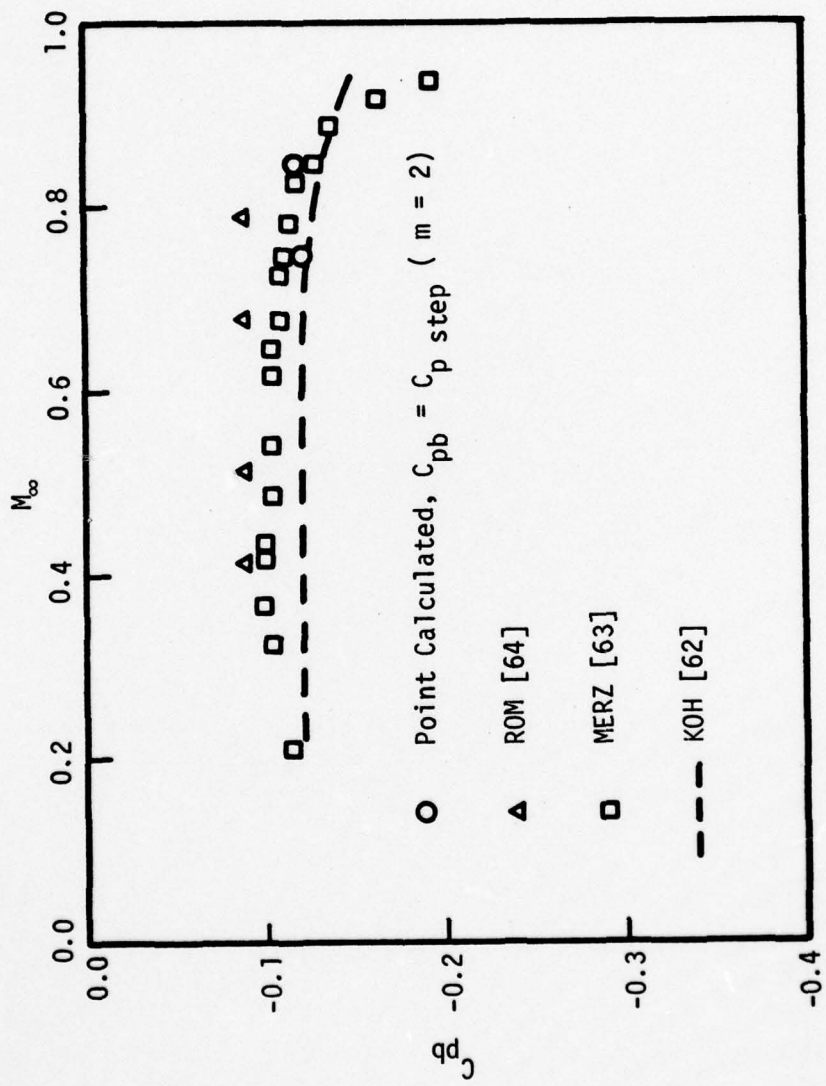


Figure 37 Comparison of Base Pressure
with Experimental Data

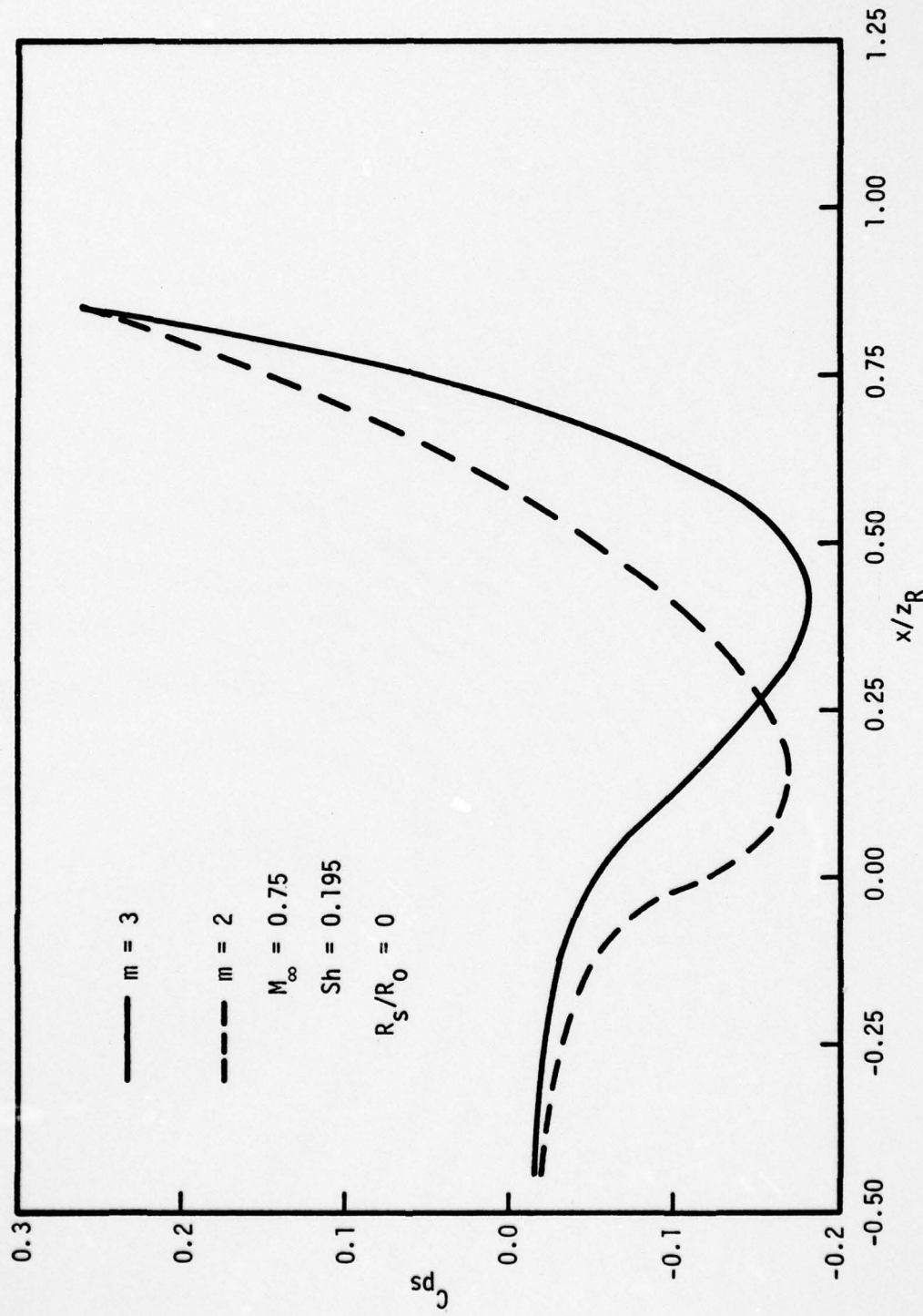


Figure 38 Comparison of Pressure Distribution of Inviscid Calculation of $m = 3$ and $m = 2$

AD-A050 658

ILLINOIS UNIV AT URBANA-CHAMPAIGN DEPT OF MECHANICAL --ETC F/G 20/4
BASE PRESSURE PROBLEMS ASSOCIATED WITH AN AXISYMMETRIC TRANSONIC--ETC(U).
NOV 77 J S LIU, W L CHOW

DAAG29-76-6-0199

UNCLASSIFIED

ME-TR-395-5

ARO-13510.3-E

NL

2 OF 2
AD
A050 658



END
DATE
FILED
4-78
DDC

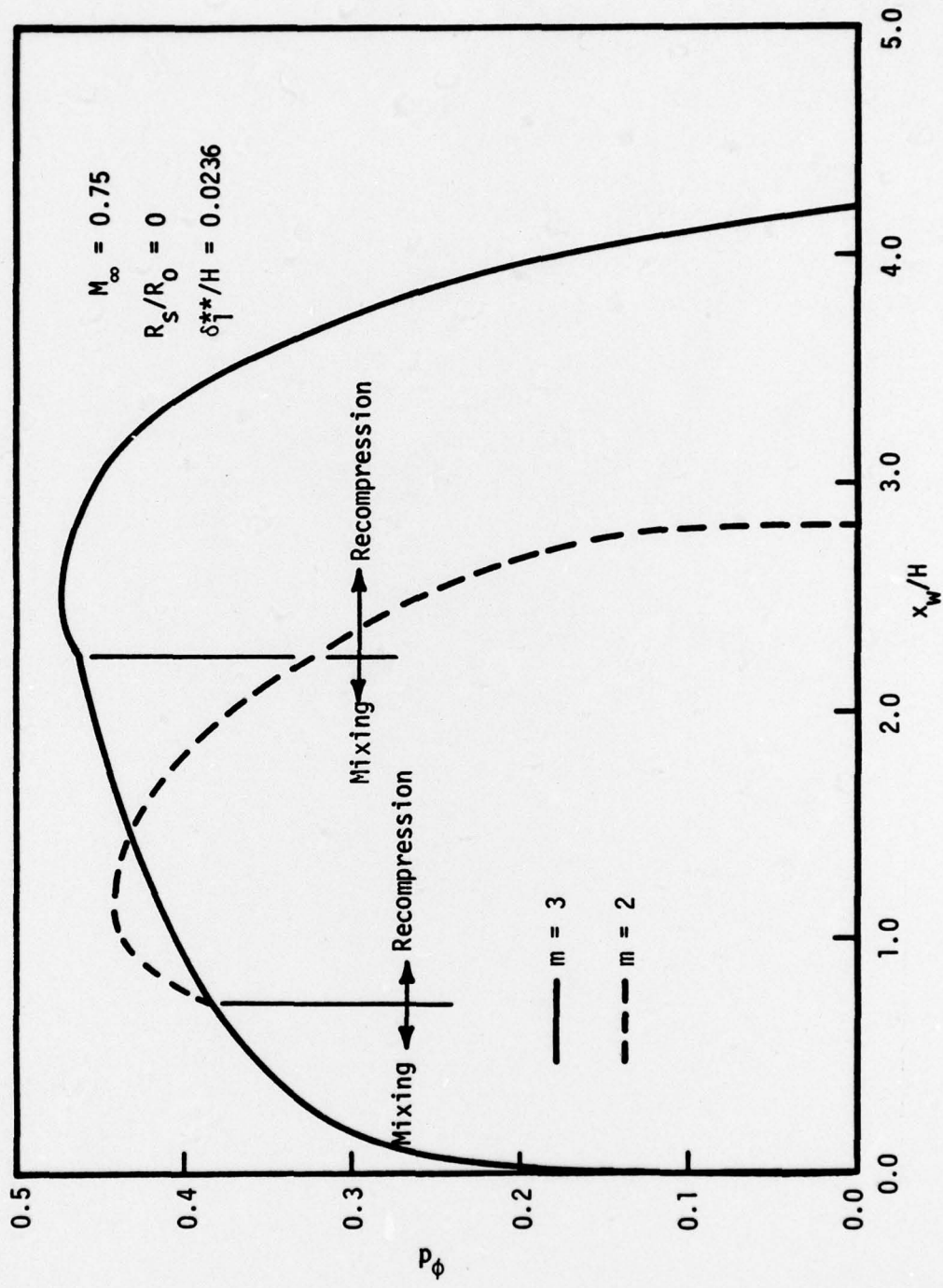


Figure 39 Comparison of ϕ_d in the Wake Region of $m = 3$ and $m = 2$

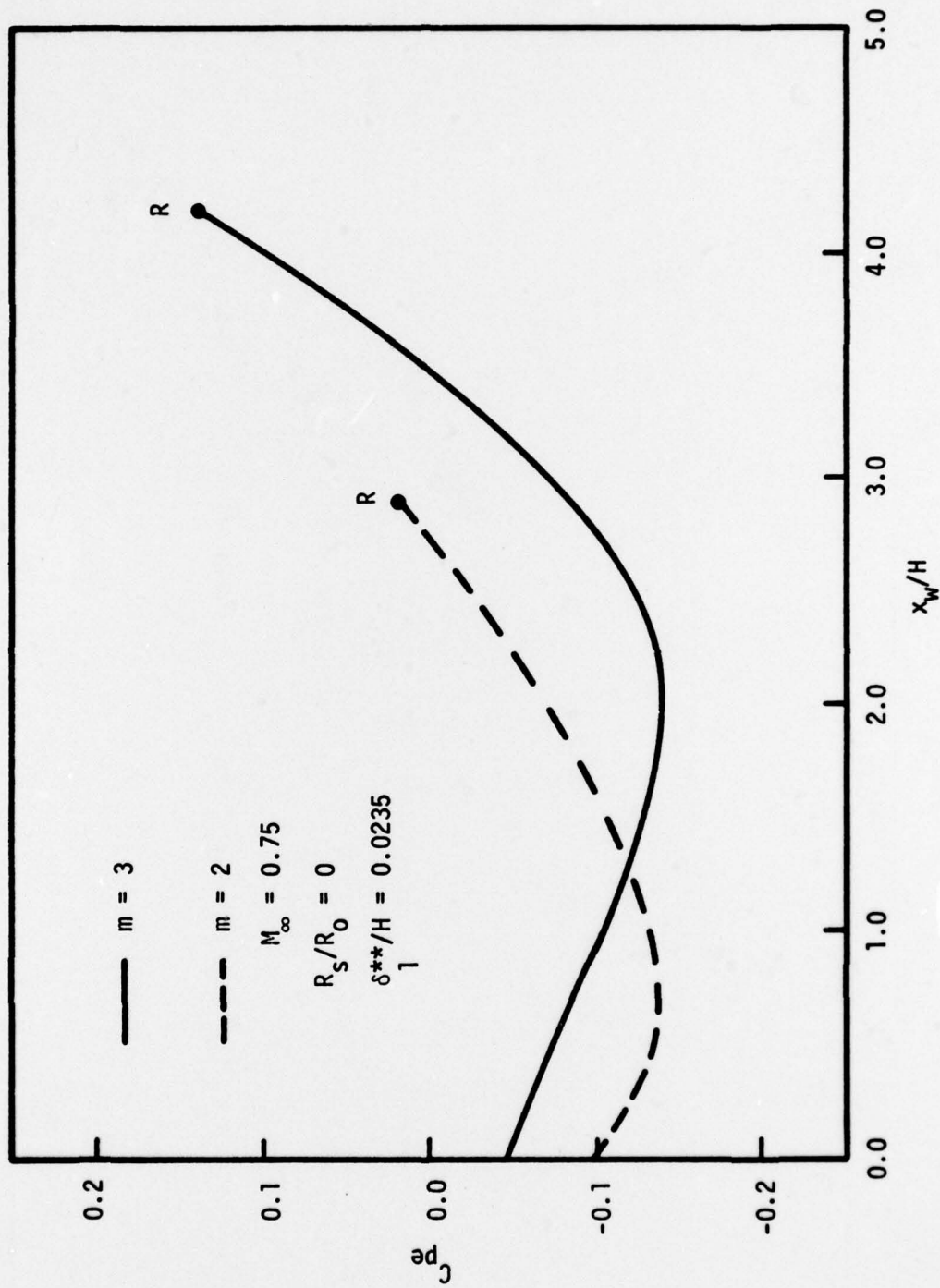


Figure 40 Comparison of Pressure Distribution in the Wake Region of $m = 3$ and $m = 2$

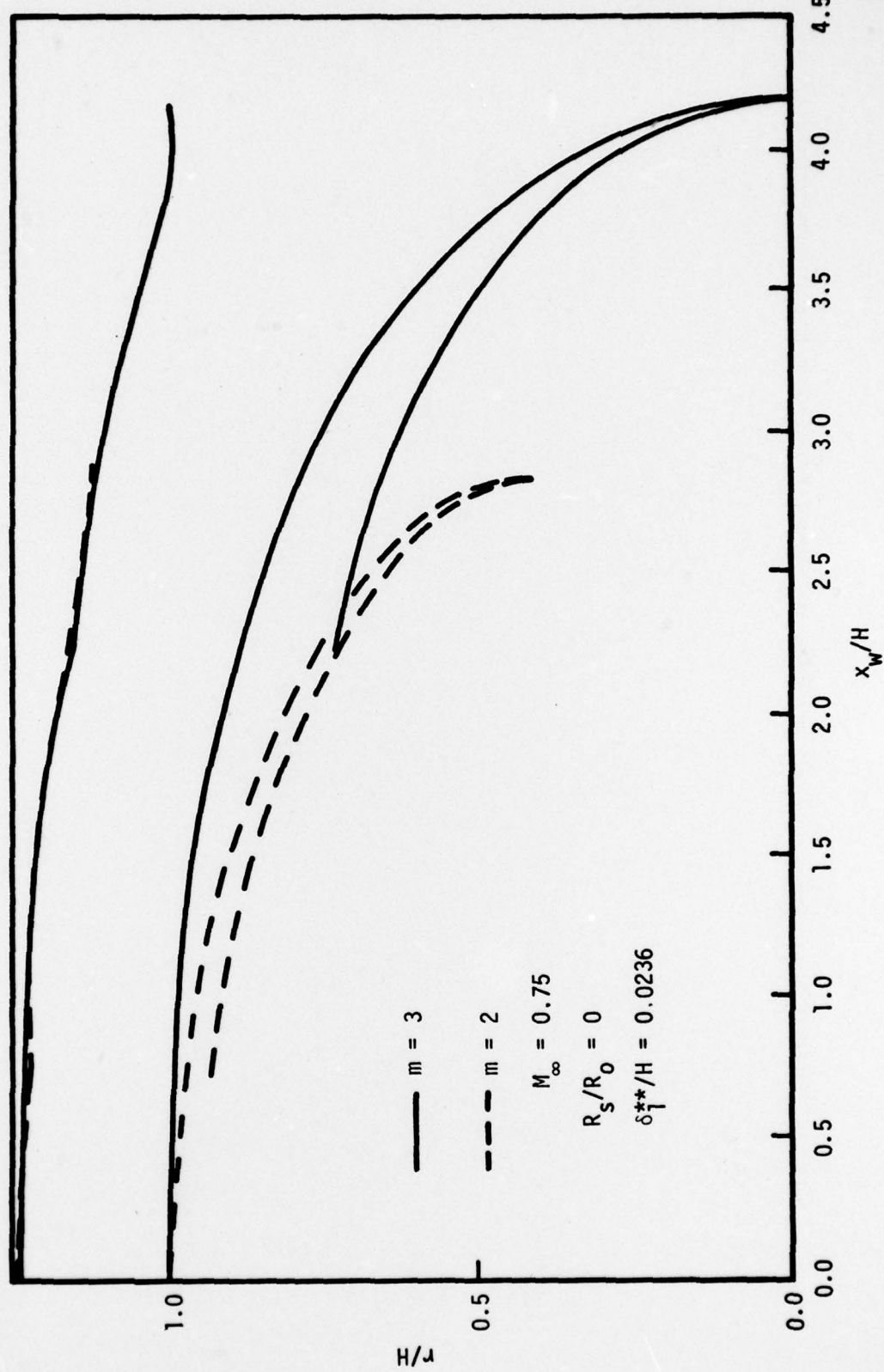


Figure 41 Comparison of Wake Geometry of $m = 3$ and $m = 2$

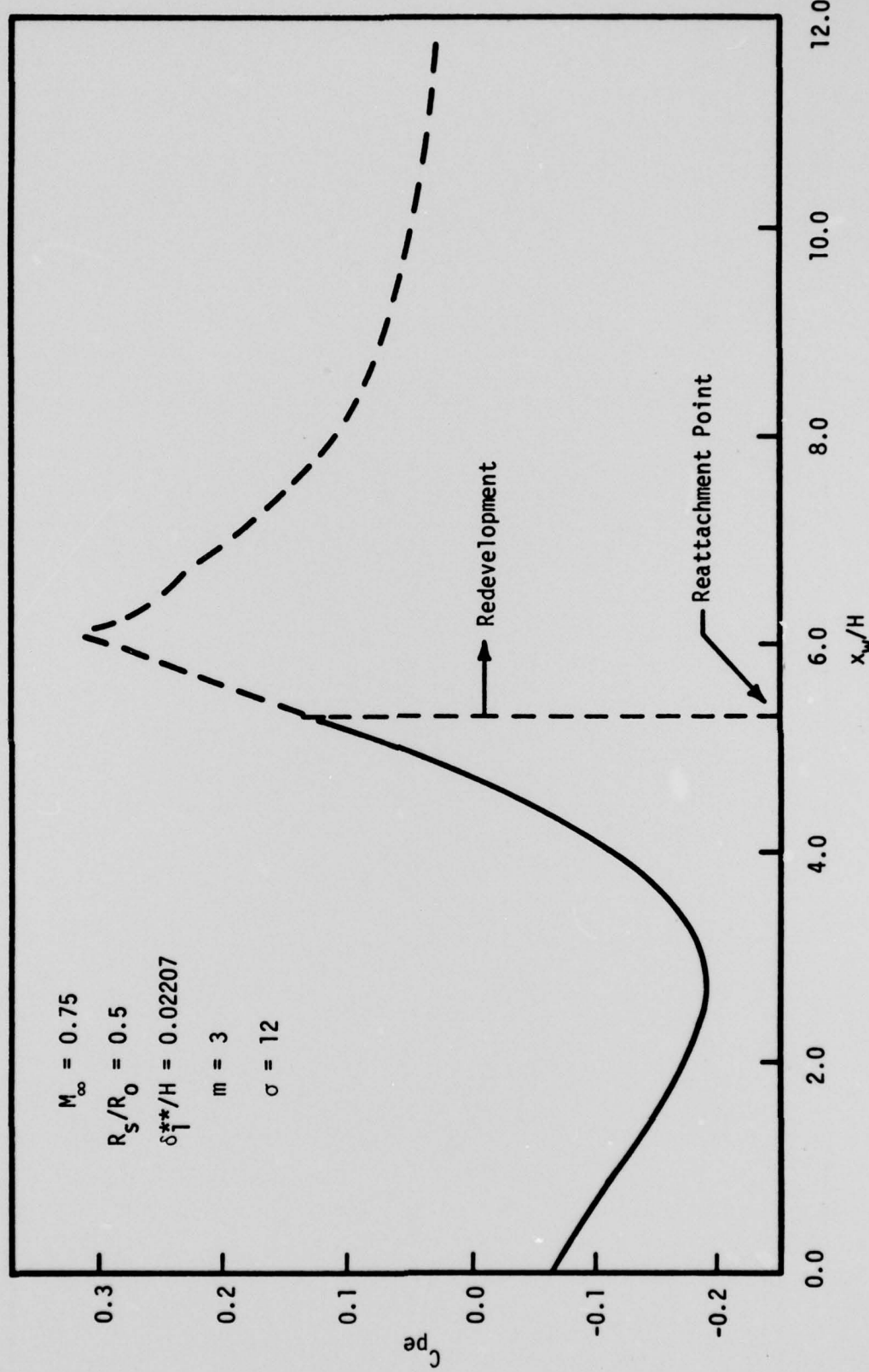


Figure 42 Pressure Distribution in the Wake Region with Rederevelopment
Pressure obtained by Streamline Tracing

BIBLIOGRAPHY

1. Liu, J. S. K., "Base Pressure Problems associated with an Axisymmetric Transonic Flow past a Backward Facing Step," Ph.D. Thesis, Department of Mech. and Ind. Engr., University of Illinois at Urbana-Champaign, October 1977.
2. Korst, H. H., R. H. Page, and M. E. Childs, "A Theory for Base Pressure in Transonic and Supersonic Flow," ME TN-392-2, Department of Mech. and Ind. Engr., University of Illinois, 1955.
3. Wuerer, J. E., and F. I. Clayton, "Flow Separation in High Speed Flight--A Review of the State of the Art," Douglas Report SM-46429, Missile and Space Systems Division, Douglas Aircraft Co., Inc., Santa Monica, California, April 1965.
4. Carpenter, P. W., and W. Tabakoff, "Survey and Evaluation of Supersonic Base Flow Theories," NASA CR-97129, 1968.
5. Chang, P. K., Separation of Flow, Pergamon Press, London, 1970.
6. Berger, S. A., Laminar Wakes, American Elsevier Publishing Co., Inc., New York, 1971.
7. Page, R. H., "A Review of Component Analysis of Base Pressure for Supersonic Turbulent Flow," Proc., Tenth International Symposium on Space Technology and Science, Tokyo, 1973. pp. 459-469.
8. Crocco, L., and L. Lees, "A Mixing Theory for the Interaction between Dissipative Flows and Nearly Isentropic Streams," J. of Aerospace Sci., Vol. 19, 1952, pp. 649-676.
9. Lees, L., and B. L. Reeves, "Supersonic Separated and Reattaching Laminar Flows: I. General Theory and Application to Adiabatic Boundary Layer/Shock Wave Interactions," AIAA J., Vol. 2, 1964, pp. 1907-1920.
10. Reeves, B. L., and L. Lees, "Theory of Laminar Near Wake of Blunt Bodies in Hypersonic Flow," AIAA J., Vol. 3, 1965, pp. 2061-2074.
11. Stewartson, K., "Further Solutions of the Falkner-Skan Equation," Proc., Cambridge Phil. Soc., Vol. 50, 1954, pp. 454-465.
12. Alber, I. E., "Integral Theory for Turbulent Base Flows at Subsonic and Supersonic Speeds," Ph.D. Thesis, California Institute of Technology, Pasadena, Cal., June 1967.
13. Alber, I. E., and L. Lees, "Integral Theory for Supersonic Turbulent Base Flows," AIAA J., Vol. 6, 1968, pp. 1343-1351.
14. Todisco, A., and B. L. Reeves, "Turbulent Boundary Layer Separation and Reattachment at Supersonic and Hypersonic Speeds," Proc., Symposium on Viscous Interaction Phenomena in Supersonic and Hypersonic Flow, 1969, University of Dayton Press, pp. 139-179.

15. Hunter, L. G., Jr., and B. L. Reeves, "Results of a Strong Interaction, Wake-like Model of Supersonic Separated and Reattaching Turbulent Flows," AIAA J., Vol. 9, 1971, pp. 703-712.
16. Shamroth, S. J., and H. McDonald, "A New Solution of the Turbulent Near-Wake Recompression Problem," AIAA Paper No. 70-228, 1970.
17. Strahle, W. C., and Mehta, G., "Turbulent Axisymmetric Base Flow Studies for External Burning Propulsion," 11th JANNAF Combustion Meeting, Vol. II, CPIA Publication 261, December 1974, pp. 441-448.
18. Strahle, W. C., et al., "Turbulent Axisymmetric Base Flow Studies for External Burning Propulsion," Paper presented at 12th JANNAF Combustion Meeting, Newport, Rhode Island, August 1975.
19. Chapman, D. R., "An Analysis of Base Pressure at Supersonic Velocities and Comparison with Experiment," NACA TN-2137, 1950.
20. Chapman, D. R., "An Analysis of Base Pressure at Supersonic Velocities and Comparison with Experiment," NACA Report 1051, 1951.
21. Korst, H. H., "A Theory for Base Pressure in Transonic and Supersonic Flow," J. Appl. Mech., Vol. 23, 1956, pp. 593-600.
22. Korst, H. H., "Auflösung eines ebenen Freistrahrlandes bei Berücksichtigung der ursprünglichen Grenzschichtströmung," Osterreichisches Ingenieur-Archiv., Vol. 7, No. 2, 1954.
23. Korst, H. H., R. H. Page, and M. E. Childs, "Compressible Two-Dimensional Jet Mixing at Constant Pressure," ME-TN 392-1, Department of Mechanical and Industrial Engineering, University of Illinois, 1954.
24. Korst, H. H., W. L. Chow, and G. W. Zumwalt, "Research on Transonic and Supersonic Flow of a Real Fluid at Abrupt Increases in Cross Section," ME TR 392-5, Department of Mechanical and Industrial Engineering, University of Illinois, 1959.
25. Chapman, D. R., D. M. Kuehn, and H. K. Larson, "Investigation of Separated Flows in Supersonic and Subsonic Streams with Emphasis on the Effect of Transition," NACA TN 3869, 1957.
26. Chapman, D. R., D. M. Kuehn, and H. K. Larson, "An Investigation of Separated Flows in Supersonic and Subsonic Streams with Emphasis on the Effect of Transition," NACA Report 1356, 1958.
27. Nash, J. F., "An Analysis of Two-dimensional Turbulent Base Flow Including the Effect of the Approaching Boundary Layer," NPL Aero. Report 1036, 1962.
28. Carriere, P., and M. Sirieix, "Facteurs d'Influence du Recollement d'un Ecollement Supersonique," Proc., 10th International Congress of Applied Mechanics, Italy, September 1960.

29. Golik, R. J., "On the Dissipative Mechanisms within Separated Flow Regions," Ph.D. Thesis, Department of Mechanical and Industrial Engineering, University of Illinois, 1962.
30. Hill, W. G., Jr., and R. H. Page, "Initial Development of Turbulent Compressible Free Shear Layers," J. of Basic Engineering, Vol. 91, 1969, pp. 67-73.
31. Zumwalt, G. W., "Analytical and Experimental Study of the Axially-Symmetric Supersonic Base Pressure Problem," Ph.D. Thesis, Department of Mechanical and Industrial Engineering, University of Illinois, 1959.
32. Mueller, T. J., "Determination of the Turbulent Base Pressure in Supersonic Axisymmetric Flow," J. of Spacecraft and Rockets, Vol. 5, No. 1, 1968. pp. 101-107.
33. McDonald, H., "Turbulent Shear Layer Reattachment with Special Emphasis on the Base Pressure Problem," Aeronautical Quarterly, Vol. XV, August 1964, pp. 247-280.
34. McDonald, H., "An Analysis of the Turbulent Base Pressure Problem in Supersonic Axisymmetric Flow," Aeronautical Quarterly, Vol. XVI, May 1965, pp. 97-121.
35. Nielson, J. N., L. K. Lynes, and F. K. Goodwin, "Calculation of Laminar Separation with Free Interaction by the Method of Integral Relations," Report AFFDL-TR-65-107, Part II, VIDYA Div., ITEK Corp., January 1966.
36. Roache, P. J., and T. J. Mueller, "Numerical Solution of Laminar Separated Flows," AIAA J., Vol. 8, 1970, pp. 530-538.
37. Lamb, J. P., and C. G. Hood, "An Integral Analysis of Turbulent Reattachment Applied to Plane Supersonic Base Flow," J. of Engineering for Industry, November 1966, pp. 553-560.
38. Reda, D. C., and R. H. Page, "Supersonic Turbulent Flow Reattachment Downstream of a Two-dimensional Backstep," AIAA Paper No. 70-108, 1970.
39. Gerhart, P. M., "A Study of the Reattachment of a Turbulent Supersonic Shear Layer with the Closure Condition provided by a Control Volume Analysis," Ph.D. Thesis, Department of Mechanical and Industrial Engineering, University of Illinois at Urbana-Champaign, 1971.
40. Chow, W. L., "Recompression of a Two-dimensional Supersonic Turbulent Free Shear Layer," Development in Mechanics, Proc., 12th Mid-western Mechanics Conference, University of Notre Dame, Notre Dame, Indiana, Vol. 6, August 1971, pp. 319-332.

41. Spring, D. J., "Supersonic Laminar Flow Reattachment and Redevelopment behind a Two-dimensional Rearward Facing Step," Ph.D. Thesis, Department of Mechanical and Industrial Engineering, University of Illinois at Urbana-Champaign, 1972.
42. Chow, W. L., and D. J. Spring, "Viscous Interaction of Flow Redvelopment after Flow Reattachment with Supersonic External Streams," AIAA J., Vol. 13, No. 12, 1975, pp. 1576-1584.
43. Weng, C. H., "Base Pressure Problems associated with Supersonic Axisymmetric External Flow Configurations," Ph.D. Thesis, Department of Mechanical and Industrial Engineering, University of Illinois at Urbana-Champaign, 1975.
44. Peters, C. E., and W. J. Phares, "Analytical Model of Supersonic, Turbulent, Near-wake Flows," AEDC-TR-76-127, Arnold Engineering Development Center, Arnold Air Force Station, Tennessee, September 1976.
45. Chow, W. L., and D. J. Spring, "The Viscous Interaction of Incompressible Separated Flows," TR RD-73-22, U.S. Army Missile Command, Redstone Arsenal, Ala., May 1974.
46. Chow, W. L., and D. J. Spring, "Viscid-Inviscid Interaction of Incompressible Separated Flows," J. of Applied Mechanics, Vol. 98, No. 3, September 1976, pp. 387-395.
47. Warpinski, N. R., "Incompressible Flow past Wedges at High Reynolds Numbers," Ph.D. Thesis, Department of Mechanical and Industrial Engineering, University of Illinois at Urbana-Champaign, 1977.
48. Warpinski, N. R., and W. L. Chow, "Viscid-Inviscid Interaction associated with Incompressible Flow past Wedges at High Reynolds Numbers," ME-TR-395-4. Department of Mechanical and Industrial Engineering, University of Illinois, Feb. 1977; also, NASA CR-135246. August 1977.
49. Murman, E. M., and J. D. Cole, "Calculation of Plane Steady Transonic Flows," AIAA J., Vol. 9, No. 1, January 1971, pp. 114-121.
50. Krupp, J. A., and E. M. Murman, "Computation of Transonic Flows past Lifting Airfoils and Slender Bodies," AIAA J., Vol. 10, No. 7, July 1972, pp. 880-886.
51. Bailey, F. R., "Numerical Calculation of Transonic Flow about Slender Bodies of Revolution," NASA TN D-6582, 1971.
52. Steger, J. L., and H. Lomax, "Numerical Calculation of Transonic Flow about Two-dimensional Airfoils by Relaxation Procedures," AIAA J., Vol. 10, No. 1, January 1972, pp. 49-54.
53. South, J.C., Jr., and A. Jameson, "Relaxation Solutions for Inviscid Axisymmetric Transonic Flow over Blunt or Pointed Bodies," Computational Fluid Dynamics Conference Proceedings, Palm Springs, Cal., 19-20 July 1973, pp. 8-17.

54. Chow, W. L., L. J. Bober, and B. H. Anderson, "Strong Interaction associated with Transonic Flow past Boattailed Afterbodies," AIAA J., Vol. 13, No. 1, January 1975, pp. 112-113.
55. Chow, W. L., L. J. Boboer, and B. H. Anderson, "Numerical Calculations of Transonic Boattail Flow," NASA TN D-7984, June 1975.
56. Deiwert, G. S., "Computation of Separated Transonic Turbulent Flows," AIAA J., Vol. 14, No. 6, June 1976, pp. 735-740.
57. Chow, W. L., and T. S. Shih, "The Viscid-Inviscid Interaction associated with a Two-dimensional Transonic Flow past a Backstep," ME-TR-395-3, Department of Mechanical and Industrial Engineering; also, UILU ENG 75-4003, Engineering Experiment Station, University of Illinois at Urbana-Champaign, October 1975.
58. Chow, W. L., and T. S. Shih, "Transonic Flow past a Backward Facing Step," AIAA J., Vol. 15, No. 9, 1977, pp. 1342-1343.
59. Kline, S., M. Morkovin, G. Sovran, and D. Cockrell, eds., Proc., Computation of Turbulent Boundary Layers, Stanford University Press, 1968.
60. Sasman, P. K., and R. J. Cresci, "Compressible Turbulent Boundary Layer with Pressure Gradient and Heat Transfer," AIAA J., Vol. 4, No. 1, January 1966, pp. 19-25.
61. Brink, D. F., and W. L. Chow, "Two-dimensional Jet Mixing with a Pressure Gradient," J. of Applied Mechanics, Vol. 42, Series E, No. 1, 1975, pp. 55-60.
62. Korst, H. H., and W. L. Chow, "Nonisoenergetic Turbulent Jet Mixing between Two Compressible Streams at Constant Pressure," NASA CR-419, 1965.
63. Koh, J.C.Y., "A New Wind Tunnel Technique for providing Simulation of Flight Base Flow," J. of Spacecraft and Rockets, Vol. 8, No. 10, October 1971, pp. 1095-1096.
64. Merz, R. A., "The Turbulent Near-wake of an Axisymmetric Blunt based Body at Subsonic Speeds," Ph.D. Thesis, Department of Mechanical, Industrial, and Aerospace Engineering, Rutgers University, New Brunswick, New Jersey, May 1975.
65. Rom, J., M. Victor, M. Reichenberg, and M. Salomon, "Wind Tunnel Measurements of the Base Pressure of an Axially Symmetric Model in Subsonic, Transonic, and Supersonic Speeds at High Reynolds Numbers," Technion-Israel Institute of Technology, T.A.E. Report No. 134, September 1972.
66. Tanner, M., "Theoretical Prediction of Base Pressure for Steady Base Flow," Progress in Aerospace Sciences, Vol. 14, Pergamon Press, London, 1973, pp. 177-225.

APPENDIX

INTEGRALS ASSOCIATED WITH THE VISCOUS LAYER

In the present analysis, it is assumed that the velocity profile of viscous layer above the dividing streamline follows a polynomial of the form given by

$$\phi = \frac{u}{u_e} = \phi_d + s\zeta_a + [3(1 - \phi_d) - 2s] \zeta_a^2 + [s - 2(1 - \phi_d)] \zeta_a^3$$

$$(0 \leq \zeta_a \leq 1)$$

where

$$\phi_d = \frac{u_d}{u_e}, \quad s = \left. \frac{\partial \phi}{\partial \zeta_a} \right|_d, \quad \zeta_a = \frac{y - y_d}{\delta_a};$$

a linear velocity profile given by

$$\phi = \frac{u}{u_e} = \phi_d \zeta_l \quad (0 \leq \zeta_l \leq 1)$$

for the forward flow of the viscous layer below the dividing streamline where

$$\zeta_l = \frac{y - y_d + \delta_b}{\delta_b}$$

and

$$\phi = \frac{u}{u_e} = -\phi_b \cos \frac{\pi}{2} \zeta_b \quad (0 \leq \zeta_b \leq 1)$$

for the reverse flow where

$$\phi_b = \frac{u_b}{u_e} \text{ and } \zeta_b = \frac{y_w - R_s}{h_b}.$$

It is further assumed that the slope parameter s is coupled with ϕ_d through $s = g \phi_d$; therefore,

$$\Gamma = \frac{\partial \phi}{\partial \phi_d} = 1 + g \zeta_a - (3 + 2g) \zeta_a^2 + (2 + g) \zeta_a^3.$$

Thus, the integrals F1 through F28 can be represented by

$$F1 = \int_0^1 \frac{\phi}{1 - C_e^2 \phi^2} d \zeta_a$$

$$F2 = \int_0^1 \frac{\phi}{1 - C_e^2 \phi^2} \zeta_a d \zeta_a$$

$$F3 = \int_0^1 \frac{1 + C_e^2 \phi^2}{(1 - C_e^2 \phi^2)^2} \Gamma d \zeta_a$$

$$F4 = \int_0^1 \frac{1 + C_e^2 \phi^2}{(1 - C_e^2 \phi^2)^2} \Gamma \zeta_a d \zeta_a$$

$$F5 = \int_0^1 \frac{\phi^3}{(1 - C_e^2 \phi^2)^2} d \zeta_a$$

$$F6 = \int_0^1 \frac{\phi^3}{(1 - C_e^2 \phi^2)^2} \zeta_a d \zeta_a$$

$$F7 = \int_0^1 \frac{\phi(1 - \phi)}{1 - C_e^2 \phi^2} d \zeta_a$$

$$F8 = \int_0^1 \frac{\phi(1 - \phi)}{1 - C_e^2 \phi^2} \zeta_a d \zeta_a$$

$$F9 = \int_0^1 \frac{1 - 2\phi + C_e^2 \phi^2}{(1 - C_e^2 \phi^2)^2} \Gamma d \zeta_a$$

$$F10 = \int_0^1 \frac{1 - 2\phi + C_e^2 \phi^2}{(1 - C_e^2 \phi^2)^2} \Gamma \zeta_a d \zeta_a$$

$$F11 = \int_0^1 \frac{\phi^3(1 - \phi)}{(1 - C_e^2 \phi^2)^2} d \zeta_a$$

$$F12 = \int_0^1 \frac{\phi^3(1 - \phi)}{(1 - C_e^2 \phi^2)^2} \zeta_a d \zeta_a$$

$$F13 = \int_0^1 \frac{u/u_d}{1 - C_d^2 (\frac{u}{u_d})^2} d \zeta_\ell$$

$$F14 = \int_0^1 \frac{u/u_d}{1 - C_d^2 (\frac{u}{u_d})^2} \zeta_\ell d \zeta_\ell$$

$$F15 = \int_0^1 \frac{u/u_b}{1 - C_b^2 (\frac{u}{u_b})^2} d \zeta_b$$

$$F16 = \int_0^1 \frac{u/u_b}{1 - C_b^2 (\frac{u}{u_b})^2} \zeta_b d \zeta_b$$

$$F17 = \int_0^1 \frac{(u/u_d)^3}{(1 - C_d^2 (\frac{u}{u_d})^2)^2} d \zeta_\ell$$

$$F18 = \int_0^1 \frac{(u/u_d)^3}{(1 - C_d^2 (\frac{u}{u_d})^2)^2} \zeta_\ell d \zeta_\ell$$

$$F19 = \int_0^1 \frac{(u/u_b)^3}{(1 - c_b^2 (\frac{u}{u_b})^2)^2} d \zeta_b$$

$$F21 = \int_0^1 \frac{(u/u_d)^2}{1 - c_d^2 (\frac{u}{u_d})^2} d \zeta_d$$

$$F23 = \int_0^1 \frac{(u/u_b)^2}{1 - c_b^2 (\frac{u}{u_b})^2} d \zeta_b$$

$$F25 = \int_0^1 \frac{(u/u_d)^4}{(1 - c_d^2 (\frac{u}{u_d})^2)^2} d \zeta_d$$

$$F27 = \int_0^1 \frac{(u/u_b)^4}{(1 - c_b^2 (\frac{u}{u_b})^2)^2} d \zeta_b$$

$$F20 = \int_0^1 \frac{(u/u_b)^3}{(1 - c_b^2 (\frac{u}{u_b})^2)^2} \zeta_b d \zeta_b$$

$$F22 = \int_0^1 \frac{(u/u_d)^2}{1 - c_d^2 (\frac{u}{u_d})^2} \zeta_d d \zeta_d$$

$$F24 = \int_0^1 \frac{(u/u_b)^2}{1 - c_b^2 (\frac{u}{u_b})^2} \zeta_b d \zeta_b$$

$$F26 = \int_0^1 \frac{(u/u_d)^4}{(1 - c_d^2 (\frac{u}{u_d})^2)^2} \zeta_d d \zeta_d$$

$$F28 = \int_0^1 \frac{(u/u_b)^4}{(1 - c_b^2 (\frac{u}{u_b})^2)^2} \zeta_b d \zeta_b$$

These integrals can only be evaluated through numerical integrations.